Fabrication and applications of supercharged, unfolded proteins

Kolbe, Anke

Fabrication and Applications of Supercharged, Unfolded Proteins

Anke Kolbe

Fabrication and Applications of Supercharged, Unfolded Proteins

Anke Kolbe

Zernike Institute Ph.D. thesis series 2012-26
ISSN: 1570-1530
ISBN: 978-90-817891-0-3 (printed version)
ISBN: 978-90-817891-1-0 (electronic version)
The work described in this thesis was carried out in the group "Polymer Chemistry and Bioengineering" at the Department of Polymer Chemistry, Zernike Institute for Advanced Materials, University of Groningen.
Cover design by Hester Nijhoff
Printed by Chris Russell, Groningen, the Netherlands
Publisher: BMC Netherlands, Groningen, the Netherlands

RIJKSUNIVERSITEIT GRONINGEN

Fabrication and Applications of Supercharged, Unfolded Proteins

Proefschrift

ter verkrijging van het doctoraat in de
Wiskunde en Natuurwetenschapen
aan de Rijksuniversiteit Groningen
op gezag van de
Rector Magnificus, dr. E. Sterken,
in het openbaar te verdedigen op
vrijdag 30 november 2012
om 14.30 uur

door

Anke Kolbe
geboren op 13 september 1979
te Stuttgart, Duitsland

Promotor:	Prof. dr. A. Herrmann
Beoordelingscommissie:	Prof. dr. K.U. Loos
	Prof. dr. B. Poolman
	Prof. dr. W.J. Parak

CONTENT

Chapter 1

Supercharged Proteins and Their Applications in Biomedicine and Biotechnology

Electrostatic interactions play a vital role in the interplay of biomacromolecules, such as protein and nucleic acids. Electrostatic repulsion, on the other hand, prevents unfavorable interactions that might lead to uncontrolled aggregation. Most naturally occurring proteins are only moderately charged at physiological conditions. Natural proteins with uncommonly high net charges are often partially or completely disordered in solution, due to repulsion forces between uncompensated charges. Moreover, many highly charged, disordered proteins are resilient to heat inactivation. Attempts to increase the net charge of (mostly folded) proteins include chemical modification of charged residues on the protein surface and genetic engineering. The latter method includes exchange of solvent-exposed amino acids, also known as "supercharging", and increase of the overall charge by means of a highly charged tag. Examples from the literature are presented and advantages as well as disadvantages of both methods in regard to applications are discussed. A focus is given to polyionic variants of genetically engineered, unfolded polypeptides on the basis of elastin and their potential as versatile materials for applications in biomedicine and biotechnology is highlighted.

1. HIGHLY CHARGED PROTEINS IN NATURE

1.1 Highly charged proteins and their functions

Electrostatic interactions play an important role in many intra- and extracellular processes in nature. The four charged amino acids lysine, arginine, glutamic acid and aspartic acid are present in most naturally occurring proteins and are often involved in protein-protein interactions.[1-4] Furthermore, electrostatic attraction mediates interactions between proteins and nucleic acids,[5-9] membranes[10-13] or small molecules.[14-16] In other cases proteins possess highly charged, surface-exposed regions to prevent unfavorable interactions that might lead to aggregation.[17] Analysis of the protein databank SwissProt[18] revealed that most proteins in nature are moderately charged. Only five percent of all proteins contained in the databank possess one or more uncompensated charges per ten amino acids. Table 1 summarizes the proteins with the highest net charge density (NCD; column 5), which was calculated according to

$$NCD = (\#posAA - \#negAA)/\#AA \quad (1)$$

with #posAA (#negAA) = number of positively (negatively) charged amino acids and #AA = total number of amino acids. For the sake of clarity, only the protein with the highest net charge density of a set of similar proteins is listed.

Among the most positively charged proteins in nature are histones, histone-like proteins and protamines (Table 1a, entries 1, 5, 6, 7 and 13). Histones are responsible for DNA condensation in eukaryotic cells; together with DNA they form the major building blocks of chromatin.[19] During the post-meiotic maturation of male haploid germ cells, histones are replaced by protamines and transition proteins, small basic proteins.[20,21] Sperm protamine P3 of *Murex brandaris*, a predatory sea snail, contains 40 positively charged residues on a total length of 54 amino acids, and is the most highly charged natural protein contained in the protein databank SwissProt to date. Moreover, highly charged proteins are involved in protein synthesis as subunits of the ribosome complex (Table 1a, entries 2-4, and Table 1b, entry 4). Other cationic polypeptides act as neurotoxins by blocking potassium or sodium channels (entries 14 and 16) or are involved in bacterial spore coat formation (entry 15). Furthermore, a number of antimicrobial polypeptides like cryptonin[22], misgurin[23] and androctonin[24] can be found among highly cationic proteins (entries 9, 11 and 12). Antimicrobial (poly) peptides (AMPs) comprise a first line of host defense against microbial pathogens in

a wide variety of organisms ranging from invertebrates and vertebrates to plants.[25,26] Cryptonin was isolated from the Korean blackish cicada, *Cryptotympana dubia*. It forms a linear amphipathic alpha-helix upon binding to negatively charged cell surfaces and kills microbial cells by increasing cell permeability, probably due to pore formation.[22] Misgurin, an AMP from the loach (mudfish) *Misgurnus anguillicaudatus,* belongs to the same structural class of peptides as cryptonin and exhibits antibacterial activity by a similar mechanism.[23] Androctonin, a 25-residue peptide with two disulfide bridges, was isolated from the hemolymph of the scorpion *Androctonus australis* and was found to be active against a broad spectrum of both gram-positive and gram-negative bacteria and fungi.[24] Unlike cryptonin and misgurin, androctonin does not form pores, but disintegrates cytoplasmic membranes by micellization in a detergent-like manner.[27,28] AMPs usually do not exhibit significant hemolytic activity, as their cationic charge promotes selectivity for negatively charged microbial cytoplasmic membranes over zwitterionic membranes of plants and animals.[29,30] Moreover, AMPs show broad activity spectra against bacteria and fungi as well as viruses and parasites. This makes these compounds promising candidates for the treatment of infections where resistance has rendered antibiotics ineffective.[31]

Among the most negatively charged, naturally occurring proteins are prothymosin and parathymosin (Table 1b, entries 1 and 13). Both proteins are expressed in a wide variety of tissues and cell lines and are believed to have vital housekeeping functions.[32] Prothymosin alpha is the most negatively charged natural protein in the SwissProt protein database with 54 aspartic and glutamic acid residues, 10 lysine and arginine residues and a total length of 111 amino acids. Prothymosin alpha is an oncoprotein transcription factor and is involved in cell cycle progression and proliferation.[33] Parathymosin, on the other hand, is associated with early DNA replication.[32] It modulates the interaction of the linker histone H1 with the nucleosome, thereby inducing chromatin decondensation.[34] Another protein that is involved in chromatin modulation is Chz1, a highly negatively charged nuclear chaperone of the histone variant H2AZ (Table 1b, entry 6).[35] H2AZ replaces conventional histone H2A in budding yeast and is found in close proximity to the promoters of most genes.[36] Chz1 aids in the proper incorporation of histones into nucleosomes by shielding their positive charge and by blocking crucial surface sites.[36] Furthermore, highly negatively charged proteins are involved in transcriptional and translational regulation (Table 1b, entries 3, 7 and 15), cell-cycle control (entry 8), ubiquitin-dependent proteolysis (entry 9), electron transport in mitochondria (entry 10) and receptor-mediated endocytosis (entry 12). Other anionic proteins are components of calcified shell layers (entry 5) and building blocks of bacteriophage or virion particles (entries 11 and 14).

Table 1. An overview of the most highly charged, naturally occurring proteins, as derived from the protein databank SwissProt. For the sake of clarity, only the protein with the highest net charge density of a set of similar proteins is listed.

a) Cationic proteins

	Protein	Function	UniProt code	NCD*	length (#AA)	# posAA	# negAA	Organism
1	sperm protamine P3	DNA condensation	P83213	0.74	54	40	0	Murex brandaris (Purple dye murex)
2	60S ribosomal protein L41	protein synthesis	P62945	0.68	25	17	0	Homo sapiens (Human) and other organisms
3	50S ribosomal protein L41e	protein synthesis	P54025	0.55	22	13	1	Methanocaldococcus jannaschii
4	30S ribosomal protein Thx	protein synthesis	P62611	0.44	27	13	1	Thermus aquaticus
5	DNA-binding protein	DNA condensation (suggested)	P24648	0.43	51	23	1	Orgyia pseudotsugata multicapsid polyhedrosis virus
6	Histone-like protein Hq1	DNA condensation	Q45881	0.42	117	53	4	Coxiella burnetii
7	Histone H1.C8/H1.M1	DNA condensation	P40270	0.41	74	31	1	Trypanosoma cruzi
8	Spermatid nuclear transition protein 1	DNA condensation	P22613	0.35	54	21	2	Ovis aries (Sheep)
9	Cryptonin	antimicrobial	P85028	0.33	24	8	0	Cryptotympana dubia (Korean horse cicada)
10	Small core protein	core protein	P69548	0.33	24	8	0	Enterobacteria phage alpha3
11	Misgurin	antimicrobial	P81474	0.33	21	9	2	Misgurnus anguillicaudatus (Oriental weatherfish)
12	Androctonin	antimicrobial	P56684	0.32	25	8	0	Androctonus australis (Sahara scorpion)
13	Histone H5	DNA condensation	P02258	0.32	193	67	5	Anser anser anser (Western graylag goose)
14	Potassium channel toxin alpha-KTx 13.1	blocks reversibly Shaker B K^+ channels	P83243	0.30	23	7	0	Tityus obscurus (Amazonian scorpion)
15	Spore coat protein G	incorporation of CotB into spore coat (suggested)	P39801	0.30	195	71	13	Bacillus subtilis
16	Mu-conotoxin GIIIB	blocks voltagegated N^+ channels	P01524	0.27	22	8	2	Conus geographus (Geography cone)

*NCD = net charge density

b) Anionic proteins

	Protein	Function	UniProt code	NCD*	length (#AA)	# posAA	# negAA	Organism
1	Prothymosin alpha	immune function (suggested)	P06454	-0.40	111	10	54	Homo sapiens (Human)
2	UPF0473 protein Helmi_02360	uncharacterized	B0TFZ1	-0.39	89	4	39	Heliobacterium modesticaldum
3	Testis ecdysiotropin peptide 1	start or boost ecdysteroid synthesis in testis of larvae and pupae	P80936	-0.38	21	0	8	Lymantria dispar (Gypsy moth)
4	50S ribosomal protein L12P	binding site for factors involved in protein synthesis	P15772	-0.36	115	2	43	Haloarcula marismortui
5	Coiled-coil domain-containing protein 1	component of organic matrix of calcified layers of the shell	B3A0Q3	-0.35	396	24	164	Lottia gigantea (Owl limpet)
6	Histone H2A.Z-specific chaperone chz-1	histone replacement in chromatin	Q9P534	-0.35	114	7	47	Neurospora crassa
7	Probable DNA-directed RNA polymerase subunit delta	initiation and recycling phases of transcription	Q49Z74	-0.35	182	12	75	Staphylococcus saprophyticus subsp. saprophyticus
8	Anaphase-promoting complex subunit 15	controlling progression through mitosis and the G1 phase	A9JSB3	-0.34	120	3	44	Xenopus tropicalis (Western clawed frog)
9	26S proteasome complex subunit DSS1	ubiquitin-dependent proteolysis	Q3ZBR6	-0.31	70	5	27	Bos taurus (Bovine) and other
10	Cytochrome b-c1 complex subunit 6	mitochondrial respiratory chain	P00127	-0.31	147	12	58	Saccharomyces cerevisiae
11	Prehead core component PIP	phage particle	P03720	-0.31	80	10	35	Enterobacteria phage T4
12	Cysteine-rich, acidic integral membrane protein	receptor-mediated endocytosis (suggested)	Q03650	-0.31	945	9	301	Trypanosoma brucei brucei
13	Parathymosin	immune function: blocking prothymosin α	P08814	-0.30	102	16	47	Bos taurus (Bovine)
14	Protein 6	virion structural protein (suggested)	O70791	-0.30	93	4	32	Rice yellow stunt virus
15	Regulator of ribonuclease activity B	modulating RNA abundance	C9XUB3	-0.30	140	6	48	Cronobacter turicensis

*NCD = net charge density

1.2 Intrinsically disordered proteins

Several of the most highly charged, natural proteins are characterized as natively unfolded in solution. Natively unfolded or intrinsically disordered proteins (IDPs) are divided into two classes: completely and partly unfolded proteins. The proteins of the former class are disordered throughout the entire polypeptide chain and can be further divided into proteins with no secondary structure at all, and proteins with residual secondary structure, but without any tertiary structure.[37] IDPs are generally characterized by a low content of hydrophobic amino acid residues and a relatively high percentage of uncompensated charged groups, which leads to a large net charge at neutral pH.[37] Folding of these proteins into a compact structure is unfavorable due to repelling forces of charges. At the same time these forces are not balanced by hydrophobic interactions that would promote folding.[38] Consistent with these characteristics, IDPs are often found to be highly resistant to heat denaturation, aggregation and chemical denaturation.[39] Table 2 provides an overview of proteins with the highest net charge listed in DisProt[40], the databank of protein disorder. This databank does not contain all disordered proteins, but only those that have been characterized as disordered. Among the most cationic, disordered proteins are the protamine variant chicken sperm histone and several other histone and non-histone, chromosomal proteins (Table 2a, entries 1 to 4, 6, 9 and 12). Variants of these proteins were also found among the most highly charged proteins in the databank SwissProt (Table 1a, entries 1, 6 and 7). Chicken sperm histone, a protamine variant, exhibits the highest charge density with 36 positive charges and a total length of 62 amino acids. Furthermore, several polypeptides with antibacterial activity like non-histone chromosomal protein H6, cathelicidin antimicrobial peptide and beta-defensin are disordered (Table 2a, entries 6, 13 and 15). It was suggested that cationic antimicrobial peptides adopt a secondary structure and become amphiphilic upon interaction with the target structure, i.e. the bacterial membrane.[41] Rat prothymosin α was found to be the protein with the most negative charge density (-0.38) in the databank DisProt (Table 2b, entry 1). It is therefore assumed that human prothymosin α, which exhibits a slightly higher charge density (-0.40) is disordered as well (Table 1b, entry 1). Besides DNA condensation and antimicrobial activity, highly charged, intrinsically disordered proteins are involved in fatty acid synthesis, protein synthesis (Table 2a, entries 8, 11 and 14, and Table 2b, entry 9) and protein degradation (Table 2b, entries 2 and 7). Furthermore, anionic, disordered proteins are associated with mineralization processes (Table 2b, entries 3 and 11), calcium storage (entry 5), muscle contraction (entry 8), and conductance regulation of chloride channels (entry 10).

Table 2. A summary of highly charged, intrinsically disordered proteins, as derived from DisProt[40], the databank of protein disorder.

a) Cationic, disordered proteins

	Protein Name	Function	UniProt code / DisProt no.	NCD*	length (#AA)	# posAA	# negAA	Organism
1	Sperm histone (protamine)	DNA condensation	P15340/ DP00057	0.58	62	36	0	Gallus gallus (Chicken)
2	Histone H5	DNA condensation	P02259/ DP00044	0.32	189	66	5	Gallus gallus (Chicken)
3	Histone H1.0	DNA condensation	P10922/ DP00097	0.27	193	62	9	Mus musculus (Mouse)
4	Histone H1.2	DNA condensation	P15865/ DP00136	0.27	217	66	7	Rattus norvegicus (Rat)
5	genome polyprotein	several	P06935/ DP00148_ C004	0.20	55	15	4	Human immunodeficiency virus type 1
6	Non-histone chromosomal protein H6	tuning DNA condensation (sugg.); antibacterial activity	P02315/ DP00042	0.20	70	20	6	Oncorhynchus mykiss (Rainbow trout) (Salmo gairdneri)
7	Protein LLP	transcriptional activator	B0FRH7/ DP00544	0.18	120	36	14	Aplysia kurodai (Kuroda's sea hare)
8	50S ribosomal protein L33	protein synthesis	P0A7N9/ DP00143	0.18	55	15	5	Escherichia coli
9	Non-histone chromosomal protein HMG-17	tuning DNA condensation	P02313/ DP00195	0.18	89	26	10	Bos taurus (Bovine)
10	Cyclin-dependent kinase inhibitor 2A [Isoform 3]	negative regulator of proliferation	Q64364-1/ DP00335	0.18	169	38	8	Mus musculus (Mouse)
11	30S ribosomal protein S12	protein synthesis	P0A7S3/ DP00145	0.17	124	28	7	Escherichia coli
12	Histone H1	DNA condensation	P53551/ DP00423	0.16	258	62	20	Saccharomyces cerevisiae (Baker's yeast)
13	Cathelicidin antimicrobial peptide (LL-37)	antibacterial activity	P49913/ DP00004 _C002	0.16	37	11	5	Homo sapiens (Human)
14	30S ribosomal protein S18	protein synthesis	P0A7T7/ DP00146	0.16	75	18	6	Escherichia coli
15	Beta-defensin 12	antibacterial activity	P46170/ DP00209	0.16	38	6	0	Bos taurus (Bovine)

*NCD = net charge density

b) Anionic, disordered proteins

	Protein Name	Function	UniProt code / DisProt no.	NCD*	length (#AA)	# posAA	# negAA	Organism
1	Prothymosin alpha	transcription factor (cell cycle progression and proliferation)	P06302 / DP00058	-0.38	112	11	53	Rattus norvegicus (rat)
2	26S proteasome complex subunit DSS1	ubiquitin-dependent proteolysis	P60896 / DP00617	-0.31	70	5	27	Homo Sapiens (Human)
3	Protein starmaker	formation of otoliths in the inner ear	A2VD23/ DP00584	-0.24	613	70	216	Danio rerio (Zebrafish) (Brachydanio rerio)
4	Cyclic nucleotide-gated cation channel beta-1 [Isoform GARP1]	visual and olfactory signal transduction	Q28181-4/ DP00441	-0.20	590	46	165	Bos taurus (Bovine)
5	Calsequestrin-1	internal calcium store in muscle	P07221/ DP00132	-0.20	395	32	111	Oryctolagus cuniculus (Rabbit)
6	Acyl carrier protein	fatty acid biosynthesis	P0A6A8/ DP00416	-0.19	78	5	20	Escherichia coli
7	Prokaryotic ubiquitin-like protein pup	marker for proteasomal degradation	O33246/ DP00293	-0.19	64	7	19	Mycobacterium tuberculosis
8	Troponin C, slow skeletal and cardiac muscles	striated muscle contraction	P63315/ DP00249	-0.18	161	17	46	Bos taurus (Bovine)
9	60S acidic ribosomal protein P1-alpha	protein synthesis	P05318/ DP00164	-0.18	106	5	24	Saccharomyces cerevisiae (Baker's yeast)
10	Methylosome subunit pICln	chloride conductance regulatory protein	P35521/ DP00717	-0.17	235	13	53	Canis lupus familiaris (Dog)
11	Bone sialoprotein 2	integral part of mineralized matrix	P21815/ DP00332	-0.17	317	23	76	Homo sapiens (Human)
12	Calmodulin	calcium signal transduction	P62152/ DP00344	-0.16	149	14	38	Drosophila melanogaster (Fruit fly)
13	Latent membrane protein 2A	blocks tyrosine kinase signaling	A8CDV5/ DP00538	-0.16	118	4	23	Epstein-Barr virus (Human herpesvirus 4)
14	RWD domain-containing protein 1	cell signaling	Q9CQK7/ DP00587	-0.16	243	24	62	Mus musculus (Mouse)

*NCD = net charge density

IDPs often play a role in transcriptional and translational regulation (Table 2a, entry 7), signal transduction (Table 2b, entries 4, 12 to 14) and cell-cycle control (Table 2a, entry 10 and Table 2b, entry 1). This indicates that IDPs are involved in processes which require certain flexibility, for example as linkers or as binding partners for multiple target structures.[38,42] Furthermore, IDPs are associated with a number of diseases such as prion diseases, Parkinson's disease, Alzheimer and Huntington's disease.[37,42] Both protein aggregation and amyloidosis, the ordered aggregation of proteins into fibers, are implicated to contribute negatively to the development of these diseases. Interestingly, it was found that mutants of an amyloid disease related protein with reduced net charge promote its aggregation.[43] These findings suggest that surface charge plays a crucial role in the aggregation behavior of proteins.

2. CHANGING THE NET CHARGE OF PROTEINS

So far, natural proteins with high net charges and their functions in nature have been discussed. In particular, intrinsically disordered proteins were highlighted. In the context of IDPs that are associated with amyloidosis, it was mentioned that protein aggregation is closely linked to surface charge. Aggregation of proteins can be induced by changing the pH, the composition of a solution or by a temperature increase. Although protein aggregation is desired under certain circumstances, it is highly unfavorable in most cases, because it often results in irreversible protein inactivation. This poses a problem in biotechnology where enzymes are used as catalysts for chemical reactions in industrial processes and as additives in washing powders. These processes usually take place under conditions that promote protein aggregation like elevated temperature, addition of organic solvents and high concentrations of surfactants.[44] Consequently, strategies were developed to influence the aggregation behavior of proteins.[45] One strategy is to increase a protein's net charge, which increases the repellence of partly unfolded chains and makes protein aggregation unfavorable. To this end, several methods for introducing charges into proteins are described and will be discussed regarding their effectiveness and applicability. Furthermore, possible applications of highly charged proteins will be described.

2.1 Post-translational, chemical modification

A simple, inexpensive way of changing the net charge of a protein is the post-translational, chemical modification of solvent-exposed amino acid residues.

Methods like acetylation and succinylation of lysine residues as well as amidation of carboxylic groups date back to the late 1960s (Figure 1).[46-49] Although initially employed for the characterization of proteins, these methods gained increased attention in the following decades due to their effect on protein net charge, which alters a protein's solubility and interaction with oppositely charged molecules.[50-54] Acetylation of lysine ε-amino groups, for example, decreases the number of positive charges and thereby leads to variants with a higher net negative charge (Figure 1, pathway 1).

By reaction with acetic anhydride, Shaw *et al.* created highly negatively charged variants of bacterial α-amylase, an industrially relevant hydrolase, without perturbing its structural integrity or decreasing its thermostability.[55] The modified variant with approximately 17 acetyl modifications proved to be more resistant to irreversible inactivation and aggregation in the presence of anionic and

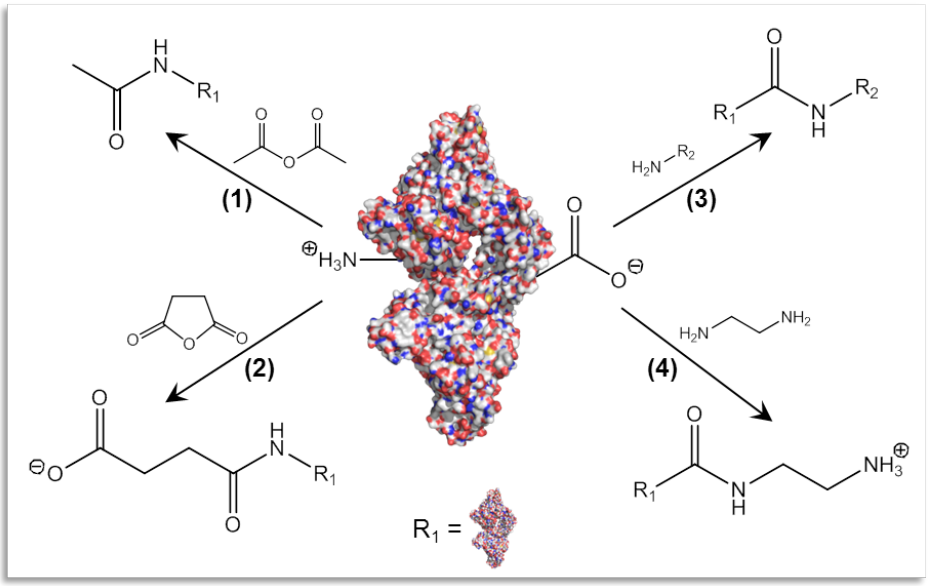

Figure 1. An overview of post-translational, chemical modifications of proteins. The net charge of a protein can be increased by elimination (1, 3) or inversion (2, 4) of charges. Amine groups are neutralized by acetylation (1) or their charge is reversed by succinylation (2). Amidation (3) of carboxyl groups eliminates negative charges on the protein surface. In the special case of amination (4), a positively charged group is introduced instead.

neutral surfactants that are commonly used in industrial applications.[56] However, acetylation of lysine residues simultaneously increases the hydrophobicity of the protein surface and can even reduce the stability of a protein towards denaturants and/or heat, which was shown for the enzyme bovine carbonic anhydrase.[57] Similarly, it was demonstrated that ovalbumin was more prone to urea and heat-induced unfolding after amidation of its carboxyl groups.[58,59] As an alternative to neutralization, charges of residues can be reversed. This increases the net charge of the protein, and at the same time the generation of a more hydrophobic protein surface is avoided. Upon reaction with succinic anhydride, lysine ε-amino groups are converted from basic to acidic groups (Figure 1, pathway 2).[48,54] Interestingly, succinylation of lysine residues was also shown to greatly enhance the activity of cyclodextrin glycosyltransferase from *Thermoanaerobacter*.[60] However, like acetylation, succinylation might lead to destabilization and increased aggregation of the modified protein.[58,59,61] The underlying mechanisms of destabilization have not been fully elucidated yet. It was suggested that charge modification might interfere with the ion pair network, thereby destabilizing the protein structure.[59] This statement is in line with the finding that protein stability after succinylation seems to be dependent on the number and sites of modification(s).[54]

Instead of creating highly anionic variants by reversing the charge of lysine, proteins can be cationized by substituting carboxylic groups with amine groups (Figure 1, pathway 4).[50] As carboxylates are less reactive than amine groups, activation of the carboxylic acid group by a carbodiimide needs to be performed before reaction with the diamine takes place. Several proteins, like ferritin, catalase, superoxide dismutase, bovine serum albumin (BSA) and ovalbumin, were modified by amidation to increase their interaction with negatively charged tissues.[50,51] It was found that cationized enzymes were much longer retained in cartilaginous tissue than their natural counterparts and their anti-inflammatory effect was prolonged.[51] Cationization does not only promote adhesion to tissues and cell membranes, but can stimulate uptake of the modified proteins by cells. Cationized BSA (cBSA) was taken up by isolated bovine brain microvessels *in vitro* and was shown to pass the blood-brain barrier *in vivo* after carotid infusion in rat models.[62] These findings raised expectations that cationized proteins might initiate the uptake of biologically active materials like drugs, DNA or proteins. Indeed, cBSA coupled to liposomes induced endocytosis by brain capillary endothelial cells via a caveolin-associated pathway.[63] Furthermore, cBSA was found to form polyplexes with plasmid DNA and to efficiently transfect A-549 human epithelial cells *in vitro*.[64,65] Biocoatings of cBSA variants promoted immobilization of lipid vesicles and

formation of bacterial biofilms.[66,67] In order to stimulate adhesion of mammalian cells *in vitro*, cyclic derivatives of the arginine-glycine-aspartate (RGD) sequence were grafted to cBSA.[67] Coatings of these RGD-cBSA derivatives on glass surfaces were shown to support cell-matrix adhesion of fibroblast cells.[68]

Taken together, chemical modifications can be used to change a protein's overall charge and to decrease unfavorable interactions in order to increase aggregation resistance. Alternatively, favorable interactions with oppositely charged molecules and structures can be enhanced, thereby promoting adhesion or even uptake of biologically active molecules into cells. Although chemical modification of charged, solution-exposed residues is a simple method to change a protein's net charge, its applicability needs to be evaluated for individual proteins. Furthermore, chemical modification results in a mixture of variants with different net charges and modification patterns. To yield fractions with a narrow net charge distribution, an extra purification step needs to be performed.[64] This method is therefore favorable in cases where the protein is directly extracted from its natural source. For proteins that are produced in a heterologous host organism, however, the gene encoding for the protein is already available in the respective vector, and surface charges are easily modified by genetic engineering. This method results in well-defined protein variants and therefore presents an elegant alternative to chemical modification as described in the following paragraph.

2.2 Modification of solvent-exposed amino acids by genetic mutation

The genetic engineering approach to dramatically increase a protein's net charge was first exploited by Liu and co-workers in 2007 and was referred to as "supercharging of proteins": charged, solvent-exposed amino acids were identified by analysis of the crystal structure and modified by genetic mutation.[69] Negatively charged residues (aspartic and glutamic acid) were exchanged by positively charged amino acids (lysine and arginine) and *vice versa* to create "superpositive" and "supernegative" variants, respectively (Figure 2).

With this strategy, the net charge density of a superfolder variant of green fluorescent protein (sfGFP) was tuned between -0.12 and +0.19 (as shown in Table 3). These supercharged GFPs retained their fluorescence and exhibited circular dichroism spectra similar to stGFP, indicating that proper folding of the protein was not impaired by the mutations that had been introduced. More interestingly, GFP(+36) and GFP(-30) showed extraordinary aggregation resistance: both variants remained soluble when heated to 100 °C and recovered significant fluorescence upon cooling.[69] Liu and co-workers also demonstrated that a

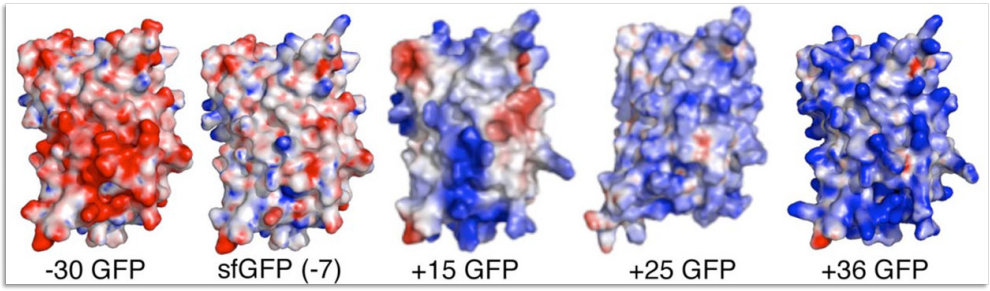

Figure 2. Positively (blue) and negatively (red) supercharged GFP variants created by genetic engineering from a superfolder variant (sfGFP). Reproduced from ref.[70].

negatively supercharged variant of glutathione-S-transferase (GST) exhibited catalytic activity similar to wild-type GST (wtGST) and retained 40% of its catalytic activity after heating to 100 °C and subsequent cooling, while wtGST was irreversibly aggregated and its activity reduced to zero.[69] Like cBSA, a superpositively charged GFP variant carrying 36 positive charges (+36GFP) readily penetrated several mammalian cell types by an endocytotic pathway.[70] Cationized GFP was therefore expected to likewise complex with nucleic acids and to mediate their transport into mammalian cells. +36GFP formed complexes with and delivered silencing RNA (siRNA) into various cell lines, causing gene silencing.[70] Moreover, fusion proteins containing +36 GFP rapidly and potently penetrated mammalian cells *in vitro* without toxicity and were able to access the cytosol.[71] A +36 GFP fusion to Cre recombinase effected recombination in transiently transfected HeLa cells *in vitro* and in mouse retinal cells *in vivo*.[71]

Considering that thermostability of proteins from thermophilic and hyperthermophilic organisms is in part conveyed by salt bridges between charged amino acid residues on the protein surface, it is somewhat surprising that thermoresistance can be achieved by exhaustive supercharging of folded proteins.[72-75] Reversing solvent-exposed charges that are employed in electrostatic interactions leads to a decrease in thermostability due to intramolecular repulsion, which might not be balanced by the gain in thermostability. This might explain why some designs for supercharged variants were not functional or failed to express.[69] Elimination of favorable interactions or introduction of unfavorable interactions might also be the reason why post-translational, chemical modification results in increased aggregation in some cases. Based on these considerations, Miklos et al.

Table 3. Genetically engineered, supercharged proteins

	Protein Name	NCD*	length (#AA)	# posAA	# negAA	net charge
1	-30GFP	-0.12	248	19	49	-7
2	-25GFP	-0.10	248	21	46	-30
3	sfGFP	-0.03	248	27	34	-25
4	+36GFP	+0.15	248	56	20	+36
5	+48GFP	+0.19	248	63	15	+48
6	scFv anti-MS3	+0.02	233	24	19	+5
7	scFv anti-MS3 (K-pos-1)	+0.06	233	32	19	+13
8	scFv anti-MS3 (K-pos-2)	+0.07	233	35	19	+16
9	scFv anti-MS3 (K-pos-3)	+0.09	233	38	18	+20
10	wild type caveolin (IMD$^{\#}$)	0	33	0	0	0
11	caveolin selectant 11 (IMD$^{\#}$)	+0.03	33	5	4	1

*NCD = net charge density. $^{\#}$NCD was only calculated for the intra-membrane domain (IMD), as it was not clear from the given information in ref. [77] which caveolin variant was used.

used a structure-based computational design to create thermoresistant single-chain F_v antibody fragments (scF_vs).[76] In this approach, the energetic consequences of each amino acid substitution were considered for the design of positively and negatively supercharged scF_v variants. Of all expressed and purified variants, three positive variants with net charge densities between +0.06 and +0.09 displayed strong binding to the antigen and at the same time moderate to high thermal stability (Table 3). For comparison, a series of supercharged scF_v variants was created based on the approach of Liu's group, which all failed to be thermoresistant.[76] These results demonstrate that the supercharging approach yields functional variants only of certain proteins, whereas for other proteins the more elaborate rational design approach has to be applied.

An alternative to rational design is the creation of a library of supercharged variants combined with simultaneous screening for the desired property and for function preservation. The group of Weiss used this alternative strategy for the solubilization of the membrane protein caveolin.[77] In order to fully elucidate structure, function and interacting factors of a membrane protein, relatively large amounts of the respective protein are required. To this end, heterologous production

is a highly suitable method. However, membrane proteins either contain one to several hydrophobic transmembrane segments or amphiphatic β-strands. Since their hydrophobicity renders them prone to aggregation in aqueous environment they cannot be overexpressed in the cytoplasm, but have to be targeted to the membrane. Consequently, protein yields are low. To overcome this bottleneck in membrane protein research, a two-step phage display assay was developed, as it allows for screening of a large library of variants: in the anti-selection step hydrophobic variants were removed by binding to resin, whereas in the positive selection step functional, folded variants which were bound to the caveolin ligand HIV gp41 (cavin) were selected (Figure 3).

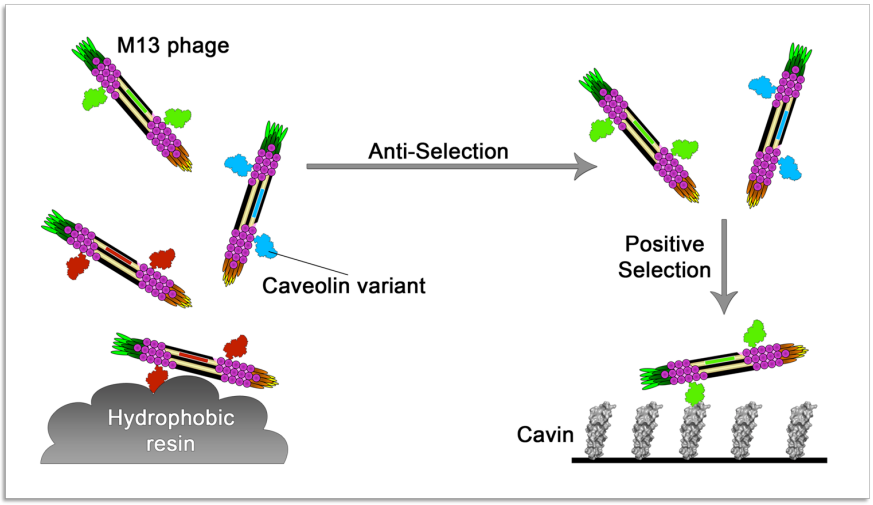

Figure 3. A two-step phage display for the selection of a functional, soluble, full-length variant of the membrane protein caveolin. A single phage contains the gene encoding for a protein variant and at the same time displays the protein on its surface. In this way, the genetic information is co-selected with the protein variant that carries the desired properties. Adapted from ref. [77].

By this method a functional, soluble, full-length caveolin variant was selected from the library (Table 3). This variant was successfully objected to direct interaction studies of caveolin and its ligand cavin.[77]

It can be concluded that rational design considering intramolecular interactions or a concept with direct selection for desired property as well as function is preferable to random supercharging of solvent-exposed amino acids.

2.3 Supercharging by means of a highly charged peptide tag

All methods discussed so far rely on modification of the protein itself. Alternatively, a highly charged tag can be attached to a protein of interest in order to increase its overall charge. This method bears the advantage that the protein itself remains unchanged and therefore obviates the need for rational design or extensive screening for functional variants. Negatively supercharged tags are used to significantly enhance the stability of proteins in solution.[78-80] Examples are the protein G B1 domain (Table 4, entry 1), the protein B domain of bacteriophage T7 (T7B; entry 2) and its more acidic variant T7B9 (entry 3) as well as the acidic tail of synuclein (ATS; entry 4).[78-80] Fusion of these anionic peptides to aggregation-prone proteins prevented their aggregation during overexpression and provided sufficient solubility for structural and biological investigations.[78,79,81] Moreover, highly charged peptide extensions can significantly enhance stability and solubility of protein formulations for therapeutic purposes. Introduction of an acidic peptide derived from the C-terminal tail of synuclein (ATS) into three different therapeutic proteins (human growth hormone, granulocyte colony-stimulating factor and human leptin) resulted in higher stability against heat, agitation and freeze/thawing cycles *in vitro,* as well as improved pharmacokinetics *in vivo* (Table 4, entry 4).[80] Interestingly, anionic stabilizing tags vary considerably in their net charge density (from -0.07 to -0.41), but only moderately in their number of negative charges (from 9 to 14), indicating that their stabilizing effect is more dependent on the number of charges than on the charge density.

Positively supercharged (poly)peptides mainly belong to the group of cell-penetrating peptides (CPPs).[82] CPPs like oligo-arginine and HIV-TAT can trigger the transport of fusion proteins across membrane barriers and deliver them to the cytoplasm or other cellular compartments (Table 4, entries 5 and 6).[83,84] Recently it was shown that also naturally supercharged, cationic human protein fragments are able to stimulate uptake of proteins into mammalian cells *in vitro* and *in vivo* (Table 4, entries 7-9).[85] These human protein fragments have a much lower net charge density (0.2 vs. 0.5 to 1) than the very short peptides R9 and HIV-TAT, but comparable to the superpositive +36GFP (NCD = 0.15; entry 11). Despite their variation in length (from 9 to 248 amino acids), all these (poly)peptides were shown to penetrate cells and to deliver fusion proteins to the cytoplasm, indicating that size alone is not a critical parameter for uptake.[70,71,83-85]

Table 4. Supercharged protein tags for solubilization or uptake of proteins

	Protein Name	NCD*	length (#AA)	# posAA	# negAA	net charge
1	B1 domain of protein G	-0.07	56	6	10	-4
2	T7B	-0.11	44	5	10	-5
3	T7B9	-0.25	44	3	14	-11
4	ATS	-0.41	22	0	9	-9
5	oligo-arginine (R9)	+1.00	9	9	0	+9
6	HIV-TAT protein	+0.54	13	7	0	+7
7	ß-defensin 3 (fragment)	+0.24	45	13	2	+11
8	c-Jun bZIP domain	+0.21	62	19	6	+13
9	histone methyl transferase (fragment)	+0.21	72	18	3	+15
10	+36GFP	+0.15	248	56	20	+36

*NCD = net charge density

3. ELASTIN AND ELASTIN-LIKE POLYPEPTIDES

3.1 Sequences and properties of elastin-like polypeptides

In the first parts of this chapter it was discussed how proteins can be supercharged by post-translational, chemical modification or genetic engineering. Furthermore, we elaborated on highly charged proteins and their role in nature, with a focus on intrinsically disordered proteins. The last part of this chapter will focus on elastin-like polypeptides (ELPs), a class of intrinsically disordered proteins. Unlike most other disordered proteins they are not naturally occurring, but chemically synthesized or genetically engineered. Their sequences are based on the elastic parts of elastin, a component of the extracellular matrix in vertebrates.[86] The elastic parts contain repetitive sequences with repeats of four to six amino acids that are rich in valine (V), proline (P), glycine (G) and alanine (A).[87] ELPs that consist of VPGG, VPGVG or VAPGVG repeats are the most intensely studied.[88] Poly(VPGVG) or recombinant $(VPGVG)_n$ is considered the model sequence for ELPs.[89] Pioneers in the synthesis of ELPs were Urry and colleagues, who discovered that ELPs exhibit a characteristic temperature-dependent transition behavior. By heating ELPs in aqueous solution above their lower critical solution temperature (LCST), their conformation changes from a soluble random-coil to an insoluble ß-spiral, which is formed by regularly

recurring type II ß-turns.[90-94] Urry and co-workers studied the influence of different guest amino acids in ELPs that are comprised of the pentapeptide sequence VPGXG. They observed that the fourth position (X) can be exchanged by any naturally occurring amino acid except proline. The LCSTs of the resulting ELPs reflected the hydrophobicity scale of the amino acids, such that the LCST dropped with increasing hydrophobicity of the guest residue.[95,96] The first ELPs were chemically synthesized, i.e. with limited control over chain length and composition.[92,97] About ten years later the emergence of genetic engineering techniques allowed recombinant production of ELPs with precise length and composition.[98-102] However, the first cloning strategies created sets of *ELP* genes with a statistical length distribution and thus no guarantee for a defined gene length. Therefore Chilkoti and co-workers developed the "recursive directional ligation" method, which allows controlled, stepwise oligomerization of a monomeric *ELP* gene containing a defined number of repeats (Figure 4).

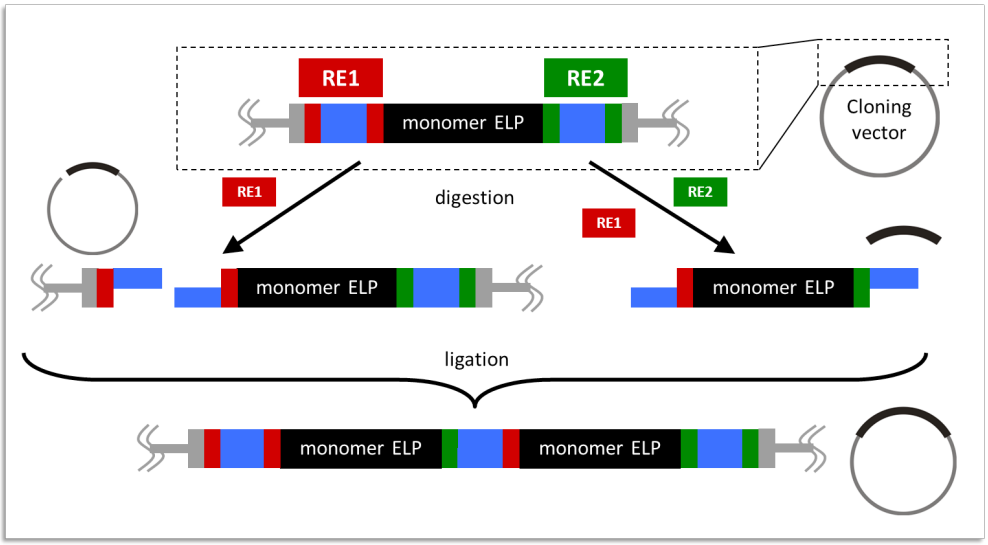

Figure 4. Recursive directional ligation for the oligomerization of elastin-like polypeptides. RE: restriction enzyme. Adapted from ref. [103].

Two monomer genes are ligated to create a dimeric gene. Due to the choice of the restriction sites flanking the gene monomer, the restriction site at the seam of the monomers is erased during ligation, whereas the restrictions sites at the termini are preserved. This allows for the dimer to be used in another round of restriction and

ligation, leading to a tetramer, which in turn can go through another round. By varying the monomer length and by repeating multiple rounds of restriction and ligation, oligomers of theoretically any desired length can be created in a controlled fashion.

Besides precise control over length and composition, genetic engineering also opened up the possibility to create fusion variants of ELPs and proteins with biological activity, which substantially increased the applicability of ELPs in biotechnology and medicine.[104] Schemes for the purification of proteins and DNA on the basis of ELPs were developed and optimized by several groups.[104-109] Furthermore, ELPs were employed for targeted delivery of therapeutic peptides,[110-112] small molecule drugs, [113-116] proteins,[117] and DNA[118]. Finally, ELPs might find applications as hydrogels for tissue engineering[119-123] and controlled release [124] of therapeutics.

3.2 Ionic ELPs

As mentioned before, the fourth position of the pentapeptide repeat in ELPs can be exchanged by any amino acid except proline. This opens up possibilities to create variations of ELPs with properties tailored for desired applications. It was already pointed out that the guest amino acids greatly influence the hydrophobicity of the polypeptide chain. By carefully choosing the guest amino acids, it is possible to fine-tune the LCST of ELPs in a range between -90 and +250 °C.[95] The greatest increase in T_t is achieved by introducing positively or negatively charged amino acids along the polypeptide chain, i.e. by creating ionic ELPs.[97,125-128] For an ELP of 81 kDa with lysine as a guest residue in every fifth repeat, for example, T_t is above 100 °C in a buffered solution of pH 7.[127] Moreover, protonation or deprotonation of the functional group determines whether a residue is charged or not. Thus, charged residues add pH responsiveness to ELPs. For the aforementioned cationic ELP, T_t drops from above 100 °C at pH 7 to 28 °C in basic conditions (0.1 N NaOH), as the ε-amine groups of the lysine residues become deprotonated, i.e. non-charged.[127] Furthermore, charged residues are able to electrostatically interact with counterions in solution, thereby reducing repelling forces between charges and drastically decreasing T_t. As a consequence, ionic ELPs are more sensitive to changes in salinity than ELPs with only aliphatic amino acids.[125-127] An overview of T_t for different ELP constructs at various conditions is given in Table 5. Taken together, by introducing charged amino acids, smart ELPs can be generated that are highly responsive towards changes in both pH and salinity.

Table 5. Transition temperatures (T_t) of cationic and anionic ELP under various conditions.

ELP	MW [kDa]	T_t [°C]			NCD*	in ref.
		basic/acidic	buffer	salt		
cationic						
poly[VPGφG] (φ=V, ca. 86%; φ=K, ca. 14%)	n.d.	n.d.	n.d.	n.d.	0.03	[97]
$[(VPGVG)_4\ (VPGKG)]_{39}$	81.1	28 [a]	>100 [b]	50 [c]	0.050	[127]
$[VPGKG(VPGVG)_6]_n$, (n = 8, 16, 32)	23.9, 47.1, 93.4	-	60, 45, 39 [d]	30, 22, 19 [e]	0.033	[126]
$[VPGKG(VPGVG)_{16}]_n$ (n = 8, 16, 32)	21.7, 42.7, 84.8	-	45, 34, 30 [d]	26, 19, 15 [e]	0.012	[126]
$[VPGKG(VPGVG)_2VPGFG]_n$ (n = 4, 8, 16, 32)	7.7, 14.6, 28.3, 55.7	-, -, -, 20 [f]	-, -, 61, 43 [d]	-, -, 17, 11 [e]	0.050	[125]
$[VPGKG(VPGVG)_7VPGFG]_n$ (n = 2, 4, 8, 16)	8.4, 15.9, 31.0, 61.1	-, -, -, 15 [f]	-, 48, 35, 26 [d]	-, 25, 16, 11 [e]	0.022	[125]
anionic						
poly[VPGφG] (φ=V, ca. 80%; φ=G, ca. 20%)	n.d.	n.d.	n.d.	n.d.	0.04	[97]
poly[IPGφG] (φ=V or E; various ratios)	n.d.	n.d.	n.d.	n.d.	0.012 - 0.2	[129]
poly[IPGφG] (φ=V or D; various ratios)	n.d.	n.d.	n.d.	n.d.	0.012 - 0.2	[130]
$[(VPGVG)_2(VPGEG)(VPGVG)_2]_n$ (n = 5, 9, 15, 30, 45)	10.4, 18.7, 31.2, 62.3, 93.5 [g]	31.5, 25.5, 23, 21, 20.5 [h]	n.d.	n.d.	0.040	[128]

*NCD = net charge density. a) 0.1 M NaOH; b) 50 mM TrisHCl, pH 7.0; c) 150 mM NaCl (, 50 mM TrisHCl, pH 7.0); d) PBS; e) PBS, 1M NaCl; f) 20 mM phosphate buffer, pH 12; g) calculated; h) phosphate buffer (pH 2.5)

The outstanding properties of these materials promoted their application in biotechnology and biomedicine. The stronger salt dependency of the cationic ELPs compared to purely aliphatic ELPs was exploited for improved purification of recombinant proteins.[131] Furthermore, introduction of charged amino acids into ELP sequences modifies their response to hydrophobic and hydrophilic surfaces, which was exploited for the formation of regularly shaped and equally distributed nanopores[132] and the fabrication of nanosized gold crystals as stimuli-responsive sensors and detectors in biological systems.[133] Next to their responsiveness, the precise incorporation of ionic guest residues in terms of their position, frequency and nature provides outstanding possibilities to crosslink or anchor functional moieties

to the polymer backbone.[97,115,127] Due to their sequence similarity to human elastin, hydrogels from ELPs are promising candidates as matrices for tissue engineering *in vitro*. Cross-linking leads to stiffening of ELP hydrogels and resistance to harsher conditions and was therefore applied to gels which were tailored for *in-situ* gelation or as matrices for tissue engineering *in vitro*.[125,126,134-137] Moreover, recombinant ELPs have the advantage that functional domains can be incorporated directly into the polypeptide sequence by genetic engineering. In this way, cell attachment sequences or protease target sequences for facilitated bioprocessability can be inserted without the need of any further coupling step.[138]

As shown so far, most applications exploit the increased pH and salt sensitivity upon introduction of ionic residues into ELPs or use these residues as anchoring moieties for chemical reactions. Few publications on ionic ELPs actually take advantage of electrostatic interactions for the (self-)assembly of supramolecular structures. A widely known technique is the so-called layer-by-layer (LbL) technology: Oppositely charged polyelectrolytes are consecutively deposited on a flat or spherical surface to build up multi-layer coatings.[139] The group of Rodríguez-Cabello used a peptide sequence rich in aspartic acid, glutamic acid and arginine flanked by cationic ELP sequences for the build-up of multiple layers with chitosan, a polysaccharide composed of β-(1-4)-linked D-glucosamine and N-acetyl-D-glucosamine.[140] Due to the fact that chitosan is positively charged at a pH below 6, the authors concluded that negatively charged sequences were employed for the electrostatic interaction between layers.[140] The same concept was used for thin coatings of cationic ELPs on chitosan. The ELP sequences flanked a short RGD sequence for enhanced cell adhesion and proliferation.[141] However, a similar sequence with purely aliphatic ELPs flanking RGD and a triple-lysine tag at the N-terminus also absorbed with chitosan in a sequential fashion. This indicates that electrostatic interactions did not seem to play a crucial role in the layer assembly of this system.[142]

To the best of our knowledge, there is only one case reported in literature apart from the work described in this thesis where electrostatic interactions were the primary force for supramolecular assembly of an ionic ELP sequence and an oppositely charged polymer or of two oppositely charged ELP sequences. For deposition on a flat surface, Golonka *et al*. used cationic and anionic ELPs, where every fifth pentapeptide contained a charged residue (either lysine or glutamic acid).[143] Due to the fact that the guest residue in all other repeats was isoleucine, which is more hydrophobic than valine, the deposited film still showed temperature-responsive collapsing and swelling upon temperature cycling between four and 40 °C. In the collapsed state the films were shown to be stable upon prolonged (72 h) incubation at close-to physiological conditions (0.1 M NaCl and 37 °C).[143] This example demonstrates that

ionic ELPs are versatile protein polyelectrolytes that might serve as building blocks in a variety of electrostatically assembled structures.

4. SUMMARY

In nature, highly charged proteins interact with a variety of biomacromolecules and structures like membranes via electrostatic forces. They are involved in DNA condensation, gene expression modulation and protein translation, or exhibit antibacterial activities by interacting with bacterial cell membranes. Furthermore, they are often resilient to aggregation at higher temperatures due to charge repulsion. By increasing the net charge of moderately charged proteins, their aggregation behavior can be tuned and their stability towards elevated temperatures and denaturants can be increased. Moreover, cationized proteins were shown to form complexes with negatively charged polynucleotides (DNA and RNA) and liposomes. They interact with bacterial and mammalian cell membranes and efficiently induce the uptake of nucleic acids and fusion proteins by mammalian cells *in vitro* and *in vivo*. Post-translational, chemical modification of surface-exposed amino acids represents a quick and simple method to increase a protein's net charge. Examples of chemically supercharged proteins exhibiting higher stability towards denaturation are reported in literature and were discussed in this chapter. However, chemical modification can also lead to loss of structural integrity and/or function. Furthermore, its heterogeneous nature makes elaborate reaction and purification schemes necessary to obtain well-characterized samples with narrow net charge distribution. Therefore, chemical modification is advantageous in cases where the protein of interest is directly extracted from its natural source and where an exactly defined product is not required. In contrast to chemical modification, genetic engineering allows for precise control over the amount and positions of modified residues on the protein scaffold. Exhaustive supercharging of solvent-exposed amino acids yielded functional, highly thermostable variants of different proteins. However, this method might also destroy stabilizing salt bridges and result in loss of stability and function. Depending on the protein, supercharging requires rational design, taking into account the microenvironment of surface charges and their interactions, or simultaneous screening for functionality and increase in net charge. Alternatively, the net charge of a protein can be increased by fusion to a supercharged tag. In the case of elastin-like polypeptides, elaborate rational design or screening is not required for supercharging, as these proteins are naturally unfolded and their repetitive sequence allows for the incorporation of charged amino acids at a high density.

5. ACKNOWLEDGEMENTS

The authors thank Ioannis Giotis for valuable assistance with the databank search. The help of Alessio Marcozzi with the graphical presentations is gratefully acknowledged.

6. MOTIVATION AND THESIS OVERVIEW

The goal of the work described in this thesis was to fabricate supercharged, unfolded proteins of varying lengths and unprecedented charge density and to evaluate their applicability in biomedicine and nanotechnology. As a starting point for the design of these proteins elastin-like polypeptides (ELPs) were chosen. ELPs are tunable, mono-disperse materials with outstanding properties (in particular biocompatibility and bioprocessability) for applications in biotechnology and medicine such as tissue engineering, scaffolds for *in-situ* repair and drug delivery systems. Ionic ELPs were designed by introducing charged amino acids as guest residues along the polymer backbone to further enhance the tuneability of the temperature-dependent ELP response to salinity, pH change and surface hydrophobicity. However, only few charged residues were incorporated into the polypeptide chain. We decided to further explore the applicability of ELPs by exchanging the aliphatic amino acids at the fourth position with the charged amino acids lysine or glutamic acid in nine out of ten pentapeptide repeats, thereby creating cationic and anionic supercharged variants of much higher charge density than reported before. **Chapter 2** describes the design and expression of these supercharged, unfolded polypeptides (SUPs). The protein polyelectrolytes were monodisperse and had a precisely defined amino acid composition, sequence and stereochemistry. Furthermore, cytotoxicity assays revealed that positively charged SUPs are considerably less cytotoxic than cationic polyelectrolytes commonly used for biomedical applications. Considering their polyelectrolyte nature we assumed that SUPs might be transferred into electrostatically assembled superstructures. It is well known that electrostatic assemblies can be fabricated from oppositely charged polyelectrolytes using the layer-by-layer technique. This technique was employed to create capsules composed of SUPs. These capsules were stable after core removal, showing that the charge density of the SUPs was sufficient to maintain capsule wall integrity.

Encouraged by these findings, we decided to assess the interaction of cationic SUPs with naturally occurring polyelectrolyte films and investigated their effect on the properties of these films. Salivary conditioning films (SCFs) were chosen as an example because of their biomedical relevance. Highly glycosylated, negatively

charged proteins, so called mucins, are mainly responsible for the lubricating properties of SCF in the mouth. To provide efficient biolubrication, these mucins have to be constantly replenished by saliva flow. In patients with dry-mouth disease saliva flow is dramatically decreased, leading to increased friction between surfaces and pain during speaking and mastication. The question arose whether cationic SUPs (CSUPs) are able to electrostatically interact with the negatively charged mucins, thereby stabilizing the SCF. *In-vitro* experiments demonstrated that cationic SUPs indeed interact with SCF, as described in detail in **chapter 3**. This interaction resulted in increased rigidity of the film and consequently in lower friction forces. However, efficient biolubrication is not only dependent on film rigidity; structural integrity at higher normal friction forces has to be maintained as well. It was observed that structural integrity is strongly dependent on the length of the CSUP, as only SCF treated with a high molecular weight CSUP variant maintained integrity, whereas untreated film and SCF treated with a shorter variant failed at higher normal forces. Concluding, it was shown in **chapter 3** that treatment of SCF with the long CSUP variant can increase its resistance against interfacial shear stress and damage. As an additive to mouth sprays that are routinely prescribed for the treatment of dry-mouth disease, CSUPs might greatly improve the duration of effect and substantially reduce dryness perception.

In addition to their low toxicity, SUPs surpass other polyelectrolytes in regard to functionalization. Genetic engineering provides the possibility to fuse SUPs to a protein carrying a (biological) function, thereby obviating the need of an extra conjugation step after production. As a proof-of principle, SUPs were designed as fusion proteins with green fluorescent protein (GFP). **Chapter 4** describes the successful expression and purification of GFP-SUP fusion variants carrying between -144 and +72 charges in the SUP part. The supercharged tag can be employed to equip electrostatic assemblies with a function, in this case fluorescence. Capsules were prepared according to procedures described in chapter 2, but this time one layer was composed of GFP fused to a SUP with 72 positive charges. Due to the intrinsic fluorescence of GFP, uptake of the capsules by cells and their intracellular fate could be followed by fluorescence microscopy. Applying this principle, other functions like enzymatic activity or ligands for targeted delivery can be introduced to capsules, complex coacervate micelles and other superstructures.

Supercharged protein tags can not only be exploited for functionalization of electrostatically assembled structures; they might also greatly enhance recognition of proteins in detectors that rely on changes in the electric field. In **chapter 5** cationic and anionic GFP-SUPs with different lengths of the ELP block, i.e. various amounts of charges, were compared regarding their performance in devices for protein detection

based on nanowire field-effect transistors. It was found that the response was clearly dependent on the sort of charge. Binding of cationic GFP-SUPs to the immobilized receptor on the nanowire surface resulted in a conductivity decrease, whereas anionic GFP-SUPs increased conductivity. Already short SUP tags with nine positive or negative charges were sufficient to induce a change in nanowire conductivity upon binding of the GFP part, whereas binding of GFP without a charged tag could not elicit a signal. In general, cationic SUP tags performed better than anionic tags. Further research is required to determine the optimum tag length, but the preliminary results confirm that SUP tags indeed enable recognition of GFP in nanowire field-effect transistors.

7. REFERENCES

[1] F. Dong, H. Zhou, *Proteins.* **2006**, *65*, 87-102.

[2] D. Morikis, J. Lambris, *J.Immunol.* **2004**, *172*, 7537-7547.

[3] A. S. Cheung, C. A. Kieslich, J. Yang, D. Morikis, *Biopolymers.* **2010**, *93*, 509-519.

[4] J. Gruber, A. Zawaira, R. Saunders, C. P. Barrett, M. E. M. Noble, *Acta Crystallogr.Sect.D-Biol. Crystallogr.* **2007**, *63*, 50-57.

[5] P. L. Privalov, A. I. Dragan, C. Crane-Robinson, *Nucleic Acids Res.* **2011**, *39*, 2483-2491.

[6] A. B. Kolomeisky, *Phys.Chem.Chem.Phys.* **2011**, *13*, 2088-2095.

[7] N. Korolev, O. V. Vorontsova, L. Nordenskiold, *Prog.Biophys.Mol.Biol.* **2007**, *95*, 23-49.

[8] J. Iwakiri, H. Tateishi, A. Chakraborty, P. Patil, N. Kenmochi, *Nucleic Acids Res.* **2012**, *40*, 3299-3306.

[9] M. Doetsch, R. Schroeder, B. Fuertig, *Febs J.* **2011**, *278*, 1634-1642.

[10] O. Vogler, J. M. Barcelo, C. Ribas, P. V. Escriba, *Biochim.Biophys.Acta-Biomembr.* **2008**, *1778*, 1640-1652.

[11] J. Li, Z. M. James, X. Dong, C. B. Karim, D. D. Thomas, *J.Mol.Biol.* **2012**, *418*, 379-389.

[12] J. Saarikangas, H. Zhao, A. Pykalainen, P. Laurinmaki, P. K. Mattila, P. K. J. Kinnunen, S. J. Butcher, P. Lappalainen, *Curr.Biol.* **2009**, *19*, 95-107.

[13] J. Boggs, G. Rangaraj, C. Hill, I. Bates, Y. Heng, G. Harauz, *Biochemistry (N.Y.).* **2005**, *44*, 3524-3534.

[14] J. Zhao, J. Rowe, J. Franzen, C. He, S. Franzen, *Biochem.Biophys.Res.Commun.* **2012**, *420*, 733-737.

[15] M. M. Malabanan, T. L. Amyes, J. P. Richard, *Curr.Opin.Struct.Biol.* **2010**, *20*, 702-710.

[16] J. Tejero, L. Hannibal, A. Mustovich, D. J. Stuehr, *J.Biol.Chem.* **2010***, 285*, 27232-27240.

[17] N. Wayne, D. N. Bolon, *J.Mol.Biol.* **2010***, 401*, 931-939.

[18] UniProt Consortium, *Nucleic Acids Res.* **2012***, 40*, D71-D75.

[19] T. D. Pollard, W. C. Earnshaw, "Chapter 13: DNA packaging in chromatin and chromosomes", in: *Cell Biology*, 2nd edition, Elsevier, 2004, p. 209-230.

[20] S. K. Kota, R. Feil, *Developmental Cell.* **2010***, 19*, 675-686.

[21] J. Govin, C. Caron, C. Lestrat, S. Rousseaux, S. Khochbin, *European Journal of Biochemistry.* **2004***, 271*, 3459-3469.

[22] D. Park, J. Y. Leem, E. Y. Suh, J. H. Hur, H. Oh, H. Park, *Arch.Insect Biochem.Physiol.* **2007***, 66*, 204-213.

[23] C. B. Park, J. H. Lee, I. Y. Park, M. S. Kim, S. C. Kim, *FEBS Lett.* **1997***, 411*, 173-178.

[24] L. EhretSabatier, D. Loew, M. Goyffon, P. Fehlbaum, J. A. Hoffmann, A. vanDorsselaer, P. Bulet, *J.Biol.Chem.* **1996***, 271*, 29537-29544.

[25] M. Zasloff, *Nature.* **2002***, 415*, 389-395.

[26] P. Bulet, R. Stocklin, L. Menin, *Immunol.Rev.* **2004***, 198*, 169-184.

[27] C. Hetru, L. Letellier, Z. Oren, J. Hoffmann, Y. Shai, *Biochem.J.* **2000***, 345*, 653-664.

[28] N. Mandard, H. Labbe, P. Da Silva, C. Hetru, C. Landon, F. Vovelle, *Comptes Rendus De L Academie Des Sciences Serie Ii Fascicule C-Chimie.* **2001***, 4*, 735-738.

[29] K. Matsuzaki, *Biochim.Biophys.Acta-Biomembr.* **1999***, 1462*, 1-10.

[30] L. T. Nguyen, E. F. Haney, H. J. Vogel, *Trends Biotechnol.* **2011***, 29*, 464-472.

[31] R. E. W. Hancock, H. Sahl, *Nat.Biotechnol.* **2006***, 24*, 1551-1557.

[32] K. Vareli, M. Frangou-Lazaridis, I. van der Kraan, O. Tsolas, R. van Driel, *Exp.Cell Res.* **2000***, 257*, 152-161.

[33] K. Letsas, M. Frangou-Lazaridis, *Neoplasma.* **2006***, 53*, 92-96.

[34] G. Martic, Z. Karetsou, K. Kefala, A. S. Politou, C. R. Clapier, T. Straub, T. Papamarcaki, *J.Biol. Chem.* **2005***, 280*, 16143-16150.

[35] E. Luk, N. Vu, K. Patteson, G. Mizuguchi, W. Wu, A. Ranjan, J. Backus, S. Sen, M. Lewis, Y. Bai, C. Wu, *Mol.Cell.* **2007***, 25*, 357-368.

[36] M. Hondele, A. G. Ladurner, *Curr:Opin.Struct.Biol.* **2011***, 21*, 698-708.

[37] A. L. Fink, *Curr. Opin. Struct. Biol.* **2005***, 15*, 35-41.

[38] V. N. Uversky, J. R. Gillespie, A. L. Fink, *Proteins.* **2000***, 41*, 415-427.

[39] V. N. Uversky, *Journal of biomedicine & biotechnology.* **2010***, 2010*, 568068.

[40] M. Sickmeier, J. A. Hamilton, T. LeGall, V. Vacic, M. S. Cortese, A. Tantos, B. Szabo, P. Tompa,

J. Chen, V. N. Uversky, Z. Obradovic, A. K. Dunker, *Nucleic Acids Res.* **2007***, 35*, D786-D793.

[41] S. K. Straus, R. E. W. Hancock, *Biochimica Et Biophysica Acta-Biomembranes.* **2006***, 1758*, 1215-1223.

[42] H. J. Dyson, P. E. Wright, *Nature Reviews Molecular Cell Biology.* **2005***, 6*, 197-208.

[43] F. Chiti, M. Calamai, N. Taddei, M. Stefani, G. Ramponi, C. Dobson, *Proc.Natl.Acad.Sci.U.S.A.* **2002***, 99*, 16419-16426.

[44] O. Kirk, T. V. Borchert, C. C. Fuglsang, *Curr.Opin.Biotechnol.* **2002***, 13*, 345-351.

[45] U. T. Bornscheuer, G. W. Huisman, R. J. Kazlauskas, S. Lutz, J. C. Moore, K. Robins, *Nature.* **2012***, 485*, 185-194.

[46] M. Klapper, Klotz IM, *Methods in Enzymology.* **1972***, 25*, 531-536.

[47] I. M. Klotz, *Methods in Enzymology.* **1967***, 11*, 576-580.

[48] A. D. Gounaris, G. E. Perlmann, *J.Biol.Chem.* **1967***, 242*, 2739-&.

[49] D. G. Hoare, D. E. Koshland, *J.Biol.Chem.* **1967***, 242*, 2447-&.

[50] D. Danon, E. Skutelsky, Y. Marikovsky, L. Goldstein, *J.Ultrastruct.Res.* **1972***, 38*, 500-&.

[51] J. Schalkwijk, W. B. Vandenberg, L. B. A. Vandeputte, L. A. B. Joosten, L. Vandenbersselaar, *J.Clin.Invest.* **1985***, 76*, 198-205.

[52] L. Gruener, M. Ismond, *Food Chem.* **1997***, 60*, 357-363.

[53] A. Achouri, W. Zhang, *Food Res.Int.* **2001***, 34*, 507-514.

[54] M. Hollecker, T. E. Creighton, *Biochim.Biophys.Acta.* **1982***, 701*, 395-404.

[55] B. F. Shaw, H. Arthanari, M. Narovlyansky, A. Durazo, D. P. Frueh, M. P. Pollastri, A. Lee, B. Bilgicer, S. P. Gygi, G. Wagner, G. M. Whitesides, *J.Am.Chem.Soc.* **2010***, 132*, 17411-17425.

[56] B. F. Shaw, G. F. Schneider, B. Bilgicer, G. K. Kaufman, J. M. Neveu, W. S. Lane, J. P. Whitelegge, G. M. Whitesides, *Protein Sci.* **2008***, 17*, 1446-1455.

[57] I. Gitlin, K. L. Gudiksen, G. M. Whitesides, *ChemBioChem.* **2006***, 7*, 1241-1250.

[58] H. A. Kosters, K. Broersen, J. de Groot, J. W. F. A. Simons, P. Wierenga, H. H. J. de Jongh, *Biotechnol.Bioeng.* **2003***, 84*, 61-70.

[59] K. Broersen, M. Weijers, J. de Groot, R. J. Hamer, H. H. J. de Jongh, *Biomacromolecules.* **2007***, 8*, 1648-1656.

[60] M. Alcalde, F. J. Plou, M. T. Martin, I. Valdes, E. Mendez, A. Ballesteros, *J.Biotechnol.* **2001***, 86*, 71-80.

[61] H. N. Ong, B. Arumugam, S. Tayyab, *J.Biochem.* **2009***, 146*, 895-904.

[62] A. K. Kumargai, J. B. Eisenberg, W. M. Partridge, *J.Biol.Chem.* **1987***, 262*, 15214-15219.

[63] M. Thole, S. Nobmann, J. Huwyler, A. Bartmann, G. Fricker, *J.Drug Target.* **2002***, 10*, 337-344.

[64] K. Eisele, R. A. Gropeanu, C. M. Zehendner, A. Rouhanipour, A. Ramanathan, G. Mihov, K. Koynov, C. R. W. Kuhlmann, S. G. Vasudevan, H. J. Luhmann, T. Weil, *Biomaterials.* **2010***, 31*, 8789-8801.

[65] L. Zoephel, K. Eisele, R. Gropeanu, A. Rouhanipour, K. Koynov, I. Lieberwirth, K. Muellen, T. Weil, *Macromolecular Chemistry and Physics.* **2010***, 211*, 146-153.

[66] S. Ritz, K. Eisele, J. Dorn, Shaohua Ding, D. Vollmer, S. Puumltz, T. Weil, E. -. Sinner, *Biointerphases Journal.* **2010***, 5*.

[67] J. F. Ng, S. Jaenicke, K. Eisele, J. Dorn, T. Weil, *Biointerphases.* **2010***, 5*, FA41-FA47.

[68] J. F. Ng, T. Weil, S. Jaenicke, *J.Biomed.Mater.Res.Part B.* **2011***, 99B*, 282-290.

[69] M. S. Lawrence, K. J. Phillips, D. R. Liu, *J. Am. Chem. Soc.* **2007***, 129*, 10110-+.

[70] B. R. McNaughton, J. J. Cronican, D. B. Thompson, D. R. Liu, *Proc.Natl.Acad.Sci.U.S.A.* **2009***, 106*, 6111-6116.

[71] J. J. Cronican, D. B. Thompson, K. T. Beier, B. R. McNaughton, C. L. Cepko, D. R. Liu, *Acs Chemical Biology.* **2010***, 5*, 747-752.

[72] K. Shiraki, S. Nishikori, S. Fujiwara, T. Imanaka, M. Takagi, *J.Biosci.Bioeng.* **2004***, 97*, 75-77.

[73] L. Xiao, B. Honig, *J.Mol.Biol.* **1999***, 289*, 1435-1444.

[74] G. I. Makhatadze, V. V. Loladze, D. N. Ermolenko, X. F. Chen, S. T. Thomas, *J.Mol.Biol.* **2003***, 327*, 1135-1148.

[75] A. Karshikoff, R. Ladenstein, *Trends Biochem.Sci.* **2001***, 26*, 550-556.

[76] A. E. Miklos, C. Kluwe, B. S. Der, S. Pai, A. Sircar, R. A. Hughes, M. Berrondo, J. Xu, V. Codrea, P. E. Buckley, A. M. Calm, H. S. Welsh, C. R. Warner, M. A. Zacharko, J. P. Carney, J. J. Gray, G. Georgiou, B. Kuhlman, A. D. Ellington, *Chem.Biol.* **2012***, 19*, 449-455.

[77] A. Hajduczki, S. Majumdar, M. Fricke, I. A. M. Brown, G. A. Weiss, *ACS Chem.Biol.* **2011***, 6*, 301-307.

[78] P. Zhou, A. Lugovskoy, G. Wagner, *J.Biomol.NMR.* **2001***, 20*, 11-14.

[79] Y. Zhang, J. Howitt, S. McCorkle, P. Lawrence, K. Springer, P. Freimuth, *Protein Expr.Purif.* **2004***, 36*, 207-216.

[80] E. Lee, Y. Kim, H. Lee, S. Park, H. Jung, J. Lee, Y. Ahn, J. Kim, *Pharm.Res.* **2005***, 22*, 1735-1746.

[81] Y. Cheng, D. Patel, *Biochem.Biophys.Res.Commun.* **2004***, 317*, 401-405.

[82] F. Heitz, M. C. Morris, G. Divita, *Br.J.Pharmacol.* **2009***, 157*, 195-206.

[83] H. Mitsui, T. Inozume, R. Kitamura, N. Shibagaki, S. Shimada, *J.Invest.Dermatol.* **2006***, 126*, 1804-1812.

[84] E. L. Snyder, S. F. Dowdy, *Expert opinion on drug delivery.* **2005***, 2*, 43-51.

[85] J. J. Cronican, K. T. Beier, T. N. Davis, J. Tseng, W. Li, D. B. Thompson, A. F. Shih, E. M. May, C.

L. Cepko, A. L. Kung, Q. Zhou, D. R. Liu, *Chem.Biol.* **2011**, *18*, 833-838.

[86] L. D. Muiznieks, A. S. Weiss, F. W. Keeley, *Biochem.Cell Biol.* **2010**, *88*, 239-250.

[87] J. Rosenbloom, W. R. Abrams, R. Mecham, *FASEB J.* **1993**, *7*, 1208-1218.

[88] A. S. Tatham, P. R. Shewry, *Trends Biochem.Sci.* **2000**, *25*, 567-571.

[89] A. Ribeiro, F. J. Arias, J. Reguera, M. Alonso, J. C. Rodriguez-Cabello, *Biophys.J.* **2009**, *97*, 312-320.

[90] D. W. Urry, M. M. Long, T. Ohnishi, M. Jacobs, *Biochem.Biophys.Res.Commun.* **1974**, *61*, 1427-1433.

[91] D. W. Urry, M. M. Long, B. A. Cox, T. Ohnishi, L. W. Mitchell, M. Jacobs, *Biochim.Biophys.Acta.* **1974**, *371*, 597-602.

[92] V. Renugopalakrishnan, D. W. Urry, *International Journal of Quantum Chemistry.* **1976**, 13-19.

[93] K. Okamoto, D. W. Urry, *Biopolymers.* **1976**, *15*, 2337-2351.

[94] D. URRY, *J.Protein Chem.* **1984**, *3*, 403-436.

[95] D. Urry, *J Phys Chem B.* **1997**, *101*, 11007-11028.

[96] D. Urry, *Chem.Phys.Lett.* **2004**, *399*, 177-183.

[97] D. W. Urry, K. Okamoto, R. D. Harris, C. F. Hendrix, M. M. Long, *Biochemistry (N.Y.).* **1976**, *15*, 4083-4089.

[98] D. T. McPherson, C. Morrow, D. S. Minehan, J. G. Wu, E. Hunter, D. W. Urry, *Biotechnol.Prog.* **1992**, *8*, 347-352.

[99] J. Kostal, A. Mulchandani, W. Chen, *Macromolecules.* **2001**, *34*, 2257-2261.

[100] J. Cappello, J. Crissman, M. Dorman, M. Mikolajczak, G. Textor, M. Marquet, F. Ferrari, *Biotechnol.Prog.* **1990**, *6*, 198-202.

[101] M. J. Fournier, H. S. Creel, M. T. Krejchi, T. L. Mason, D. A. Tirrell, K. P. McGrath, E. D. T. Atkins, *J.Bioact.Compatible Polym.* **1991**, *6*, 326-338.

[102] R. McMillan, T. Lee, V. Conticello, *Macromolecules.* **1999**, *32*, 3643-3648.

[103] D. E. Meyer, A. Chilkoti, *Biomacromolecules.* **2002**, *3*, 357-367.

[104] D. T. McPherson, J. Xu, D. W. Urry, *Protein Expr. Purif.* **1996**, *7*, 51-57.

[105] D. E. Meyer, A. Chilkoti, *Nat. Biotechnol.* **1999**, *17*, 1112-1115.

[106] M. Shimazu, A. Mulchandani, W. Chen, *Biotechnol. Bioeng.* **2003**, *81*, 74-79.

[107] K. Trabbic-Carlson, L. Liu, B. Kim, A. Chilkoti, *Protein Sci.* **2004**, *13*, 3274-3284.

[108] W. Y. Wu, C. Mee, F. Califano, R. Banki, D. W. Wood, *Nat. Protoc.* **2006**, *1*, 2257-2262.

[109] U. L. Lao, J. Kostal, A. Mulchandani, W. Chen, *Nat. Protoc.* **2007**, *2*, 1263-1268.

[110] I. Massodi, S. Moktan, A. Rawat, G. L. Bidwell III, D. Raucher, *International Journal of Cancer.*

2010, *126*, 533-544.

[111] G. L. Bidwell III, A. N. Davis, D. Raucher, *J.Controlled Release.* **2009**, *135*, 2-10.

[112] I. Massodi, E. Thomas, D. Raucher, *Molecules.* **2009**, *14*, 1999-2015.

[113] G. L. Bidwell III, A. N. Davis, I. Fokt, W. Priebe, D. Raucher, *Invest.New Drugs.* **2007**, *25*, 313-326.

[114] Y. Q. Wu, J. A. MacKay, J. R. McDaniel, A. Chilkoti, R. L. Clark, *Biomacromolecules.* **2009**, *10*, 19-24.

[115] D. Kaufmann, R. Weberskirch, *Macromol. Biosci.* **2006**, *6*, 952-958.

[116] D. Y. Furgeson, M. R. Dreher, A. Chilkoti, *J. Control. Release.* **2006**, *110*, 362-369.

[117] M. F. Shamji, J. Chen, A. H. Friedman, W. J. Richardson, A. Chilkoti, L. A. Setton, *J.Controlled Release.* **2008**, *129*, 179-186.

[118] T. H. Chen, Y. Bae, D. Y. Furgeson, *Pharm.Res.* **2008**, *25*, 683-691.

[119] H. L. Zhang, M. Iwama, T. Akaike, D. W. Urry, A. Pattanaik, T. M. Parker, I. Konishi, T. Nikaido, *Tissue Eng.* **2006**, *12*, 391-401.

[120] J. C. Liu, D. A. Tirrell, *Biomacromolecules.* **2008**, *9*, 2984-2988.

[121] S. C. Heilshorn, K. A. DiZio, E. R. Welsh, D. A. Tirrell, *Biomaterials.* **2003**, *24*, 4245-4252.

[122] Y. Garcia, N. Hemantkumar, R. Collighan, M. Griffin, J. C. Rodriguez-Cabello, A. Pandit, *Tissue Engineering Part a.* **2009**, *15*, 887-899.

[123] X. Wu, R. E. Sallach, J. M. Caves, V. P. Conticello, E. L. Chaikof, *Biomacromolecules.* **2008**, *9*, 1787-1794.

[124] Z. Megeed, M. Haider, D. Q. Li, B. W. O'Malley, J. Cappello, H. Ghandehari, *J. Control. Release.* **2004**, *94*, 433-445.

[125] D. W. Lim, D. L. Nettles, L. A. Setton, A. Chilkoti, *Biomacromolecules.* **2007**, *8*, 1463-1470.

[126] K. Trabbic-Carlson, L. Setton, A. Chilkoti, *Biomacromolecules.* **2003**, *4*, 572-580.

[127] R. McMillan, V. Conticello, *Macromolecules.* **2000**, *33*, 4809-4821.

[128] A. Girotti, J. Reguera, F. J. Arias, M. Alonso, A. M. Testera, J. C. Rodriguez-Cabello, *Macromolecules.* **2004**, *37*, 3396-3400.

[129] D. W. Urry, S. Peng, T. Parker, *J.Am.Chem.Soc.* **1993**, *115*, 7509-7510.

[130] D. W. Urry, S. Q. Peng, T. M. Parker, D. C. Gowda, R. D. Harris, *Angew.Chem.-Int.Edit.Engl.* **1993**, *32*, 1440-1442.

[131] D. W. Lim, K. Trabbic-Carlson, J. A. MacKay, A. Chilkoti, *Biomacromolecules.* **2007**, *8*, 1417-1424.

[132] J. Reguera, A. Fahmi, P. Moriarty, A. Girotti, J. Rodriguez-Cabello, *J.Am.Chem.Soc.* **2004**, *126*, 13212-13213.

[133] R. Alvarez-Rodriguez, M. Alonso, A. Girotti, V. Reboto, J. Carlos Rodriguez-Cabello, *Eur. Polym.J.* **2010**, *46*, 643-650.

[134] A. Junger, D. Kaufmann, T. Scheibel, R. Weberskirch, *Macromol. Biosci.* **2005**, *5*, 494-501.

[135] D. Kaufmann, A. Fiedler, A. Junger, J. Auernheimer, H. Kessler, R. Weberskirch, *Macromol. Biosci.* **2008**, *8*, 577-588.

[136] M. K. McHale, L. A. Setton, A. Chilkoti, *Tissue Eng.* **2005**, *11*, 1768-1779.

[137] D. L. Nettles, K. Kitaoka, N. A. Hanson, C. M. Flahiff, B. A. Mata, E. W. Hsu, A. Chilkoti, L. A. Setton, *Tissue Eng.Part A.* **2008**, *14*, 1133-1140.

[138] A. Girotti, J. Reguera, J. C. Rodriguez-Cabello, F. J. Arias, M. Alonso, A. M. Testera, **2004**, 479-484.

[139] E. Donath, G. Sukhorukov, F. Caruso, S. Davis, H. Mohwald, *Angew.Chem.-Int.Edit.* **1998**, *37*, 2202-2205.

[140] J. S. Barbosa, R. R. Costa, A. M. Testera, M. Alonso, J. C. Rodriguez-Cabello, J. F. Mano, *Nanoscale Res.Lett.* **2009**, *4*, 1247-1253.

[141] R. R. Costa, C. A. Custodio, A. M. Testero, F. J. Arias, J. C. Rodriguez-Cabello, N. M. Alves, J. F. Mano, *Adv.Funct.Mater.* **2009**, *19*, 3210-3218.

[142] R. R. Costa, C. A. Custodio, F. J. Arias, J. C. Rodriguez-Cabello, J. F. Mano, *Small.* **2011**, *7*, 2640-2649.

[143] M. Golonka, M. Bulwan, M. Nowakowska, A. Maria Testera, J. Carlos Rodriguez-Cabello, S. Zapotoczny, *Soft Matter.* **2011**, *7*, 9402-9409.

Chapter 2

De Novo Design of Supercharged, Unfolded Protein Polymers and their Assembly into Supramolecular Aggregates

Anke Kolbe, Loretta L. del Mercato, Azhar Z. Abbasi, Pilar Rivera Gil, Sekineh J. Gorzini, Wim H.C.Huibers, Bert Poolman, Wolfgang J. Parak, and Andreas Herrmann

Macromolecular Rapid Communications, Vol. 32 (2), pp. 186-190, 2011

Here we report for the first time the design and expression of highly charged, unfolded protein polymers based on elastin-like peptides (ELPs). Positively and negatively charged variants were achieved by introducing lysine and glutamic acid residues, respectively, within the repetitive pentapeptide units. Subsequently it was demonstrated that the monodisperse protein polyelectrolytes with precisely defined amino acid compositions, sequences and stereochemistries can be transferred into superstructures exploiting their electrostatic interactions. Hollow capsules were assembled from oppositely charged protein chains by using the layer-by-layer technique. The structures of the capsules were analyzed by various microscopy techniques revealing the fabrication of multilayer containers. Due to their low toxicity in comparison to other polyelectrolytes, supercharged ELPs are appealing candidates for the construction of electrostatically induced scaffolds in biomedicine.

Genetically encoded polypeptides with repetitive motifs have gained increasing attention in recent years due to their high potential for biotechnological and biomedical applications. This development was mainly fueled by progress in recombinant DNA technology allowing precise control of the structure of the resulting macromolecules.[1,2] Important examples are silk-like,[3] collagen-like[4,5] and elastin-like proteins (ELPs)[6]. The latter are derived from a repeating motif within a hydrophobic domain of mammalian tropoelastin. The most common pentapeptide motif has the sequence $(VPGXG)_n$ with X being any guest amino acid except proline and n denoting the number of repeats.[7] The structural and physical properties of ELPs, such as their elastic/mechanical as well as thermoresponsive behavior, have been investigated.[8-10] Their ability to undergo a reversible phase transition at the so-called lower critical solution temperature (LCST) has been exploited for the purification of proteins[11] and DNA.[12] For tissue engineering purposes, ELPs were designed as thermally sensitive hydrogels that solidify when injected into the body.[13] Furthermore, their temperature responsiveness was utilized for drug delivery applications. In hyperthermia treatment, ELPs were accumulated in tumors[14] and the LCST-behavior was employed to induce micelle formation of block ELP structures.[15]

RESULTS AND DISCUSSION

Design, Preparation and Characterization of Elastin-like Polypeptides

The choice of different guest amino acids within the ELP motif allows the precise control of LCST and the incorporation of chemical modifications.[16] Here, we took advantage of the flexibility of amino acid composition at the fourth position within the repeat to transform ELPs into unprecedented highly charged anionic and cationic polyelectrolytes. These structures of biosynthetic origin are much better defined than their chemically synthesized counterparts. To assess their viability in a common application for polyelectrolytes in a biomedical context, these materials were transformed into superstructures, i.e. hollow capsules, employing the electrostatic interactions of oppositely charged variants.

We thus decided to introduce lysine and glutamic acid residues in order to obtain highly positively and negatively charged polypeptide chains, respectively. Monomer units of the ELP gene encoded nine to twelve pentapeptide repeats (Val-Pro-Gly-Lys/Glu-Gly) and were multimerized using recursive directional ligation, as described by Chilkoti and co-workers.[10] ELPs with 48 positive (K48) or 57 negative (E57) charges were produced in *E. coli* and purified. Protein yields were 1 and 5 mg per liter of bacterial cell culture for K48 and E57, respectively. The purity of the products was

analyzed by polyacrylamide gel electrophoresis and subsequent staining with either SimplyBlue™ SafeStain (Invitrogen) or copper(II) chloride (Figure 1a, left pane). ELPs exhibited reduced electrophoretic mobilities compared to globular proteins, a finding widely observed with ELPs.[10] It was also observed that the negatively charged variant E57 was poorly stained with the SimplyBlue™ SafeStain as well as with Coomassie brilliant blue R-250 (data not shown). Staining with copper(II) chloride, however, led to a clear E57 protein band and a white K48 protein band against an opaque, whitish-blue background (Figure 1a, right pane). Mass spectra yielded sharp peaks for all three variants (Figure 1b). Determined masses were 24,105 +/- 50 Da for K48 and 28,967 +/- 50 Da for E57, which is in excellent agreement with the calculated masses of 24,151 and 28,971 Da, respectively. As expected,[17] K48 and E57 do not exhibit LCST behavior until 90°C. Transition of ELPs from the soluble to the insoluble state was determined by measuring absorbance at 350 nm (OD_{350}) at temperatures ranging from 20 to 90°C. No significant increase in the OD_{350} values for either of the ELP variants could be observed at any temperature measured (data not shown). This finding is in line with published data, where the incorporation of increasing numbers of lysine or glutamic acid residues in ELPs led to an increase in the lower critical solution temperature (LCST) at neutral pH values.[7,16] ELPs below their critical solution temperature exhibit extensive random coil formation in water.[18,19] To determine the secondary structure of K48 and E57, CD spectra were recorded at 20°C. The spectra of both polypeptides showed a smaller trough at around 220 nm and a larger trough at around 200 nm (Figure 1c). This spectral behavior is usually interpreted to represent largely random coil structure with some contribution of α-helical segments.[19,20]

Capsule Preparation and Characterization

After successful expression our next goal was to exploit the high net charges of K48 and E57 for self-assembly of the ELP variants into supramolecular structures, namely multilayer polypeptide capsules, using a Layer-by-Layer (LbL) technique[21] (Figure 2). This technique is based on the consecutive assembly of oppositely charged polymers around a preformed charged spherical template[21] with typical diameter from a few hundred nm to a few mm. At the end of the LbL adsorption process, the cores can be successfully removed to obtain hollow and intact capsules. Polymer containers based on the LbL technique have recently attracted high interest for a variety of different applications, ranging from drug delivery systems and targeted gene therapy to biosensor devices.[22,23] To date, capsules have been made of synthetic and biodegradable polyelectrolytes,[24,25] comprising natural molecules such as oligonucleotides[26] and proteins,[27,28] which demonstrates the high versatility of LbL assembly.

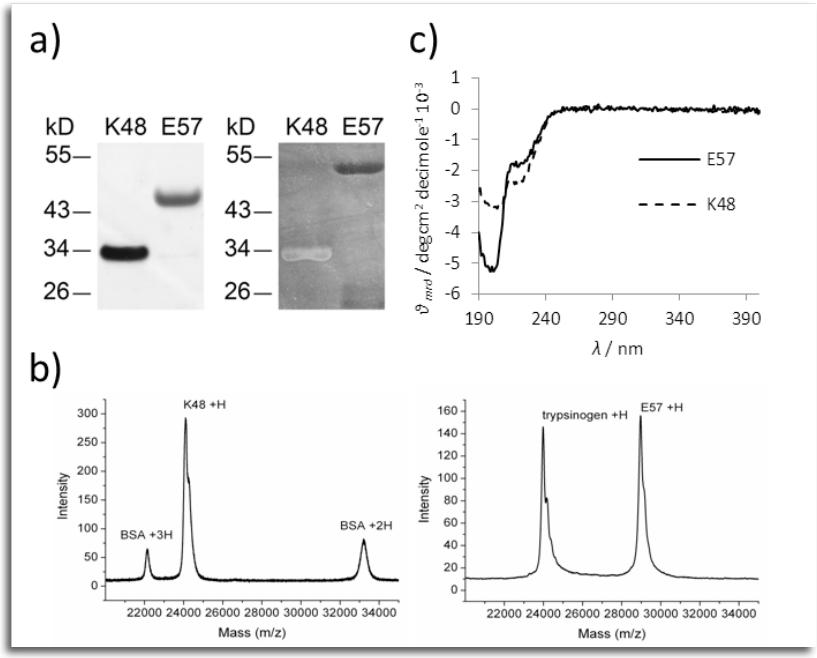

Figure 1. Characterization of unfolded, supercharged proteins. a) Purified ELP variants K48 and E57 examined by SDS-PAGE. Left: 4-12% NuPAGE® gel stained with SimplyBlue™ safe stain (K48: 2 µg, E57: 8 µg). Right: 12% SDS-PAGE gel stained with a 0.3 M copper (II) chloride solution (K48: 2 µg, E57: 4 µg). b) MALDI-TOF mass spectra of supercharged elastin-like proteins K48 and E57. Left: mass spectrum of K48 (m/z is 24,104.6) with internal standard bovine serum albumin (BSA; m/z is 22,135.5 for BSA +3H and m/z is 33,215.3 for BSA +2H). Right: Mass spectrum of E57 (m/z is 28,967.1) with internal standard trypsinogen (m/z is 23,982.0). *I* = absolute intensity. c) Circular dichroism (CD) spectra of aqueous solutions of ELPs K48 (10 µM) and E57 (5µM). Data represent averages of 25 scans.

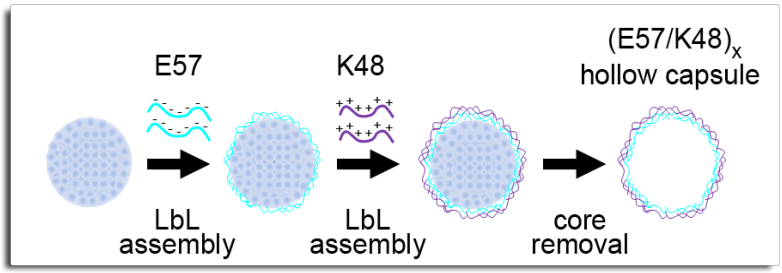

Figure 2. Schematic illustration of the multiple assembly of the two oppositely supercharged proteins onto spherical $CaCO_3$ porous microparticles via LbL assembly technique, and fabrication of a hollow protein-based capsule by dissolution of the template core. The turquoise lines represent the supercharged negative E57 ELP, the violet lines represent the supercharged positive K48 ELP. For simplicity, only two layers are shown. Capsules are not drawn to scale.

The main driving force in alternate LBL assembly of multilayer capsules is the electrostatic interaction between oppositely charged species. Hence, the number of charges per molecule of the two supercharged unfolded proteins K48 and E57, employed as component layers of ELP-derived capsules, was calculated and compared to the number of charges per molecule of polyelectrolytes (PEs) commonly used for capsule synthesis, which served as controls in this work (Table 1). As expected, all control PEs have a higher number of charges per molecule than the ELPs except for DEXS, which has around 27 charges per molecule. The μmol charges per 1 mg are also higher for all control PEs than for the ELPs.

Table 1. Calculation of the charges per molecule (ch./mol.) and μmol charges per 1 mg of the polyelectrolytes (PE) used in this work.

PE	**full name**	**MW (average) [Da]**	**ch./mol. at pH 7.0**	**μmol charges in 1 mg**
E57	ELP-glutamic acid	28,970	57	1.97
K48	ELP-lysine	24,150	48	1.99
DEXS	Dextran sulfate sodium salt from *Leuconostoc* spp.	6,500-10,000	27.79	3.37
pARG	Poly-L-arginine hydrochloride	70,000	498	7.11
PSS	Poly(sodium 4-styrenesulfonate)	70,000	339	4.84
PAH	Poly(allylamine hydrochloride)	56,000	605	10.8
pLL	poly-L-lysine hydrobromide	15,000-30,000	108	4.8

Using standard LbL preparation techniques[21] and employing supercharged proteins E57 and K48 as building blocks, we generated capsules exhibiting the following wall structure: (DEXS/pARG)(E57/K48)$_3$(E57/K48$_{AF488}$)E57, where DEXS denotes dextran sulfate and pARG poly(L-arginine), two charged biodegradable polymers made from naturally occurring monomers.[24] The use of DEXS/pARG as a first bi-layer proved crucial to growing a stable multilayer (E57/K48) wall. In a previous experiment, protein capsules assembled by using E57 as first layer showed diffusion of the fluorescent layer K48$_{AF488}$ into the capsule cavity during the LbL steps (data not shown). Moreover, after core removal no spherical capsules were detectable by fluorescence microscopy, thus confirming that both E57 and K48 were mostly localized as complexes inside the $CaCO_3$ cores instead of alternately depositing on the template surface (data not shown). It is worth noting that $CaCO_3$ microparticles are high

porous with pore diameters ranging from 20 to 60 nm.[29] This allows small molecules with a size of several nanometers to penetrate into the template during LbL assembly. Thus, in order to prevent diffusion of ELP into the cavities, we decided to assemble the ELP multilayer shell after adsorption of one biodegradable bi-layer composed of (DEXS/pARG) polymers. As control samples, capsules made of degradable and non-degradable polyelectrolytes were fabricated. Degradable capsules, which are susceptible to enzymatic degradation, were composed of dextran sulfate (DEXS) as the polyanion and of poly(L-arginine) (pARG) as the polycation.[24] Non-degradable capsules were made of poly(sodium 4-styrenesulfonate) (PSS) as the polyanion and of polyallylamine hydrochloride (PAH) as the polycation. For visualization purposes, one layer was fluorescently labeled with Alexa Fluor 488 (AF488; labeling of K48 and pARG) or fluorescein isothiocyanate (FITC; labeling of PAH).

The typical morphologies of core-shell microparticles after LbL assembly with the same number of layers but different layer components are presented in Figure 3. In the three systems investigated the diameter of the microparticles was found to be

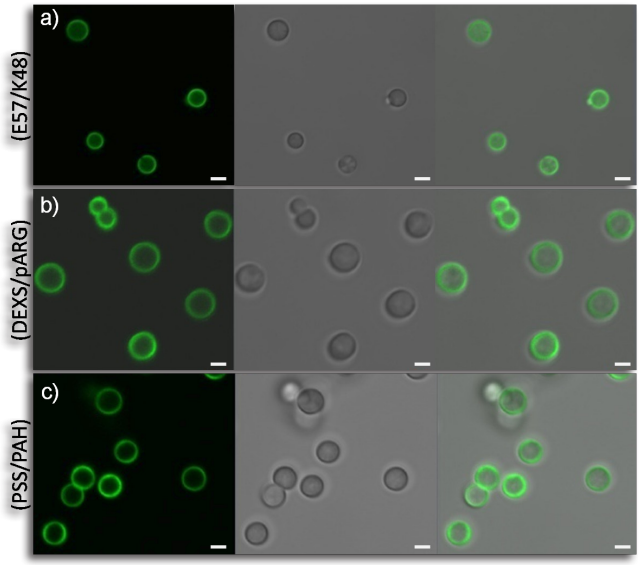

Figure 3. CLSM images of (a) (DEXS/pARG)(E57/K48)$_3$(E57/K48$_{AF488}$)E57, (b) (DEXS/pARG)$_3$(DEXS/pARG$_{AF488}$)(DEXS/pARG)DEXS and (c) (PSS/PAH)$_3$(PSS/PAH$_{FITC}$)(PSS/PAH)PSS capsules before core removal. The capsule walls were labeled with AF488 (a, b) and FITC (c). Left panels: Fluorescence images of green emitting dyes. Central panels: optical transmission images. Right panels: corresponding overlay of both fluorescence and transmission channels. The fluorescence signal coming from the capsule walls can be seen whereas the spherical shape of $CaCO_3$ porous cores can be observed in the corresponding transmission images. Scale bars represent 1 µm.

in the range of 2-2.5 μm. As shown in the fluorescence channels, the fluorescence signal corresponding to the labeled layers, which had been added as tenth layer in the ELP capsules and as eighth layer in the biodegradable and non-degradable capsules, was detected only in the walls. This indicates that the layers were efficiently adsorbed around the spherical templates during the LbL assembly. As expected, the $CaCO_3$ cores were clearly visible in the corresponding transmission channels.

After core removal, confocal laser scanning microscopy (CLSM) pictures of the resulting capsules were taken (Figure 4). Notably, the dissolution of the core is a critical step in the preparation of hollow capsules, as it may result in capsules breaking or swelling due to decomposition conditions (i.e., low pH). The fluorescence signal in the ELP capsules was found to be still confined to the walls even after core removal, showing that the integrity of the multilayer protein shell was not affected during core dissolution. In some of the biodegradable (DEXS/pARG) capsules a slight diffusion of the labeled polymer $pARG_{AF488}$ into the cavities was observed, owing to the above

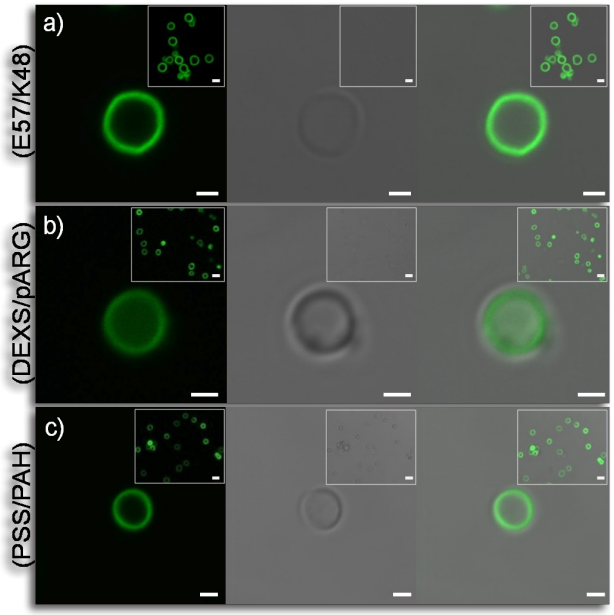

Figure 4. CLSM images of (a) (DEXS/pARG)(E57/K48)$_3$(E57/K48$_{AF488}$)E57, (b) (DEXS/pARG)$_3$(DEXS/pARG$_{AF488}$)(DEXS/pARG)DEXS and (c) (PSS/PAH)$_3$(PSS/PAH$_{FITC}$)(PSS/PAH)PSS single capsule after core removal. The capsule walls were labeled with AF 488 (a, b) and FITC (c). Left column: fluorescence image; middle column: transmission image; right column: overlay. The absence of the $CaCO_3$ cores can be clearly observed in the transmission images. Inset: CLSM images of several capsules showing spherical and intact capsules after core removal. Scale bars represent 1 μm.

mentioned porosity of the $CaCO_3$ cores.[29] The absence of the cores was clearly detected in each capsule sample, as shown in the transmission channels.

The efficient assembly of the protein layers was confirmed by the following control experiment: $CaCO_3$ particles were coated with one bi-layer of $DEXS/pARG_{AF488}$ and analyzed by CLSM before and after core removal. Before core removal, the typical morphology of capsules enclosed by a fluorescently labeled wall was observed (data not shown). After core removal, no capsules were observed in the bulk solution indicating that capsules made of only one bi-layer are not stable against the dissolution conditions. This result confirms that the protein-based capsules prepared by LbL assembly of E57/K48 onto one bi-layer of (DEXS/pARG) were actually composed of alternating protein layers with the fluorescently labeled $K48_{AF488}$ as second-last layer.

Capsules permeability

In order to compare the permeability behavior of protein capsules and control capsules based on DEXS/pARG and PSS/PAH layers, dextran with a molecular weight of 500 kDa and labeled with red fluorescent Alexa Fluor 594, was entrapped inside the cavities during synthesis of the $CaCO_3$ cores. After core removal diffusion of dextran across the wall of (E57/K48) capsules was observed, whereas no diffusion was observed for the control capsules (Figure 5). These data suggest the existence of large pores in the wall of supercharged protein-based capsules.

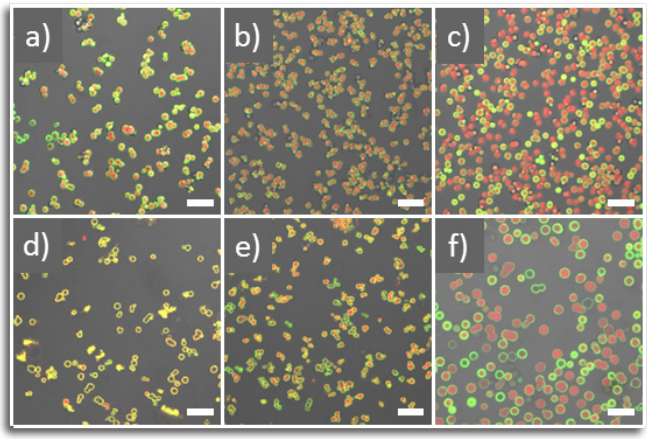

Figure 5. CLSM overlay images of 11-layer (a, d) (E57/K48), (b, e) (DEXS/pARG) and (c, f) (PSS/PAH) capsules. Capsules are shown before (a-c) and after (d-f) core removal. Capsule cavities were loaded with dextran (MW 500 kDa), labeled with red fluorescent AF543. Capsule walls were labeled with green fluorescent AF488 (a, b, d, e) or FITC (c, f). After core removal dextran diffused through the walls of (E57/K48) capsules, suggesting a higher porosity of the wall compared to the control capsules. Scale bars represent 10 µm.

Protein capsules were then analyzed by Scanning Electron Microscopy (SEM) and Transmission Electron Microscopy (TEM) to gain deeper insight into the structure and morphology of the multilayer polypeptide wall, both before and after core removal, and to compare their properties to the control capsules. Figure 6 shows the SEM images corresponding to the core-shell microparticles previously presented in Figure 3. Protein-coated cores and (DEXS/pARG)-coated cores were characterized by a thick surface, suggesting dense packing of the polymers in the multilayer shells.

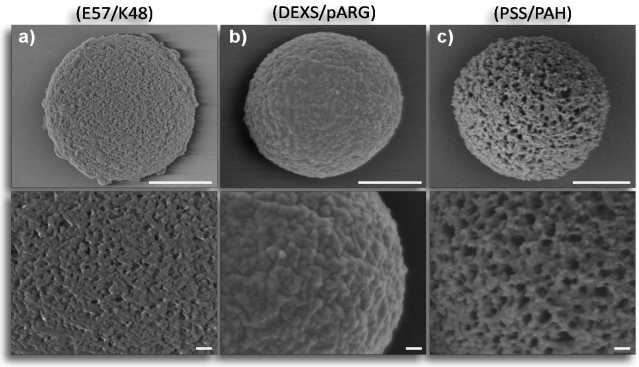

Figure 6. SEM images of $CaCO_3$ cores after coating (a) (DEXS/pARG)(E57/K48)$_3$(E57/K48$_{AF488}$)E57, (b) (DEXS/pARG)$_3$(DEXS/pARG$_{AF488}$)(DEXS/pARG)DEXS and (c) (PSS/PAH)$_3$(PSS/PAH$_{FITC}$)(PSS/PAH)PSS. The typical spherical, porous-like structure of capsules templated on $CaCO_3$ cores can be observed. Scale bars represent 1 μm (top row), 100 nm (bottom row).

In the case of capsules made up of (PSS/PAH) polyelectrolytes, a highly porous surface was observed. This might be explained by the adsorption of the polyelectrolytes onto the rough surface of the $CaCO_3$ microparticles which results in the formation of a porous polyelectrolyte network.[29] After dissolution of the templates, a porous network with clear holes was observed in the protein capsules sample (Figure 7), whereas in the capsule wall composed of biodegradable PEs no holes were detected. Non-degradable capsules exhibited a rather porous wall structure.

In line with the LSM and SEM data the walls of the protein capsules investigated under TEM were found to be more porous than biodegradable and non-degradable capsules (Figure 8), indicating that the two investigated polypeptides, E57 and K48, formed thinner shells during the LbL assembly. Nonetheless we would like to point out that the porosity, and thus the permeability, of the protein capsules could be reduced by increasing the number of layers employed to grow the multilayer wall or by cross-linking the proteins after their adsorption onto the sacrificial core surfaces (i.e., by using glutaraldehyde as a cross-linker agent).[27,28] Finally, the use of unfolded,

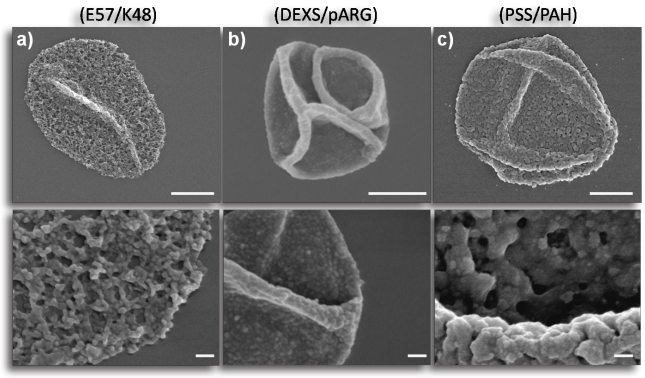

Figure 7. SEM images of (a) (DEXS/pARG)(E57/K48)$_3$(E57/K48$_{AF488}$)E57, (b) (DEXS/pARG)$_3$(DEXS/pARG$_{AF488}$)(DEXS/pARG)DEXS and (c) (PSS/PAH)$_3$(PSS/PAH$_{FITC}$)(PSS/PAH)PSS capsules after core removal. Capsules collapse after core removal indicating the absence of the cores in their cavities. Scale bars represent 1 μm (top row), 100 nm (bottom row).

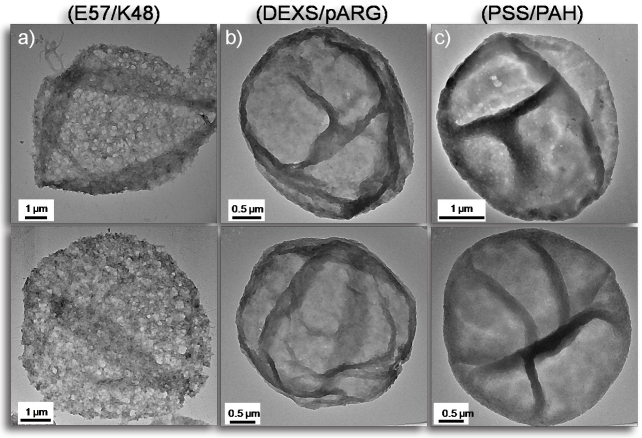

Figure 8. TEM images of (a) (DEXS/pARG)(E57/K48)$_3$(E57/K48$_{AF488}$)E57, (b) (DEXS/pARG)$_3$(DEXS/pARG$_{AF488}$)(DEXS/pARG)DEXS and (c) (PSS/PAH)$_3$(PSS/PAH$_{FITC}$)(PSS/PAH)PSS capsules after core removal. Capsules collapse after core removal indicating the absence of the cores in their cavities.

supercharged proteins with a higher number of charges per molecule (see Table 1) might be taken into account to build up a multilayer shell with stronger electrostatic attractions between each component layer.

Taken together, we successfully assembled multilayers of unfolded, supercharged proteins onto a spherical core template. After dissolution of the core the existence of capsules with empty interior and stable walls was clearly demonstrated. Compared to capsules formed by standard synthetic polyelectrolytes such as poly(styrene sulfonate) (PSS) and poly(allylamine hydrochloride) (PAH) the walls of capsules based on supercharged proteins were found to be rather porous. This may be due to the lower charge density of E57 and K48 compared to PSS and PAH (Table 1), which results in a higher mechanical pressure during the dissolution procedure. At any rate, the two structural compartments of capsules, cavity and wall, are well defined and prove successful and stable assembly.

Evaluation of *In Vitro* Cytotoxicity

Such capsules might be appealing containers for use in biomedicine. Since positively charged polymers are the most common source of toxicity in charged systems due to their interaction with anionic intracellular components,[30-32] the toxicity of K48 was investigated and compared to the other positive polyelectrolytes used for the synthesis of capsule controls (i.e. PLL, PAH, pARG). A fluorimetric metabolic assay employing NIH/3T3 embryonic fibroblast cells was utilized to assess cytotoxicity. The normalized fluorescence of Resorufin, a dye indicating metabolically active cells, was plotted against polyelectrolyte concentrations (Figure 9). The resulting

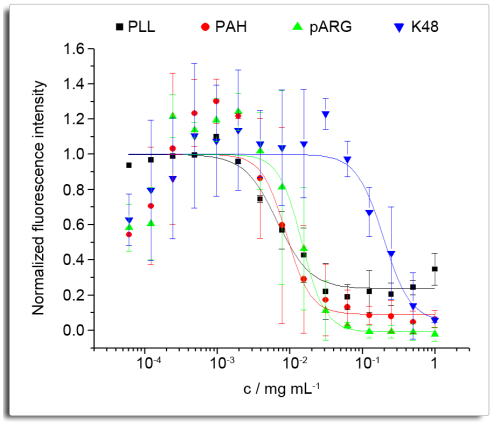

Figure 9. Comparison of the polyelectrolyte-induced toxicity on NIH/3T3 embryonic fibroblasts. Cells were incubated with the different polymers in a concentration range from 6.1 x 10^{-5} mg ml^{-1} to 1 mg ml^{-1} and some cells were left untreated as positive control for viability. Cell viability was assessed by an increase in the fluorescence signal and is given as mean of normalized intensities. The normalized fluorescent intensity is plotted against the concentration (c) and shows a sigmoidal concentration-toxicity relationship. PLL: poly(L-lysine); PAH: poly(allylamine hydrochloride); pARG: poly(L-arginine).

dose response curves yielded the following polymer concentrations causing 50% cell death (LD50, mg ml^{-1}) in decreasing order of toxicity: PLL (LD50 = 0.007), PAH (LD50 = 0.009), pARG (LD50 = 0.015) and K48 (LD50 = 0.196). PLL, PAH and pARG exhibited similar dose response curves with similar LD50 values, whereas the curve for K48 was strongly shifted to higher concentration values. This indicates that lower concentrations of PLL, PAH and pARG than of K48 are able to induce cell death. K48 induces toxicity at the maximum concentration value used (1 mg ml^{-1}) and this effect was immediately mitigated by halving the dose. A plateau level of viability was reached at a concentration of 3.1 x 10^{-2} mg ml^{-1}.

CONCLUSION

In this work we demonstrated the expression of supercharged polypeptides consisting of repetitive motifs. As a result of incorporating a single charge per almost every repeat, unfolded polyelectrolytes were obtained that are perfectly defined regarding their number and distribution of charges, monomer composition, stereochemistry and dispersity, which is almost impossible by conventional polymerization techniques. With K48 for example, 1 positive charge per 5.7 amino acids was reached. ELPs with charged amino acids as guest residues have already been produced, but with much lower charge densities than reported herein.[16] So far only a single folded protein, Green Fluorescent Protein (GFP), was equipped with similar amounts and densities of charges.[33] However, within GFP the charges were by far not as equally distributed as in the ELP backbone. In this respect we demonstrated that the concept of supercharging by genetic engineering can be extended to other peptide-based biopolymers. When comparing supercharged ELPs with naturally occurring polypeptides, we see that with K48 it was even possible to realize a charge density comparable to only a few naturally occurring unfolded proteins,[33,34] all while using a minimal set of the amino acid alphabet.

It was further shown that the high number of charges of these de novo designed proteins could be exploited for the fabrication of supramolecular structures. Oppositely charged variants were transformed into multilayer capsules by electrostatic interactions employing the widely used Layer-by-Layer technique. Due to their low toxicity, supercharged proteins like the highly charged ELPs presented in this work promise to be a favorable alternative to their chemically synthesized counterparts in the context of biomedical scaffolds. In the future we will employ supercharged ELPs for the generation of other electrostatically induced polymeric architectures such as polyplexes and hydrogels with well-defined network porosity.

EXPERIMENTAL PART

Materials

E.coli XL1-Blue competent cells were purchased from Stratagene (La Jolla, CA). The pUC19 cloning vector, restriction endonucleases, T4 DNA ligase (LC), Fast AP™ thermosensitive alkaline phosphatase (Fast AP), and GeneJET™ Plasmid Miniprep kit were purchased from Fermentas (St. Leon-Rot, Germany). Digested DNA fragments were purified using QIAquick® spin miniprep kits from QIAGEN, Inc. (Valencia, CA). The pET-25b(+) vector and *E.coli* BLR(DE3) competent cells were purchased from Novagen Inc. (Milwaukee, WI). Oligonucleotides were synthesized by biomers.net (Ulm, Germany). Bacto™ tryptone and BBL™ yeast extract were purchased from Becton, Dickinson and Co. (Sparks, MD). Potassium phosphate monobasic, potassium phosphate dibasic, sodium phosphate monobasic, sodium phosphate dibasic, sodium chloride, and glycerol were purchased from Merck KGaA (Darmstadt, Germany). Ampicillin and imidazole were purchased from Roth (Karlsruhe, Germany). Isopropyl ß-thiogalactopyranoside (IPTG) was purchased from Duchefa (Harlem, Netherlands). 3,5 dimethoxy-4-hydroxycinnamic acid and internal standards bovine serum albumin and trypsinogen were purchased from LaserBio Labs (Sophia-Antipolis, France). Poly(sodium 4-styrenesulfonate) (PSS, Mw ~70,000), poly(allylamine hydrochloride) (PAH, Mw ~56,000), poly(fluorescein isothiocyanate allylamine hydrochloride) (PAH_{FITC}, Mw ~56,000), poly-L-arginine (pARG, Mw> 70 kDa), dextran sulfate (DEXS, Mw ~10 kDa), poly-L-lysine hydrobromide (pLL, Mw 15,000 – 30,000 Da), calcium chloride dehydrate ($CaCl_2$), Sodium carbonate (Na_2CO_3) and ethylenediaminetetraacetic acid (EDTA) were purchased from Sigma-Aldrich. Alexa Fluor488, Alexa Fluor 594 carboxylic acid succinimidyl ester and amino dextran (Mw ~500,000) carboxylic acid succinimidyl ester were obtained from Molecular Probes (Invitrogen). All chemicals were used as received. Ultrapure water with a resistivity greater than 18.2 MW cm was used for all experiments.

Monomer gene synthesis and gene oligomerization

Construction of the monomer genes and subsequent multimerization were performed as described by Chilkoti and co-workers.[10] Briefly, a monomer gene was constructed from eight 5'-phosphorylated, PAGE-purified synthetic DNA oligonucleotides. For annealing, equimolar mixtures of the oligonucleotides in T4 DNA ligase buffer were heated to 94°C and then slowly cooled down to 4°C, yielding a double-stranded DNA cassette with *Eco*RI and *Hin*DIII compatible ends. PUC19 was digested with *Eco*RI and *Hin*DIII, dephosphorylated with Fast AP and run on a 1% agarose gel in TAE

buffer (per 1L, 108 g Tris base, 57.1 ml glacial acetic acid, 0.05 M EDTA, pH 8.0). The vector band was cut out and purified using a spin column purification kit. The annealed oligonucleotides were ligated to the linearized vector. For transformation, 200 µL of chemically competent *E.coli* XL1-Blue cells were combined with 5 µL of the ligation mixture and further treated according to the manufacturer's protocol. Cells were spread on Lysogeni broth (LB) agar plates (for 1L, 10 g Bacto™ tryptone, 5 g BBL™ yeast extract, 5 g NaCl, 15 g agar) supplemented with 100 µg/ml ampicillin, and incubated overnight at 37°C. Colonies were picked and grown in 6 ml LB media (for 1L, 10 g Bacto™ tryptone, 5 g BBL™ yeast extract, 5 g NaCl) supplemented with 100 µg/ml ampicillin overnight, and plasmids were isolated using the GeneJET Plasmid Miniprep kit. Positive clones were verified by plasmid digestion with *Eco*RI and *Hin*DIII and subsequent gel electrophoresis. The DNA sequence of putative inserts was further verified by DNA sequencing (SequenceXS, Leiden, The Netherlands).
Gene oligomerization was performed as described by Chilkoti and co-workers. [10] Positive clones were verified by plasmid digestion with *Eco*RI and *Hin*DIII and subsequent gel electrophoresis. The DNA sequences of putative inserts were further verified by DNA sequencing (SequenceXS, Leiden, The Netherlands). The resulting ELP gene sequences encoded for the positively charged ELP sequences $[(VPGKG)_{12}(VPGVG)]_4$, hereafter K48, and $[(VPGEG)_{10}(VPGVG)(VPGEG)_{11}(VPGVG)]_3$, hereafter E57, with V denoting valine, P proline, G glycine, K lysine, and E glutamic acid. As the recognition sites of the restriction enzymes *Pfl*MI and *Bgl*I had to be preserved, a valine residue instead of a lysine or glutamic acid residue was incorporated with every step of oligomerization.

Expression vector construction

The expression vector pET 25b(+) (Novagen) was modified by cassette mutagenesis as described by Chilkoti and co-workers.[10] The DNA sequence spanning *Nde*I to *Eco*RI was exchanged for a sequence which incorporates a unique *Sfi* I recognition site and which encodes for an affinity tag consisting of six histidine residues (Figure 10).

Insert sequence of modified expression vector pET-25b(+)-SfiI-H6

*Nde*I *Sfi*I *Eco*RI

T ATG GGC GCG GGG CCG GGC TGG CCG CAC CAC CAC CAC CAC CAC TGA TAA GAA TT

M G A G P G W P H H H H H H * *

Figure 10. Sequence inserted into pET-25b(+) between recognition sites *Nde*I and *Eco*RI. The modified pET-25b(+)-SfiI-H6 vector contains a unique *Sfi*I recognition site to insert ELP genes into the vector, and sequence encoding for a hexa-histidine (H6) tag at the C-terminus of the expressed protein for affinity purification.

The modified pET 25b(+) expression vector was digested with *Sfi*I, dephosphorylated and purified using a microcentrifuge spin column kit. The respective ELP gene was excised from the pUC19 vector by digestion with *Pfl*MI and *Bgl*I, and the excised gene was purified by agarose gel extraction following gel electrophoresis. The linearized vector and ELP-encoding gene were ligated, transformed into XL1-Blue cells, and screened as described above.

Protein expression and purification

E.coli BLR (DE3) cells (Novagen) were transformed with the pET expression vectors containing the respective ELP genes. For protein production, Terrific Broth medium (for 1L, 12 g tryptone and 24 g yeast extract) enriched with phosphate buffer (for 1L, 2.31 g potassium phosphate monobasic and 12.54 g potassium phosphate dibasic) and glycerol (4 ml per 1L TB), and supplemented with 100 µg/ml ampicillin was inoculated with an overnight starter culture to an initial OD_{600} of 0.1 and incubated at 37°C with orbital agitation at 250 rpm until OD_{600} reached 0.7. Protein production was induced by addition of IPTG to a final concentration of 1 mM. Cultures were then continued for an additional 4 h post-induction. Cells were subsequently harvested by centrifugation (7,000 x *g*, 20 min, 4°C), resuspended in lysis buffer (50 mM sodium phosphate buffer, pH 8.0, 300 mM NaCl, 20 mM imidazole) to an OD_{600} of 100 and disrupted with a French Press. Cell debris was removed by centrifugation (40,000 x *g*, 90 min, 4°C). Proteins were purified from the supernatant under native conditions by Ni-sepharose chromatography (GE Healthcare). Product-containing fractions were pooled and dialyzed against Ultrapure water (>18 MΩ). K48 was further purified by affinity chormatography using a Heparin HP column (GE Healthcare) and protein-containing fractions were dialyzed against Ultrapure water (>18 MΩ). Purified proteins were stored at -20°C or lyophilized and stored at room temperature until further use.

Protein characterization

The concentrations of the purified ELPs were determined by measuring absorbance at 280 nm using a spectrophotometer (NanoDrop™, Thermo Scientific). Protein purity was analyzed by PAGE (poly(acrylamide) gel electrophoresis) on a 4-12% NuPAGE® Bis-Tris gel (Invitrogen) and subsequent staining of the gel with SimplyBlue™ SafeStain (Invitrogen). Furthermore, purified proteins were characterized by SDS-PAGE (SDS - sodium dodecyl sulfate) on a 12% polyacrylamide gel according to Laemmli[35] and subsequent copper (II) chloride staining as reported by Lee and coworkers.[36] Mass spectrometric analysis was performed using a 4800 Plus MALDI-TOF/TOF Analyzer (Applied Biosystems, Foster City, CA, USA). The samples were

prepared in a recrystallized 3,5 dimethoxy-4-hydroxycinnamic acid matrix with the calibration standards bovine serum albumin (MW = 66,429.9) for K48 and trypsinogen (MW = 23980.9) for E57. Mass spectra were recorded in positive ion mode with the 4000 Series Explorer Software, version 3.0 (Applied Biosystems, Foster City, CA, USA). The data were analyzed in Data Explorer, version 4.9 (Applied Biosystems, Foster City, CA, USA).

Analysis of secondary structure

Circular dichroism (CD) spectra were recorded using a Jasco-815 spectropolarimeter (Jasco, Japan). Measurements were carried out at room temperature with a cell path length of 1 mm. The polypeptide concentrations in ultrapure water were 10 and 5 μM for K48 and E57, respectively.

LCST behavior analysis

To characterize the ELP inverse temperature transition, the OD_{350} of K48 and E57 ELPs in ultrapure water at a concentration of 57 and 24 μM, respectively, were measured as a function of temperature on a Jasco V630 spectrophotometer. Measurements were performed between 20 and 90°C by increasing the temperature every 10 min in 5°C increments.

Labelling of proteins

Alexa Fluor® 488 sulfodichlorophenol ester (AF488) was purchased from Molecular Probes (Invitrogen) and dissolved in DMF to a concentration of 10 mg/ml. To 3.15 mg of K48 in 0.1 M sodium carbonate buffer, pH 8.6, an equimolar amount of AF488 was added under vigorous stirring. After incubation for 2 h at room temperature under vigorous stirring, hydroxylamine solution (pH 8.6) was added to a final concentration of 0.14 M and incubated for additional 90 min at room temperature. Uncoupled dye was removed by size exclusion using an illustra NAP™-25 column (GE Healthcare) and 0.1 M sodium carbonate buffer (pH 8.6) as equilibration and elution buffer. Protein-containing fractions were pooled and dialyzed (cut-off 500 Da) against Ultrapure water (>18 MΩ). Protein concentration was determined using the following equation:

$$c\ [mg/ml] = (A_{280} - 0.11 * A_{495}) * MW_{K48} \quad (1)$$

where A_{280} and A_{495} are the absorbance values at 280 and 495 nm, respectively, and MW_{K48} is the molecular weight of K48. The labeled protein ($K48_{AF488}$) was lyophilized and stored at room temperature until further use.

Cytotoxicity assay of positively charged polyelectrolytes (PEs)

NIH/3T3 embryonic fibroblasts were seeded in a 96-well-platte (Greiner by Sigma-Aldrich) at a cell density of 10^4 cells/well in 100 µL growth medium (DMEM-F12 Ham´s basal medium supplemented with 10% calf serum, 1% L-glutamine and 1% penicillin/streptomycin whereby all material were provided by Sigma-Aldrich). The next day, the cells were incubated with the PEs under investigation (i.e. PLL, PAH, pARG, and K48) for 24h. A starting concentration of 1 mg/ml was used for each PE and consecutively halved until a final concentration of 6.1 x 10^{-5} mg/ml. All concentrations were done in duplicate. Cells that were not treated with any PE served as a positive control for viability. After 24 h, the cells were washed once with PBS, 100 µL of a 10% Resazurin (TOX-8 kit from Sigma-Aldrich) solution (in growth medium) were added to each well and incubated for 3 h at 37°C and 5% CO_2. Resazurin is a blue, non-fluorescent sodium salt, which is converted to resorufin by metabolically active cells. Resorufin is a pink, fluorescent sodium salt that accumulates outside the cells. This reduction process requires functional mitochondrial activity which is inactivated immediately after cell death. Fluorescence spectra were measured using a 96-microwell plate reader connected to a Fluorolog® spectrofluorometer (Jovin Yvon) at an excitation wavelength of 560 nm. The emission was recorded in the range of 572-650 nm with 1 nm resolution and a slit of 5 nm. Firstly, the mean of the intensities of the emission spectra of the duplicates was calculated and then, the maximum intensity values found in the range 578-585 nm were also averaged. The mean background signal (640-650 nm) was subtracted from the mean maximum emission values and subsequently normalized with the maximum fluorescence value obtained. The maximum fluorescence value corresponded not always to the untreated cells, probably due to the formation of hydroresorufin, a transparent nonfluorescent product which is formed upon further reduction of resorufin by viable cells.[37] The experiments were repeated three times for each PE. The means of the normalized fluorescence intensity values of the three experiments (I/Imax) were plotted against the different concentrations of the PEs. A sigmoidal distribution was obtained and fitted as a function of a logistic dose response curve which enables us calculating the PE concentration yielding 50% cell death (LD50).

Preparation of $CaCO_3$ microparticles

For each capsule system, $CaCO_3$ microparticles were precipitated from solutions of calcium chloride and sodium carbonate under vigorous stirring.[29] Briefly, equal volumes (0.615 ml) of aqueous $CaCl_2$ and Na_2CO_3 solutions (0.33 M) were mixed in the presence of 5 mg/ml 500 kDa dextran and thoroughly agitated on a magnetic stirrer for 30 s at room temperature. After the agitation, the mixture was left without

stirring for 4 min at room temperature. During this time precipitation of $CaCO_3$ occurs and spherical $CaCO_3$ particles with an average diameter ranging from 2.5-3.5 μm are formed. Dextran is integrated in the cores.[38] Subsequently, the precipitate was separated from the supernatant by centrifugation (6000x g, 6 s) and washed three times with pure water to remove unreacted species. In the last step, the particles were washed with acetone and air-dried. We incorporated dextran in the $CaCO_3$ cores, as dissolution of the cores including dextran by addition of EDTA was faster than that of cores without dextran. Naturally, in this way dextran remains in the capsule cavities after core dissolution. The whole powder obtained from one synthesis (about 20 mg) was employed for the LbL coating.

Fabrication of multilayer capsules

The resulting spherical cores were coated by sequential incubation of the particles in the corresponding polyanion and polycation solutions. Three different types of microcapsules made of different layer constituents were prepared by sequential adsorption of negatively charged and positively charged species on $CaCO_3$ microparticles (~20 mg per samples) to give the following shell architectures comprising 11 layers in total:

PSS/PAH - capsules: $(PSS/PAH)_3(PSS/PAH_{FITC})(PSS/PAH)PSS$,

DEXS/pARG - capsules: $(DEXS/pARG)_3(DEXS/pARG_{AF488})(DEXS/pARG)DEXS$,

and E57/K48 - capsules: $(DEXS/pARG)(E57/K48)_3(E57/K48_{AF488})E57$.

The adsorption of polyelectrolytes PSS, PAH, PAH_{FITC} and DEXS was conducted in 2 mg/ml solutions in 0.5 M NaCl, whereas the polyelectrolyte pARG and the positively charged and negatively charged proteins (K48 and E57, respectively) were suspended in 1 mg/ml solutions in 0.5 M NaCl. The pH of the polyelectrolyte solutions was adjusted to 6.5 by addition of NaOH, whereas the pH of the protein solutions was maintained neutral (~7.2-7.6). The adsorbing protocol started with the negatively charged polymer (PSS or DEXS). PAH_{FITC} (obtained from Sigma) and PAH_{AF488} (obtained by reacting NHS-ester modified Alexa488 to the amino groups of PAH or pARG) were used instead of non-labeled polycation for the eighth layer of the multilayer polymer shell, so that the capsules had a green emitting dye label in their walls. Similarly, $K48_{AF488}$ was used for the tenth layer of the protein capsules to label the capsule walls. After addition of each charged species, samples were continuously shaken for 12 min. The coated particles were then centrifuged at 6000x g for 6 s and the supernatant containing unabsorbed species was removed. This procedure was repeated three times after each absorption step. After each cycle the $CaCO_3$ suspension was resuspended with ultrasound pulses to prevent aggregation. At the end eleven layers were deposited for each capsule type, starting from the polyanion.

We want to point out that in the case of the protein capsules the first two layers were DEXS and pARG in order to mechanically stabilize the capsules. As the capsule cavities include dextran, the first layer of dextran sulfate has the same constituency as the interior of the capsule cavity. Poly-L-arginine is a polypeptide and thus similar in nature to the following layers of supercharged proteins. After assembly of the capsule walls by LbL deposition the $CaCO_3$ core was removed by complexation with EDTA. Coated $CaCO_3$ particles were shaken for 2 min with 1 ml of an EDTA solution (0.2 M, pH 5), followed by centrifugation and redispersion in 1 ml of a fresh EDTA solution (0.2 M, pH 7). The thus obtained hollow microcapsules with some dextran in their cavities were washed five times with pure water with centrifugation at 1000 x *g* for 8 min. The microcapsules were finally stored as suspension in water at 4°C.

Capsule characterization

Confocal laser scanning microscopy (CLSM)

Fluorescent images were taken by a confocal microscope (LSM 510 META, Zeiss). The excitation wavelength was 488 nm. Samples were observed through a 100X/1.45 NA oil-immersion PLAN-FLUOAR objective. Capsules labeled with FITC and Alexa488 fluorescence were studied with the Ar/Kr laser 488 nm. A 20 µL drop sample was placed onto a cover glass and imaged in liquid.

Electron Microscopy

Protein capsules were analyzed by Scanning Electron Microscopy (SEM) and Transmission Electron Microscopy (TEM). SEM micrographs were recorded on a JEOL JSM-7500F SEM at an operation voltage of 2.00 kV. A 10 µl drop sample was placed onto a cover glass, dried at room temperature, and sputtered with a platinum layer under vacuum for 90 s. TEM micrographs were recorded on a JEOL 3010 TEM operating at an accelerating voltage of 300 kV. A 10 µl drop sample was placed on a Formvar®/carbon coated TEM-grid (300 Mesh 3.05 mm Copper, Plano GmbH) and dried at room temperature before imaging.

ACKNOWLEDGEMENTS

Parts of the project were supported by an *ERC* starting grant (A.H.), and by the *BMBF ERA-NET* grant NanoSyn (W.J.P.). Azhar Z. Abbasi is grateful to HEC Pakistan / DAAD Germany for a fellowship. The research in the group of B.P. was supported by the *Netherlands Proteomics Centre (NPC*). The help of Alessio Marcozzi with preparing the graphics is gratefully acknowledged.

REFERENCES

[1] R. Langer, D. A. Tirrell, *Nature.* **2004**, *428*, 487-492.

[2] J. M. Dang, K. W. Leong, *Adv. Drug Deliv. Rev.* **2006**, *58*, 487-499.

[3] U. K. Slotta, S. Rammensee, S. Gorb, T. Scheibel, *Angew. Chem.-Int. Edit.* **2008**, *47*, 4592-4594.

[4] H. Y. Bai, K. Xu, Y. J. Xu, H. Matsui, *Angew. Chem.-Int. Edit.* **2007**, *46*, 3319-3322.

[5] H. Jia, C. Wong Po Foo, D. L. Kaplan, *Poly. Rev.* **2007**, *47*, 29-62.

[6] A. Chilkoti, T. Christensen, J. A. MacKay, *Curr. Opin. Chem. Biol.* **2006**, *10*, 652-657.

[7] K. Trabbic-Carlson, L. Setton, A. Chilkoti, *Biomacromolecules.* **2003**, *4*, 572-580.

[8] J. Gosline, M. Lillie, E. Carrington, P. Guerette, C. Ortlepp, K. Savage, *Philos.Trans.R.Soc.Lond. Ser.B-Biol.Sci.* **2002**, *357*, 121-132.

[9] L. L. del Mercato, G. Maruccio, P. P. Pompa, B. Bochicchio, A. M. Tamburro, R. Cingolani, R. Rinaldi, *Biomacromolecules.* **2008**, *9*, 796-803.

[10] D. E. Meyer, A. Chilkoti, *Biomacromolecules.* **2002**, *3*, 357-367.

[11] W. Y. Wu, C. Mee, F. Califano, R. Banki, D. W. Wood, *Nat. Protoc.* **2006**, *1*, 2257-2262.

[12] U. L. Lao, J. Kostal, A. Mulchandani, W. Chen, *Nat. Protoc.* **2007**, *2*, 1263-1268.

[13] H. Betre, L. A. Setton, D. E. Meyer, A. Chilkoti, *Biomacromolecules.* **2002**, *3*, 910-916.

[14] M. R. Dreher, W. G. Liu, C. R. Michelich, M. W. Dewhirst, F. Yuan, A. Chilkoti, *J. Natl. Cancer Inst.* **2006**, *98*, 335-344.

[15] T. A. T. Lee, A. Cooper, R. P. Apkarian, V. P. Conticello, *Adv. Mater.* **2000**, *12*, 1105-+.

[16] A. Girotti, J. Reguera, F. J. Arias, M. Alonso, A. M. Testera, J. C. Rodriguez-Cabello, *Macromolecules.* **2004**, *37*, 3396-3400.

[17] D. W. Lim, K. Trabbic-Carlson, J. A. MacKay, A. Chilkoti, *Biomacromolecules.* **2007**, *8*, 1417-1424.

[18] L. D. Muiznieks, F. W. Keeley, *J.Biol.Chem.* **2010**, *285*, 39779-39789.

[19] D. W. Urry, *J. Protein Chem.* **1988**, *7*, 1-34.

[20] M. Miao, C. M. Bellingham, R. J. Stahl, E. E. Sitarz, C. J. Lane, F. W. Keeley, *J. Biol. Chem.* **2003**, *278*, 48553-48562.

[21] E. Donath, G. Sukhorukov, F. Caruso, S. Davis, H. Mohwald, *Angew.Chem.-Int.Edit.* **1998**, *37*, 2202-2205.

[22] M. F. Bedard, B. G. De Geest, A. G. Skirtach, H. Moehwald, G. B. Sukhorukov, *Adv.Colloid Interface Sci.* **2010**, *158*, 2-14.

[23] P. Rivera Gil, L. L. del Mercato, P. del-Pino, A. Munoz-Javier, W. J. Parak, *Nano Today.* **2008**, *3*, 12-21.

[24] B. De Geest, R. Vandenbroucke, A. Guenther, G. Sukhorukov, W. Hennink, N. Sanders, J. Demeester, S. De Smedt, *Adv Mater.* **2006**, *18*, 1005-+.

[25] P. Rivera-Gil, S. De Koker, B. G. De Geest, W. J. Parak, *Nano Lett.* **2009**, *9*, 4398-4402.

[26] A. P. R. Johnston, L. Lee, Y. Wang, F. Caruso, *Small.* **2009**, *5*, 1418-1421.

[27] Y. Zhu, W. Tong, C. Gao, H. Moehwald, *J.Mater.Chem.* **2008**, *18*, 1153-1158.

[28] W. Qi, L. Duan, K. Wang, X. Yan, Y. Citi, Q. He, J. Li, *Adv Mater.* **2008**, *20*, 601-+.

[29] D. Volodkin, A. Petrov, M. Prevot, G. Sukhorukov, *Langmuir.* **2004**, *20*, 3398-3406.

[30] A. C. Hunter, *Adv.Drug Deliv.Rev.* **2006**, *58*, 1523-1531.

[31] N. Seiler, F. Raul, *J.Cell.Mol.Med.* **2005**, *9*, 623-642.

[32] D. Fischer, Y. Li, B. Ahlemeyer, J. Krieglstein, T. Kissel, *Biomaterials.* **2003**, *24*, 1121-1131.

[33] M. S. Lawrence, K. J. Phillips, D. R. Liu, *J. Am. Chem. Soc.* **2007**, *129*, 10110-+.

[34] V. N. Uversky, J. R. Gillespie, A. L. Fink, *Proteins.* **2000**, *41*, 415-427.

[35] U. Laemmli, *Nature.* **1970**, *227*, 680-&.

[36] C. Lee, A. Levin, D. Branton, *Anal. Biochem.* **1987**, *166*, 308-312.

[37] J. O'Brien, I. Wilson, T. Orton, F. Pognan, *Eur.J.Biochem.* **2000**, *267*, 5421-5426.

[38] O. Kreft, A. M. Javier, G. B. Sukhorukov, W. J. Parak, *Journal of Materials Chemistry.* **2007**, *17*, 4471-4476.

Chapter 3

A Minimally Interfering Approach to Restore and Improve Biolubrication

Deepak H. Veeregowda, Anke Kolbe, Henny C. van der Mei, Henk J. Busscher, Andreas Herrmann, and Prashant K. Sharma

Insufficient biolubrication is an increasingly acute medical problem around the world. [1-3] *It may impede proper speech, mastication and swallowing, underlie excessive friction and wear of articulating cartilage surfaces in hips and knees, cause vaginal dryness and result in dry, irritated eyes. Treatment with current biomimetic lubricants is inadequate for properly restoring the biolubrication necessary for growing number of patients. Here, we introduce a new strategy to address this need using non-toxic and biocompatible recombinant supercharged, unfolded proteins (SUPs) containing 36 (K36) or 72 (K72) positive charges and based on elastin-like polypeptides. These materials rejuvenate lubrication through naturally occurring salivary conditioning films (SCFs), a mechanism explained using surface analytical techniques. Adsorbed K36 and K72 bind with glycosylated mucins in SCFs through electrostatic interactions and induce rigidity in the film to a degree that correlates with the amount of positive charge. The extra charges in the case of K72 present residual cations in the SCFs that await further electrostatic interactions. Upon renewed exposure to saliva the K72 cations recruit negatively charged glycosylated mucins from saliva to create a soft, hydrated film. Such SCFs are marked by structural rigidity, long-range repulsive forces and a higher degree of glycosylation, which together result in effective biolubrication. Furthermore, we identify a friction force signature for the SCFs containing K72 unique among other lubricants, indicating particularly high inherent structural stability for lasting lubrication. Thus cationic SUPs represent a minimally interfering, novel therapeutic modality to improve biolubrication when availability of naturally occurring proteins is reduced.*

Biolubrication is an essential feature of health and can become impaired in the elderly or diseased. Sjögren's syndrome,[4] for instance, is a disease causing a variety of symptoms like dry eyes,[2] dry mouth,[3] vaginal dryness[5] and excessive friction and wear at the knee and hip joints.[6] Biolubrication is mediated by glandular secretions containing (glyco-)proteins that adsorb at the sliding interface and form a so-called conditioning film. Although water forms the basis of all biolubrication phenomena, it is easily removed from in between sliding surfaces during physiological activities associated with high contact pressures. To counter this, conditioning films providing biolubrication contain different glycoproteins that retain water molecules to generate repulsive hydration forces at the interface of the sliding surfaces.[7,8] Oral lubrication by adsorbed salivary conditioning films (SCFs) is essential to facilitate speaking and mastication and protects against wear due to erosion and abrasion.[7,9,10] Maintenance of adequate biolubrication in the oral cavity is not only challenged by disease and aging, but also by high contact pressures. Contact pressures on molar surfaces during mastication can be as high as 86 MPa which is one order of magnitude higher than the pressures experienced in hip and knee joints.[8,11] This load makes the maintenance and restoration of lubrication more challenging in the oral cavity than in other parts of the human body where articulating surfaces are involved.

Often, oral dryness is due to insufficient retention of water molecules in adsorbed SCFs due to low salivary flow rates (< 1 ml min^{-1}) or dysfunction of a particular salivary gland.[12] Patients suffering from oral dryness symptoms are treated with artificial salivas, often containing lubricants like pig gastric mucins, polyacrylic acid and carboxymethyl cellulose.[13] However, artificial salivas only yield temporary relief in patients, as the adsorbed conditioning films are unable to sufficiently retain water due to lack of structural integrity.

Intrigued by the facts that cationic polyelectrolytes are able to improve the mechanical strength of polysaccharide multilayers[14] and can form polymer-brush like structures,[15] we tested their ability to act as additive to improve oral lubrication. Among the existing polyelectrolytes, recombinant supercharged unfolded proteins (SUPs) derived from elastin-like polypeptides (ELPs) constitute an attractive group of proteins that may assist in restoring biolubrication. Not only can cationic SUPs interact with the negatively charged, naturally occurring mucins, they also possess significantly lower cytotoxicity than other cationic polyelectrolytes commonly used in biomedical applications.[16] Moreover, they are well-defined with respect to their length, composition and charge density and are broken down into non-toxic, naturally occurring amino acids upon digestion. However, the potential of SUPs to improve biolubrication and mechanical strength of naturally occurring conditioning films has to be investigated.

The aim of this study is to evaluate the role of SUPs with 36 (K36) and 72 (K72) positive charges in modifying the lubrication of adsorbed SCFs. A quartz crystal microbalance with dissipation monitoring (QCM-D) was used to examine changes in SCF structure after K36 and K72 adsorption and renewed exposure to saliva. Colloidal probe atomic force microscopy (AFM) was applied to determine friction and repulsive force characteristics and topography of the SCFs. Finally, X-ray photoelectron spectroscopy (XPS) was used to determine their degree of glycosylation.

RESULTS

Cationic SUPs based on ELPs consist of repeats of five amino acids, containing the aliphatic residues glycine (G), valine (V), proline (P), and positively charged lysine (K). The gene sequence of the *SUP monomer* gene *SUP K9*, which encodes for the polypeptide sequence [(GVGVP)(GKGVP)$_9$], and oligomerization of the gene are described in the supplementary information (supplementary Figures S1 and S2). After oligomerization, *SUP* genes encoding for [(GVGVP)(GKGVP)$_9$]$_4$ (K36) and [(GVGVP)(GKGVP)$_9$]$_8$ (K72) were cloned into a modified bacterial expression vector, pET25b(+)-*Sfi*IHis6, and successfully expressed in *E. coli*. SUPs were purified from the crude cell extract by affinity and ion exchange chromatography. Protein integrity and purity were confirmed by gel electrophoresis and mass spectrometry (supplementary Figure S3). Typical yields were 45 mg (K36) and 40 mg (K72) of purified recombinant protein per liter of culture.

The formation of SCFs on gold (Au) coated quartz crystals and the effects of their exposure to recombinant K36 and K72 or buffer, followed by renewed adsorption of salivary proteins, were observed real-time in the QCM-D, as presented in Figure 1a-c. Exposure of an existing SCF to buffer (Figure 1a) yielded a small change in the oscillating sensor frequency (Δf_3) and dissipation (ΔD_3), whereas exposure to K36 (Figure 1b) and K72 (Figure 1c) solutions caused significant decreases in Δf_3 and ΔD_3 that were largest for K72. Subsequent removal of the protein solution by perfusing the QCM-D chamber with buffer indicated a structural decrease in the softness of the SCFs, expressed as the ratio ($\Delta D_3/\Delta f_3$). Again, this effect was larger after exposure to K72 solution than after exposure to K36 solution (Figure 1d). Renewed salivary exposure over the SCFs was initiated immediately after treatment with buffer or recombinant protein solutions (Figure 1a-c) because such experimental conditions reflect best the *in vivo* situation of immediate reflow of saliva in the oral cavity. Renewed perfusion of the QCM-D chamber with saliva did not affect the structural

softness of the SCF exposed to buffer (Figure 1d), but salivary films formed on SCFs exposed to K36 solution became softer again to a level comparable to buffer exposed SCFs. The SCFs formed on films with adsorbed K72, however, were significantly ($p < 0.05$, two tailed Student t-test) softer than SCFs formed after exposure to buffer or adsorption of K36. Bare Au coated QCM crystals have a smooth surface (supplementary Figure S4a), presenting uneven, globular structures upon adsorption of salivary proteins (supplementary Figure S4b) with maximal heights of around 22 nm. Similar structures are observed when adsorbed K36 or K72 are part of the SCF, but their heights differ considerably from 16 nm for films comprising K36 to 32 nm when K72 is involved (supplementary Figure S4c, d).

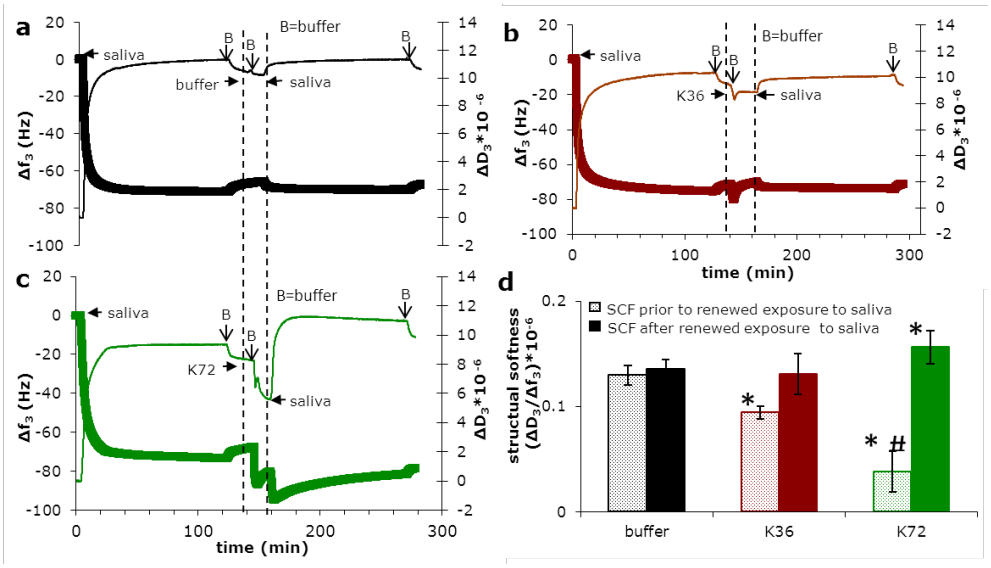

Figure 1. Influence of adsorption of recombinant cationic proteins and renewed exposure to saliva on the softness of salivary conditioning films. (a, b, c) Examples of the QCM-D response as a function of time to protein adsorption from saliva on Au coated quartz crystal surfaces, subsequent adsorption to cationic recombinant proteins (2 min) and renewed exposure to salivary proteins, expressed as changes in third harmonic frequency (Δf3, thick line) and dissipation (ΔD3, thin line), together with structural softness of the adsorbed films. (a) buffer/ no recombinant protein adsorption; (b) adsorption of recombinant K36 and; (c) adsorption of recombinant K72. (d) Structural softness of salivary conditioning films after with and without ("buffer") adsorbed recombinant cationic proteins and renewed exposure to saliva. Error bars represent the standard deviation over five independent measurements. Statistically significant ($p < 0.05$, two tailed Student t-test) differences in softness of films with adsorbed K36 or K72 with respect to control films are indicated by *. Differences in softness between films with adsorbed K72 and K36 are indicated by #.

In a next step, the lubrication properties of the SUP-modified films were investigated by colloid probe AFM. Friction forces on bare Au-coated crystals increased linearly ($R^2 = 0.95$) with normal force up to 35 nN, corresponding to a coefficient of friction (COF) of 0.28 (Figure 2a). Upon adsorption of a SCF, friction forces appeared almost two times lower than on Au coated crystals with a COF of 0.19, and linearity broke down at normal forces above 14 nN. Note that the negative friction forces at a normal force of 1.5 nN represent the known limitation of AFM to measure very low friction forces.[17] However, measurements on SCF after recombinant protein adsorption and subsequent exposure to saliva clearly showed still lower friction forces (Figure 2b). Linearity corresponding with a COF of 0.08 persisted up to a normal force of 20 nN for K36, while linearity ($R^2 = 0.94$) corresponding to an extremely low COF of 0.06 existed over the entire range of normal forces applied for K72-modified films, indicative of a high structural integrity. Contact of the AFM colloidal probe with the Au-coated quartz crystal (Figure 2c) shows a hard material compared with the softer SCFs due to long-range repulsive forces between SCFs and the approaching colloidal probe. The repulsive force range arising from the SCFs increased with the number of positive charges after adsorption of recombinant cationic SUPs (Figure 2c). To gain more insight into the structural composition of the modified SCFs, XPS was applied to measure the degree of glycosylation, which is related to the water content of the surface (see Figure 2d and supplementary Table S1). Glycosylation in the SCFs with no adsorbed SUPs amounts to 5.8 ± 0.8 % and increases with the molecular weight of the adsorbed SUPs to 6.9 ± 0.3% and 7.2 ± 0.6 % in SCFs with K36 and K72, respectively.

DISCUSSION

From the measurements described above one can conclude that cationic recombinant SUPs adsorb on SCFs and decrease their structural softness, i.e. increase their rigidity. SUPs carrying more positive charges create more rigid films, and more efficiently recruit salivary proteins to form a SCF with thicker globular structure and higher degree of glycosylation, generating a longer repulsive force range and more stable, low friction.

Patients with oral dryness symptoms have reduced salivary flow rates, but naturally occurring salivary proteins are always present. This study is the first in which naturally occurring salivary proteins are recruited through the adsorption of recombinant, cationic proteins to improve several parameters crucial for effective biolubrication. Our approach represents a groundbreaking strategy for artificial biolubrication, where

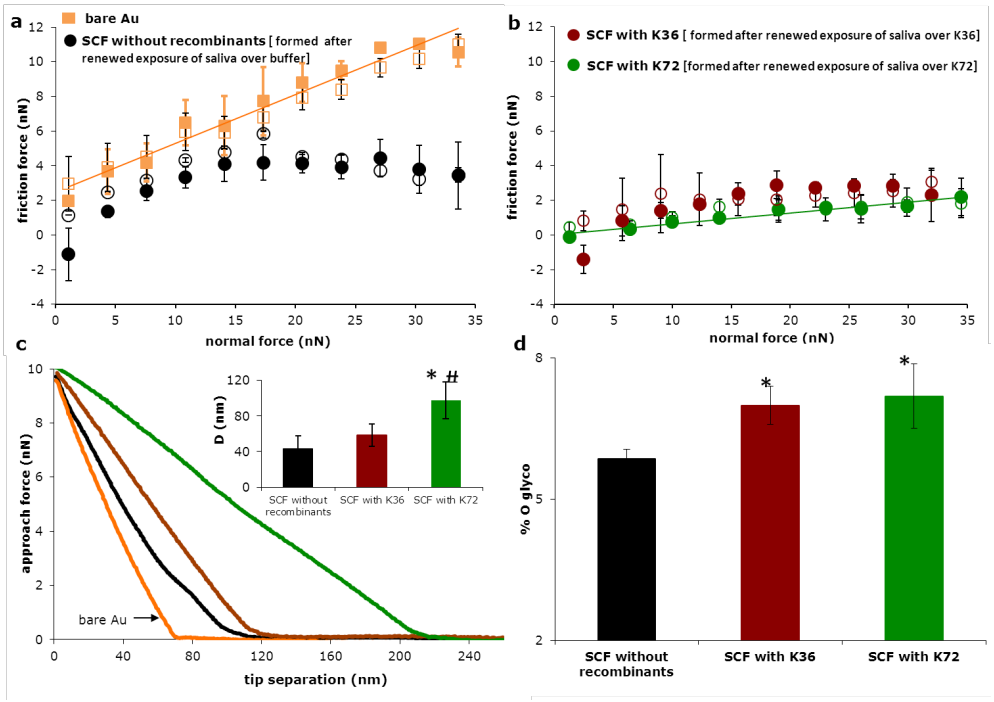

Figure 2. Influence of adsorption of recombinant cationic proteins and renewed exposure to saliva on the friction forces, repulsive force upon approach and glycosylation of salivary conditioning films. (a, b) Friction force as a function of normal force during increasing (closed symbols) and decreasing (open symbols) normal forces. (a) bare Au coated QCM crystal and SCF without adsorbed recombinant cationic proteins; (b) SCFs with adsorbed recombinant cationic proteins K36 or K72 and after renewed exposure to salivary proteins. Error bars on all the friction forces represent standard deviation over 12 measurements. (c) Example of the repulsive force as a function of tip separation distance for bare Au coated QCM crystals, SCF without adsorbed recombinant cationic proteins and with adsorbed K36 or K72. The repulsive force range (D) for all adsorbed protein films is calculated with respect to hard contact recorded on bare Au coated crystal surface (inset of Fig. 2c). Error bars represent the standard deviations over 30 force curves. (d) The degree of glycosylation ($\%O_{glyco}$) for SCFs without adsorbed recombinant cationic proteins and with adsorbed K72 or K36, obtained from a decomposition of the O_{1s} photoelectron peak in XPS. Error bars represent the standard deviations over three independent XPS measurements on differently prepared samples. Statistically significant ($p < 0.05$, two tailed Student t-test) differences in repulsive force range (c) and glycosylation (d) of SCF with K36 or K72 with respect to SCF in absence of adsorbed recombinant proteins are indicated by *signs. Differences in repulsive force range between SCF with adsorbed K36 or K72 are indicated by #sign.

additives act in concert with and enhance the natural lubricants rather than simply replacing them. A proof of principle was obtained for oral lubrication, the most

challenging environment for biolubrication, but similar recruitment mechanisms may be applied in other parts of the human body as well.

SCF is composed of glycosylated, high-molecular weight mucins that adsorb in loops and trains and thereby provide a scaffold to hold and retain water molecules at the surface, while adsorbed smaller proteins like proline-rich proteins, histatins, lysozymes, and amylases may be found underneath the loops and between the trains (Figure 3a).[18] Based on the measurements presented above, we suggest a model for the interaction of cationic SUPs with an existing SCF and for how the adsorbed cationic proteins may be further involved in the recruitment of salivary proteins during renewed exposure of saliva. K36 and K72 bind to the negatively charged mucins leading to elimination of electrostatic stabilization of the adsorbed film and its subsequent collapse, forming a rigid structure (Figure 3b). K72 is a polypeptide consisting of more than 400 amino acids with 72 positively charged groups evenly distributed along the polymer backbone. The higher number of positive charges in K72 compared with K36 neutralizes more negative charges in the SCF and positive charges of adsorbed K72 remain available for further interactions with negative charges. This can be concluded from zeta potential measurements (supplementary Figure S5), showing more positive charges on SCFs exposed to K72 than on K36-treated and untreated SCFs. Thus, uncompensated positive surface charges of adsorbed K72 on a SCF can trigger further recruitment of negatively charged glycosylated mucins during renewed exposure to saliva (Fig. 3b; right panel), resulting in a softer highly hydrated over-layer (Figure 3c). This recruitment process rejuvenates the film, as it can bind to more water molecules. This is one critical step beyond simply restoring the film structure, as observed in SCFs formed after reflow of saliva over K36-treated and buffer-treated SCFs. Note that an analogous layer-by-layer assembly of bovine mucins using chitosan as a cationic polyelectrolyte has been demonstrated previously.[19]

The rigid and hydrated SCF, modified with adsorbed K72 and after renewed exposure to saliva, shows low friction forces and a structural integrity that is not compromised at higher contact pressures, in contrast to films containing K36 or untreated films. The breakdown of structural integrity in these latter films can be seen from a discontinuity in the linearity of friction force against the normal force.[20,21] In order to determine the mechanical strength of the SCFs, we have applied Von Mises distortion energy criterion that relates the normal force at which the discontinuity arises (f_L) to the yield strength (σ_y) of the films[21,22] through

$$\sigma_y = \frac{1}{\sqrt{2}}\left[2\left(\frac{3*f_L}{2*\pi*R_{tip}*\delta}\right)^2 + 6\left(\frac{3*f_f}{2*\pi*R_{tip}*\delta}\right)^2\right]^{0.5} \quad (1)$$

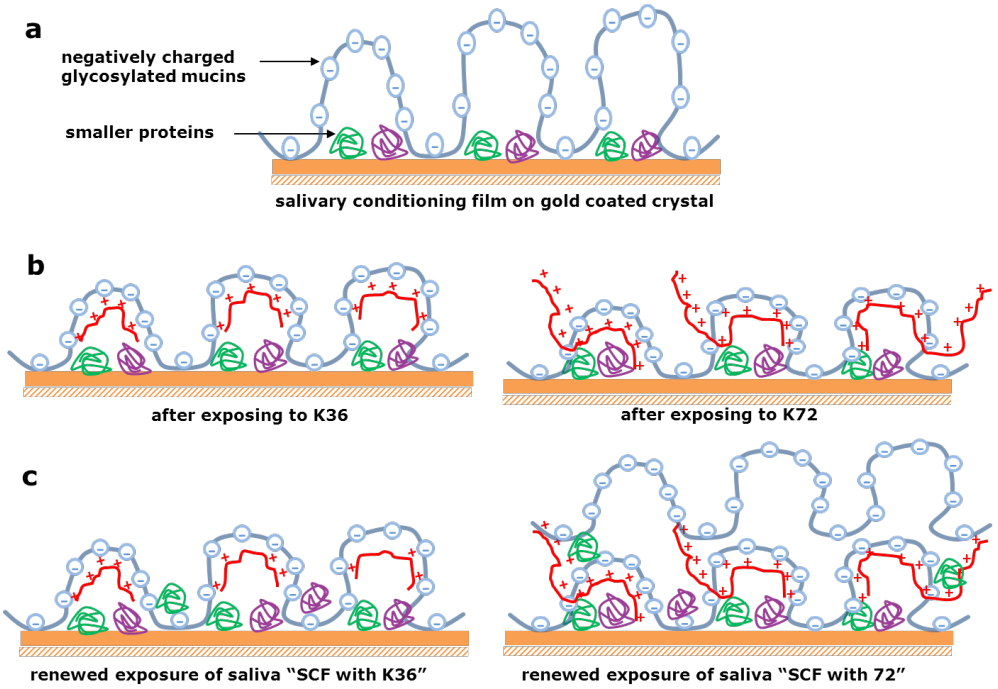

Figure 3. Architecture of salivary conditioning films after adsorption of recombinant cationic proteins with different numbers of positive charges and renewed exposure to saliva. (a) Adsorbed salivary conditioning film, showing glycosylated mucins adsorbed in loops and trains over a layer of adsorbed densely packed low-molecular weight proteins, including proline-rich proteins, histatins and lysozymes. (b) Salivary conditioning films after adsorption of K36 (left panel) and K72 (right panel). Recombinant cationic proteins interact with the negatively charged glycosylated mucins, causing collapse of the glycosylated structure through electrostatic interaction. In case of K72, not all positive charges engaged with the mucins and remain available for further interaction (right panel). (c) Salivary conditioning films with adsorbed cationic proteins and after renewed exposure to saliva. No mucins are recruited in the presence of adsorbed K36 (left panel), but remaining positive charges in the film possessing adsorbed K72 recruit mainly glycosylated mucins to form a soft mucinous layer over a compact SCF (right panel).

where, R_{tip} is the radius of the colloidal tip (2.25 µm), δ is the elastic displacement of the film determined from a Hertzian fit to the force-distance curves as obtained by colloidal probe AFM and f_f is the friction force at f_L. Accordingly, yield strength for SCF in absence of recombinant cationic SUPs is 80 ± 12 kPa, increasing to 102 ± 8

kPa in the presence of adsorbed K36. In contrast, no discontinuity in the linearity of friction force against the normal force was observed for K72-treated films within the range of normal forces applied, indicating that the yield strength of SCFs in presence of K72 exceeds 102 kPa.

An ideal biolubricant-like artificial saliva should lubricate the oral surfaces and at the same time sustain this lubrication for lasting benefits. Here we demonstrate that non-toxic, recombinant cationic SUPs adsorb on SCFs to recruit further glycosylated mucins from saliva, provided the number of positive charges is sufficiently high. These hydrated and rigid films improve interfacial lubrication and maintain their structural integrity upon high contact pressures. Current generations of artificial salivas are inadequate to restore oral lubrication on a lasting basis. Cationic recombinant SUPs as additives, however, go even beyond restoration to rejuvenation of the film, affording effective lubrication under conditions of reduced availability of naturally occurring proteins. On the basis of the cooperative layer-by-layer mechanism laid out here, cationic protein polyelectrolytes show great promise for a minimally interfering treatment of impaired biolubrication.

EXPERIMENTAL PART

Design, development and characterization of recombinant cationic proteins

Materials

All chemicals were used as received without any further purification. The pUC19 cloning vector, restriction enzymes, and GeneJET™ Plasmid Miniprep kit were purchased from Fermentas (St. Leon-Rot, Germany). T4 DNA ligase and antarctic phosphatase were obtained from New England Biolabs (Ipswich, MA). Digested DNA fragments were purified using QIAquick® spin miniprep kits from QIAGEN, Inc. (Valencia, CA). *E.coli* XL1-Blue competent cells for plasmid amplification were purchased from Stratagene (La Jolla, CA). *E.coli* BLR(DE3) competent cells were purchased from Novagen Inc. (San Diego, CA). Oligonucleotides for sequencing were ordered from Sigma-Aldrich (St. Louis, MO). A-cyano-4-hydroxycinnamic acid and internal standards trypsinogen and enolase for mass spectrometry were purchased from LaserBio Labs (Sophia-Antipolis, France). Ultrapure water, resistivity > 18 MΩ·cm, was used for all experiments.

Gene oligomerization and expression vector construction

Integrity of the DNA sequence was verified by sequencing of coding and complementary DNA strand after each cloning step (SequenceXS, Leiden, The

Netherlands). *SUP monomer* gene *SUP K9*, encoding for the polypeptide [GVGVP $(GKGVP)_9$], was ordered from Entelechon (Regensburg, Germany) and was delivered in the pEN vector. The gene sequence and the respective amino acid sequence of the monomer are shown in supplementary Figure S1. As the recognition sites of the restriction endonucleases *Pfl*MI and *Bgl*I had to be preserved, one valine residue per ten pentapeptide repeats was incorporated instead of a lysine residue. All cloning steps were performed according to standard molecular biology methods. *SUP K9* was transferred into the standard cloning vector pUC19, digested with *Eco*RI and *Hin*DIII. Plasmids were isolated and positive clones were verified by plasmid digestion with *Eco*RI and *Hin*DIII and subsequent gel electrophoresis. Gene oligomerization was performed as described by Chilkoti and co-workers.[23] Genes of correct length were identified by gel electrophoresis following plasmid digestion with *Eco*RI and *Hin*DIII (supplementary Figure S2) and by sequencing (ServiceXS, Leiden, The Netherlands).

Genes coding for K36 and K72 were cloned into the expression vector pET25b(+)-*Sfi*IHis6 as described before.[16] Positive clones were identified by gel electrophoresis following plasmid digestion with *Eco*RI and *Hin*DIII and by sequencing.

Protein expression and purification

E.coli BLR (DE3) cells were transformed with pET25b(+)-*Sfi*IHis6 containing the respective *SUP* genes. For protein production, Terrific Broth medium (for 1 L, 12 g tryptone and 24 g yeast extract) enriched with phosphate buffer (for 1 L, 2.31 g potassium phosphate monobasic and 12.54 g potassium phosphate dibasic) and glycerol (4 mL per 1 L TB), and supplemented with 100 µg/mL ampicillin was inoculated with an overnight starter culture to an initial optical density at 600 nm (OD_{600}) of 0.1 and incubated at 37 °C with orbital agitation at 250 rpm until OD_{600} reached 0.7. Cultures were shifted to 30°C and continued for additional 16 h. Cells were subsequently harvested by centrifugation (7,000 x *g*, 20 min, 4 °C), resuspended in lysis buffer (10 mM TrisHCl buffer, pH 8.0, 300 mM NaCl, 20 mM imidazole) to an OD_{600} of 100 and disrupted with a constant cell disrupter (Constant Systems Ltd., Northands, UK). Cell debris was removed by centrifugation (40,000 x *g*, 90 min, 4 °C). Proteins were purified from the supernatant under native conditions by Ni-sepharose chromatography (GE Healthcare). Protein-containing fractions were dialyzed extensively against ultrapure water (resistivity >18 MΩ cm). Purified proteins were frozen in liquid nitrogen, lyophilized and stored at -17 °C until further use.

Protein characterization

Concentrations of purified SUPs were determined by measuring absorbance at 280 nm on a SpectraMax M2 (Molecular Devices, Sunnyvale, CA). Protein purity was

determined by sodium dodecyl sulfate polyacrylamide gel electrophoresis (SDS-PAGE) on a 12% polyacrylamide gel according to Laemmli.[24] Gels were stained with coomassie staining solution (40% methanol, 10% glacial acetic acid, 1 g/L Brilliant Blue R250). Photographs of the gels were taken with a LAS-3000 Image Reader (Fuji Photo Film (Europe) GmbH, Dusseldorf, Germany) (supplementary Figure S3a). Both K36 and K72 showed reduced electrophoretic mobility compared to a commercial molecular weight standard, a well-known phenomenon for elastin-like polypeptides.[23,25] Mass spectrometric analysis was performed using a 4800 MALDI-TOF/TOF Analyzer (Applied Biosystems, Foster City, CA, USA) in the linear positive mode. The protein samples were mixed 1:1 v/v with a recrystallized a-cyano-4-hydroxycinnamic acid matrix (10 mg/mL in 50% ACN and 0.1% TFA, LaserBio Labs). Mass spectra were analyzed and calibrated internally with the Data Explorer software, version 4.9 (Applied Biosystems, Foster City, CA, USA). Trypsinogen (MW = 23980) and enolase (MW = 46672) were used as calibration standards for K36 (expected MW = 18,888) and K72 (expected MW = 36,313), respectively. Mass spectra yielded sharp peaks for both variants (supplementary Figure S3 b and c). Determined masses were 18,932 +/- 20 Da for K36 and 36,330 +/- 30 Da for K72.

Saliva collection

Human whole saliva from twenty healthy volunteers (10 men, 10 women, average age 30 ± 8 years) was collected into ice-chilled cups after stimulation of salivary flow by chewing Parafilm®. Volunteers gave their informed consent to saliva donation, in agreement with the guidelines set out by the Medical–Ethical-Committee at the University-Medical-Center-Groningen, The Netherlands. After saliva was pooled and centrifuged at 12,000 g, 15 min, 4°C, phenylmethylsulfonylfluoride was added to a concentration of 1 mM as a protease inhibitor. The solution was again centrifuged, dialyzed for 24 h, 4°C against demineralized water, and freeze-dried for storage. Lyophilized stock was prepared by mixing freeze-dried material originating from 2 L of saliva. Reconstituted saliva was prepared from the lyophilized stock by dissolution of 1.5 mg/mL in buffer (2 mM potassium phosphate, 1 mM $CaCl_2$, 50 mM KCl, pH 6.8).

Quartz crystal microbalance with dissipation monitoring (QCM-D)

Structural softness and formation kinetics of SCFs were studied using a QCM-D device, model Q-sense E4 (Q-sense, Gothenburg, Sweden). Au-coated quartz crystals with 5 MHz were used as substrata. Before each experiment, crystals were cleaned by 10 min UV/ozone treatment, followed by immersion into a 3:1:1 mixture of ultrapure water, NH_3 and H_2O_2 at 70°C for 10 min, drying with N_2 and another UV/ozone treatment. The QCM-D chamber is disc-shaped with the inlet and outlet

facing the crystal surface. The chamber was perfused with buffer by a peristaltic pump (Ismatec SA, Glattbrugg, Switzerland). When stable base lines for both frequency and dissipation at third harmonics were achieved, saliva was introduced. Saliva was perfused through the chamber at 25°C for 2h at a flow rate of 50 µL/min, corresponding with a shear rate of 3 s^{-1} after which the chamber was perfused with buffer or 0.05% w/v of either K72 or K36 for 2 min, followed by another 2 h of salivary flow. In between steps, the chamber was perfused with buffer for 15 min. The shear rate in the QCM-D represents a low oral salivary flow.[26] Frequency and dissipation were measured real-time during perfusion.

After experiments, crystals were removed from the QCM-D and immediately used for further experiments. When needed for timing, saliva-coated Au crystals were kept hydrated in a closed environment with 100% humidity.

Colloidal Probe Atomic Force Microscopy

Friction force, surface topography and repulsive force range toward a colloidal[27] AFM probe were measured in buffer with an AFM (Nanoscope IV Dimension^{tm} 3100) equipped with a Dimension Hybrid XYZ SPM scanner head (Veeco, New York, USA) on the differently adsorbed SCFs. Rectangular, tipless cantilevers were calibrated for their torsional and normal stiffness using AFM Tune IT v2.5 software.[28] The normal stiffness (K_n) was between 0.01 - 0.04 N/m and the torsional stiffness (K_t) between 2 - 4 x 10^{-9} N m/rad. Subsequently, a silica particle of 4.74 µm diameter (d) (Bangs laboratories, Fishers, IN, USA) was glued to a cantilever with an epoxy glue (Pattex, Brussels, Belgium). The deflection sensitivity (α) of the colloidal probe was recorded at a constant compliance with bare crystal in buffer to calculate the normal force (F_n) applied using

$$F_n = \Delta V_n * \alpha * K_n \qquad (2)$$

where ΔV_n is the voltage output from the AFM photodiode due to normal deflection of the colloidal probe. The torsional stiffness and geometrical parameters of the colloidal probe were used to calculate the friction force (F_f) according to

$$F_f = \frac{\Delta V_L * K_t}{2\delta * (d + t/2)} \qquad (3)$$

where t is the thickness of the cantilever, δ is the torsional detector sensitivity of the AFM and ΔV_L corresponds to the voltage output from the AFM photodiode due to lateral deflection of the probe.[19,29] Lateral deflection was observed at a scanning angle of 90 degrees over a scan area of 5x5 µm^2 and a scanning frequency of 1 Hz.

The colloidal probe was incrementally loaded and unloaded up to a maximal normal force of 35 nN. At each normal force, 10 friction loops were recorded to yield the average friction force. Repulsive force-distance curves between a colloidal probe and the films were obtained at a trigger threshold force of 10 nN and at an approach and retraction velocity of 10 μm s^{-1}. The repulsive force range (D) was determined at a point where the colloidal tip starts experiencing the repulsive force > 1 nN between the two interacting surfaces.

X-ray Photoelectron Spectroscopy (XPS)

Glycosylation of the adsorbed SCFs was determined by using XPS (S-probe, Surface Science Instruments, Mountain View, CA, USA). Films adsorbed on crystals as removed from the QCM-D chamber, were dried in the pre-vacuum chamber of the XPS, and then subjected to a vacuum of 10^{-7} Pa. X-rays (10 kV, 22 mA, spot size 250 x 1000 μm) were produced using an aluminum anode. Scans in the binding energy range of 1-1100 eV were made at low resolution (pass energy 150 eV). The area under each peak was used to yield elemental surface concentrations for C, O, N, and Au after correction with sensitivity factors provided by the manufacturer. The O_{1S} peak was split into three components for oxygen involved in amide groups (C=O-N; 531.3 eV), carboxyl groups (C-O-H; 532.7 eV) and oxygen arising from the crystal. Accordingly, the fraction of the O_{1s} peak at 532.7 eV ($\%O_{532.7}$) was used to calculate the amount of oxygen involved in glycosylated moieties ($\%O_{glyco}$) and amides ($\%O_{amides}$).

$$\%O_{glyco} = \%O_{532.7} * \%O_{total} \quad (4)$$

$$\%O_{amide} = \%O_{531.3} * \%O_{total} \quad (5)$$

where $\%O_{total}$ is the total percentage of oxygen.

SUPPLEMENTARY INFORMATION

*Eco*RI *Pfl*MI

A ATT CAT ATG GGC CAC GGC GTG GGT GTT CCG GGC AAA GGT GTT CCG GGT AAA GGT GTG CCG

G V G V P G K G V P G K G V P

GGC AAA GGT GTT CCT GGT AAA GGT GTG CCG GGT AAA GGT GTG CCG GGT AAA GGT GTA CCA

G K G V P G K G V P G K G V P G K G V P

*Bgl*I *Hind*III

GGT AAA GGT GTT CCG GGT AAA GGC GTT CCG GTT AAA GGT GTG CCG GGC GGG CTG GAA TA

G K G V P G K G V P G K G V P

Figure S1. Recombinant supercharged unfolded proteins: Monomer gene *SUP K9*. Gene sequence and corresponding polypeptide sequence in amino acid one-letter code. Recognition sites for the restriction enzymes *Eco*RI, *Pfl*MI, *Bgl*I, and *Hind*III are underlined.

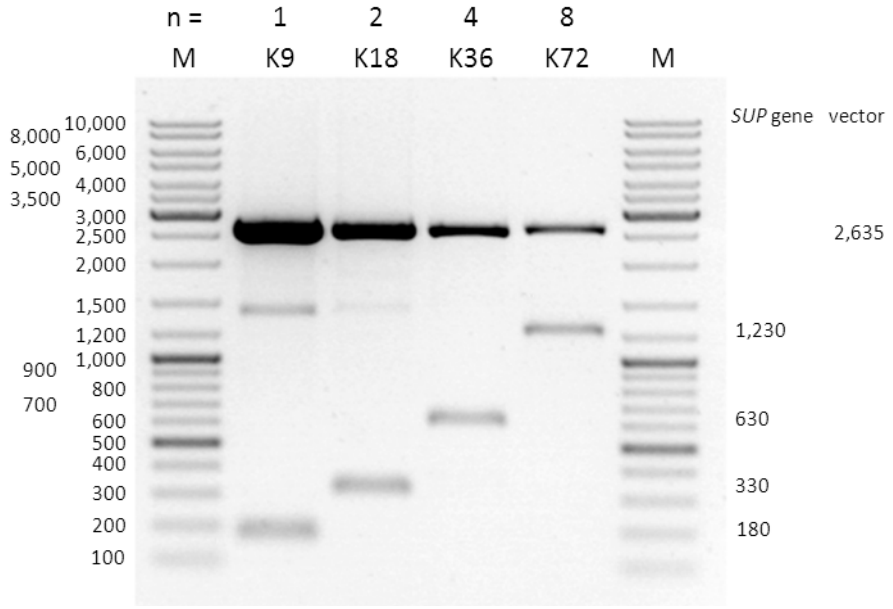

Figure S2. Gel electrophoresis of *SUP* genes encoding for positively supercharged elastin-like polypeptides. PUC vectors containing the *SUP* genes were digested with *Eco*RI and *Hin*DIII and separated on a 1% agarose gel. DNA bands were visualized by ethidium bromide staining. Digestion produced a vector fragment of 2,635 bp and a *SUP* gene fragment (size in bp is depicted on the right). n: number of repeats; K: lysine ; 9-72: number of charges in respective elastin-like polypeptide; M: size standard.

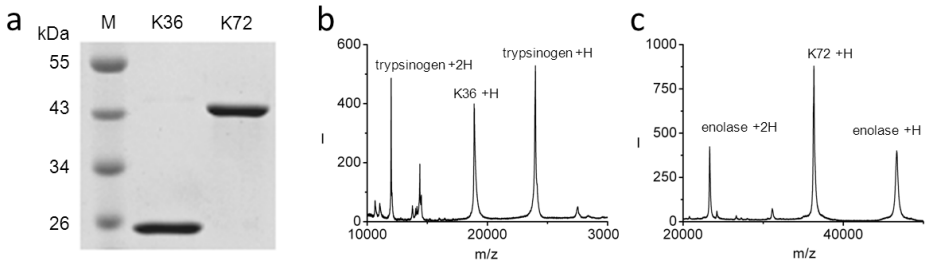

Figure S3. Characterization of recombinant supercharged unfolded proteins.
(a) Gel electrophoresis: Purified proteins were separated on a 12% SDS-PAGE gel and stained with Coomassie brilliant blue R250. M: size standard. Expected sizes were 18.9 kDa (K36) and 36.3 kDa (K72); (b-c) MALDI-TOF mass spectra. (b) K36 with internal standard trypsinogen (MW = 23981) and (c) K72 with internal standard enolase (MW = 46672). I = absolute intensity.

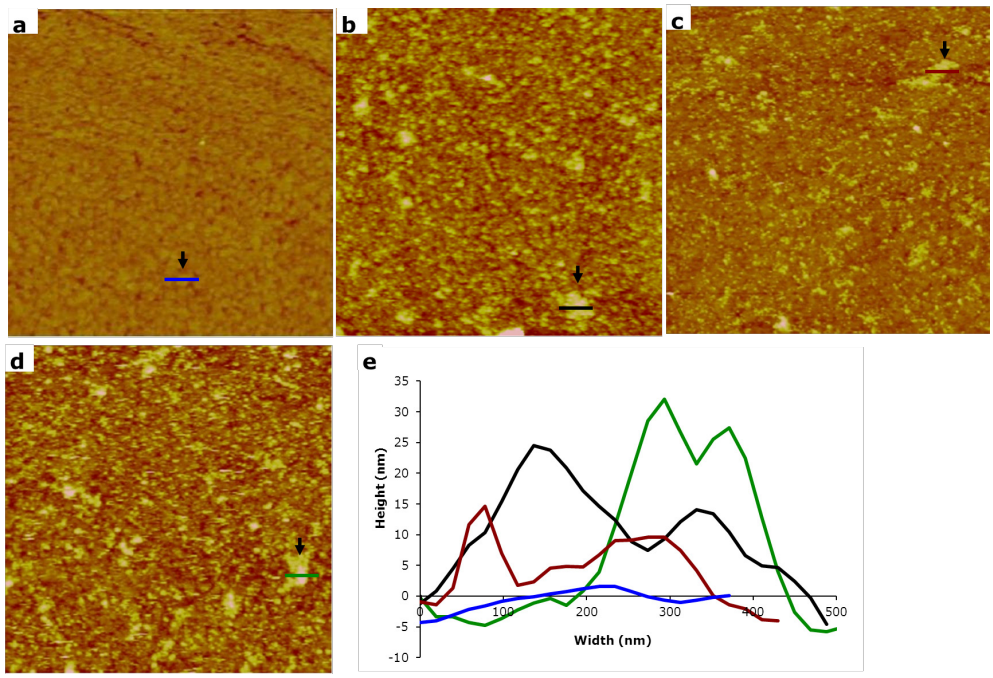

Figure S4. Surface topography of the surfaces as imaged by colloidal probe AFM. (a) Bare Au coated QCM crystal ; (b) SCF in absence of adsorbed recombinant cationic proteins; (c) SCF with adsorbed K36 and after renewed exposure to saliva; (d) SCF with adsorbed K72 and after renewed exposure to saliva; (e) height as a function of width of the globular structures found in the different adsorbed films.

Table S1. Elemental composition of the bare Au coated QCM crystals with and without an adsorbed SCF, and with SCF possessing adsorbed K36 or K72 after renewed exposure to saliva. ± indicates standard deviation over three measurements.

%	Au-coated QCM crystal		SCF without recombinants	SCF with K72	SCF with K36
C	41.3 ± 1.5		62.9 ± 2.9	62.9 ± 2.9	56.4 ± 1.40
N	Not detected		14.3 ± 1.2	13.9 ± 0.7	13.0 ± 0.4
O	O_{total}	11.7 ± 1.5	22.6 ± 1.8	24.1 ± 2.8	22.3 ± 1.9
	$\%O_{532.7}*O_{total}$	Not detected	5.8 ± 0.8	7.19 ± 0.6	6.9 ± 0.3
	$\%O_{531.2}*O_{total}$	Not detected	15.7 ± 1.7	16.8 ± 2.1	15.3 ± 1.5

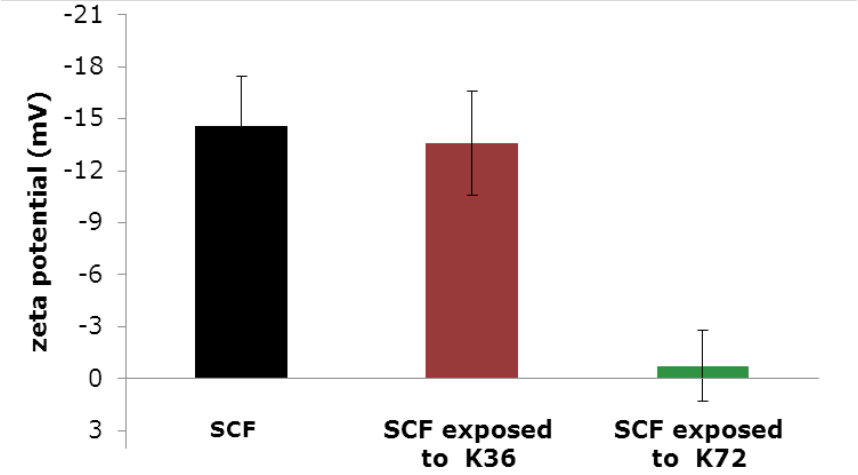

Figure S5. Zeta potentials of the SCFs in absence and presence of adsorbed SUPs. Silica spheres (diameter 970 nm) were coated with SCF by suspending in saliva for 2 h. Subsequently, the spheres were suspended in buffer or recombinant K36 or K72 solutions (0.05% w/v) for 2 min. After each coating step, the spheres were rinsed with buffer for 10 min. The zeta potential of the different spheres was measured in buffer (2 mM potassium phosphate, 1 mM $CaCl_2$, 50 mM KCl, pH 6.8) employing a Zetasizer nano series (Model Number ZEN3600, Malvern Ltd, UK). Error bars represent the standard deviation over three measurements with separately coated spheres.

REFERENCES

[1] J. M. Meijer, P. M. Meiners', J. J. R. H. Slater, F. K. L. Spijkervet, C. G. M. Kallenberg, A. Vissink, H. Bootsma, *Rheumatology.* **2009***, 48*, 1077-1082.

[2] E. K. Akpek, K. B. Lindsley, R. S. Adyanthaya, R. Swamy, A. N. Baer, P. J. McDonnell, *Ophthalmology.* **2011***, 118*, 1242-1252.

[3] C. M. Stewart, K. M. Berg, S. Cha, W. H. Reeves, *J.Am.Dent.Assoc.* **2008***, 139*, 291-299.

[4] D. W. Lim, D. L. Nettles, L. A. Setton, A. Chilkoti, *Biomacromolecules.* **2007***, 8*, 1463-1470.

[5] N. Schoofs, *Jognn-Journal of Obstetric Gynecologic and Neonatal Nursing.* **2003***, 32*, 589-593.

[6] C. T. Pease, W. Shattles, N. K. Barrett, R. N. Maini, *Rheumatology.* **1993***, 32*, 609-613.

[7] A. Joiner, A. Schwarz, C. J. Philpotts, T. F. Cox, K. Huber, M. Hannig, *J.Dent.* **2008***, 36*, 360-368.

[8] B. Dejak, A. Mlotkowski, M. Romanowicz, *J.Prosthet.Dent.* **2003***, 90*, 591-597.

[9] I. C. H. Berg, M. W. Rutland, T. Arnebrant, *Biofouling.* **2003***, 19*, 365-369.

[10] M. Hannig, M. Balz, *Caries Res.* **1999***, 33*, 372-379.

[11] K. C. Morrell, W. A. Hodge, D. E. Krebs, R. W. Mann, *Proc.Natl.Acad.Sci.U.S.A.* **2005***, 102*, 14819-14824.

[12] A. Mariotti, *The comprehensive pharmacology reference*, Elsevier, New York 2007.

[13] S. Hahnel, M. Behr, G. Handel, R. Buergers, *Supportive Care in Cancer.* **2009***, 17*, 1331-1343.

[14] M. Salomaki, J. Kankare, *Biomacromolecules.* **2009***, 10*, 294-301.

[15] U. Raviv, S. Giasson, N. Kampf, J. F. Gohy, R. Jerome, J. Klein, *Nature.* **2003***, 425*, 163-165.

[16] A. Kolbe, L. L. del Mercato, A. Z. Abbasi, P. Rivera-Gil, S. J. Gorzini, W. H. C. Huibers, B. Poolman, W. J. Parak, A. Herrmann, *Macromol.Rapid Commun.* **2011***, 32*, 186-190.

[17] L. Macakova, G. E. Yakubov, M. A. Plunkett, J. R. Stokes, *Colloids and Surfaces B-Biointerfaces.* **2010***, 77*, 31-39.

[18] O. Svensson, L. Lindh, M. Cardenas, T. Arnebrant, *J.Colloid Interface Sci.* **2006***, 299*, 608-616.

[19] T. Pettersson, A. Naderi, R. Makuska, P. M. Claesson, *Langmuir.* **2008***, 24*, 3336-3347.

[20] J. Yu, X. Banquy, G. W. Greene, D. D. Lowrey, J. N. Israelachvili, *Langmuir.* **2012***, 28*, 2244-2250.

[21] J. Sotres, A. Barrantes, T. Arnebrant, *Langmuir.* **2011***, 27*, 9439-9448.

[22] L. Y. Wang, Z. F. Yin, J. Zhang, C. I. Chen, S. Hsu, *Wear.* **2000***, 237*, 155-162.

[23] D. E. Meyer, A. Chilkoti, *Biomacromolecules.* **2002***, 3*, 357-367.

[24] U. K. Laemmli, *Nature.* **1970***, 227*, 680-&.

[25] D. T. McPherson, J. Xu, D. W. Urry, *Protein Expr. Purif.* **1996***, 7*, 51-57.

[26] S. Watanabe, C. Dawes, *J.Dent.Res.* **1990***, 69*, 1150-1153.

[27] W. A. Ducker, T. J. Senden, R. M. Pashley, *Nature.* **1991***, 353*, 239-241.

[28] T. Pettersson, N. Nordgren, M. W. Rutland, *Rev.Sci.Instrum.* **2007***, 78*, 093702.

[29] T. Pettersson, A. Dedinaite, *J.Colloid Interface Sci.* **2008***, 324*, 246-256.

Chapter 4

Supercharging of Proteins by Means of a Highly Charged Tag

Anke Kolbe, Loretta L. del Mercato, Pilar Rivera Gil, Wolfgang J. Parak, and Andreas Herrmann

In this work we present an alternative method for the fabrication of supercharged proteins, where the protein of interest is fused to a genetically engineered polypeptide tag with high charge density and tightly controlled distribution of charges along the backbone. In contrast to post-translational, chemical modification and genetic modification of surface-exposed amino acids, this method obviates the need to modify the protein of interest itself. By adjusting the length of the charged tag, we can gradually tune the overall charge of the fusion protein. Tags carrying between -144 and +72 charges were fused to green fluorescent protein (GFP). All variants were successfully produced in E.coli and purified as fluorescently active proteins. It was demonstrated that the charged tag allows incorporation of proteins with a low overall net charge into electrostatically mediated layer-by-layer assemblies. Uptake of the resulting capsules by cultured mammalian cells could be followed with fluorescence microcopy.

Methods to significantly alter a protein's overall charge are known since decades,[1] [2] but gained increased attention in recent years due to possible new applications in biotechnology and biomedicine.[3,4] A protein's net charge can be altered by post-translational, chemical modification or by genetic engineering. Post-translational, chemical modification takes advantage of reactive, solvent-exposed amino acid residues, like glutamic or aspartic acid and lysine. Charges can be neutralized by acetylation of lysine residues or by amidation of carboxylic acid groups, for example, to increase a protein's net negative or positive charge, respectively.[5,6] Highly negatively charged derivatives of an industrially relevant enzyme, α-amylase, showed increased resilience against inactivation due to temperature elevation or addition of surfactants.[3,5] On the other hand, neutralization increases surface hydrophobicity and thus can render a protein more susceptible to aggregation.[7,8] Alternatively, the charge of a residue can be reversed to yield variants with a high net charge and a high charge density. The plasma protein bovine serum albumin (BSA), which is negatively charged at neutral pH and which contains a high number of reactive, surface-exposed amino acid residues, was chemically modified to yield highly positively and negatively charged variants.[9-11] Cationized BSA variants were successfully employed as biocoatings for the immobilization of lipid vesicles and bacterial biofilms and for cell adhesion.[12-14]. Furthermore, cationized BSA was used as efficient vehicle for gene delivery.[11] A major drawback of chemical modification is its randomness which results in a mixture of proteins with different net charges. Controlled reaction schemes and elaborate purification strategies were necessary to yield protein samples with low charge distributions.[11]

As an alternative to post-translational, chemical modification, the net charge of a protein can be dramatically increased by genetic engineering. Surface-exposed amino acids were mutated individually to create superpositive and supernegative variants of green fluorescent protein (GFP) and glutathione-S-transferase (GST).[15] In most cases the function of the protein, i.e. fluorescence or catalytic activity, was not impaired. [15] Positively supercharged variants of GFP were shown to penetrate mammalian cell membranes.[16] Due to electrostatic interactions, these proteins were able to complex with silencing RNA and plasmid DNA and to transfect a variety of mammalian cell lines.[16] Moreover, functional proteins that were fused to a superpositively charged GFP variant were successfully delivered into mammalian cells *in vitro* and *in vivo*.[17] Interestingly, supercharged variants of GFP, GST and streptavidin were highly resistant to thermally induced aggregation.[15] This stabilizing effect was mainly attributed to repelling forces between proteins due to the presence of surface charges, inhibiting irreversible aggregation and enabling refolding after denaturation.[15] It has to be taken into account, however, that salt bridges between oppositely charged residues

convey conformational stability to the tertiary structure.[18,19] Deleting or inversing the charge of an amino acid can therefore destroy stabilizing salt bridges, which might counteract the gain in aggregation resistance.[20] Consequently, supercharging of a protein by genetic mutation of solution-exposed amino acids requires careful examination of the crystal structure to identify charged amino acid residues on the protein surface, mutation and shuffling of the gene sequence, and expression and screening for functional variants.[4]

In this work, we present an alternative strategy to modify the overall charge of a protein of interest. By genetic engineering, the protein is equipped with a supercharged polypeptide tag. This enables us to tune the overall charge of the protein to basically any desired value by adjusting the length of the tag, while obviating modification of the protein itself. For tag design we chose elastin-like polypeptide (ELP) as basic sequence. The suitability of ELPs as materials for biomedical applications was demonstrated in a number of publications. ELPs were employed as hydrogels for biosurface and tissue engineering and for controlled release.[21-24] Furthermore, ELPs were used for delivery of drugs, peptides, proteins and DNA.[23,25,26] We have shown earlier that ELPs can be positively and negatively supercharged by introducing a lysine or glutamic acid residue at the fourth position of the repetitive pentapeptide sequence.[27] In this work we demonstrate the supercharging of a model protein, GFP, by means of fusion with charged variants of ELP.

RESULTS AND DISCUSSION

Preparation and Characterization of supercharged GFP-ELP fusion proteins

Genes encoding for cationic and anionic supercharged protein tags of different lengths were generated by recursive directional ligation of the *elp monomer* gene (Figure S1).[28] An ELP monomer consists of 10 repeating units of the pentapeptide sequence GXGVP, with G denoting the amino acid glycine, V valine, P proline and X either glutamic acid (E), lysine (K) or V. To preserve the restriction site that is needed for multimerization, V is inserted at position X in one out of ten pentapeptide repeats (Figure 1 b). After multimerization, the *elp* genes were cloned into a bacterial expression vector containing the *gfp* gene and a sequence encoding a hexahistidine tag for affinity purification. *Gfp* encodes GFP plus, a variant of enhanced green fluorescent protein, hereafter named GFP (Figure S3). We realized fusion variants of GFP with supercharged protein containing between nine and 144 negative and between nine and 72 positive charges. In this work, GFP-Ex and GFP-Kx denote GFP with anionic and cationic tags, respectively, with x displaying the number of

charged residues in the tag. All variants were successfully expressed in and purified from *E.coli* cells. Typically, a 50 mL culture yielded up to 20 mg of purified protein. Protein integrity and purity was confirmed by gel electrophoresis (Figure 1 c) and mass spectrometry (Figure 2). Values determined by mass spectrometry were is good agreement with the masses that were calculated based on the amino acid sequence (Table S1). For all variants, GFP was found to be fluorescent. Fluorescence spectra were recorded for GFP, GFP-K72 and GFP-E72 (Figure 3). GFP fluorescence was not decreased or shifted, indicating that even the long positively and negatively charged tags did not interfere with GFP function.

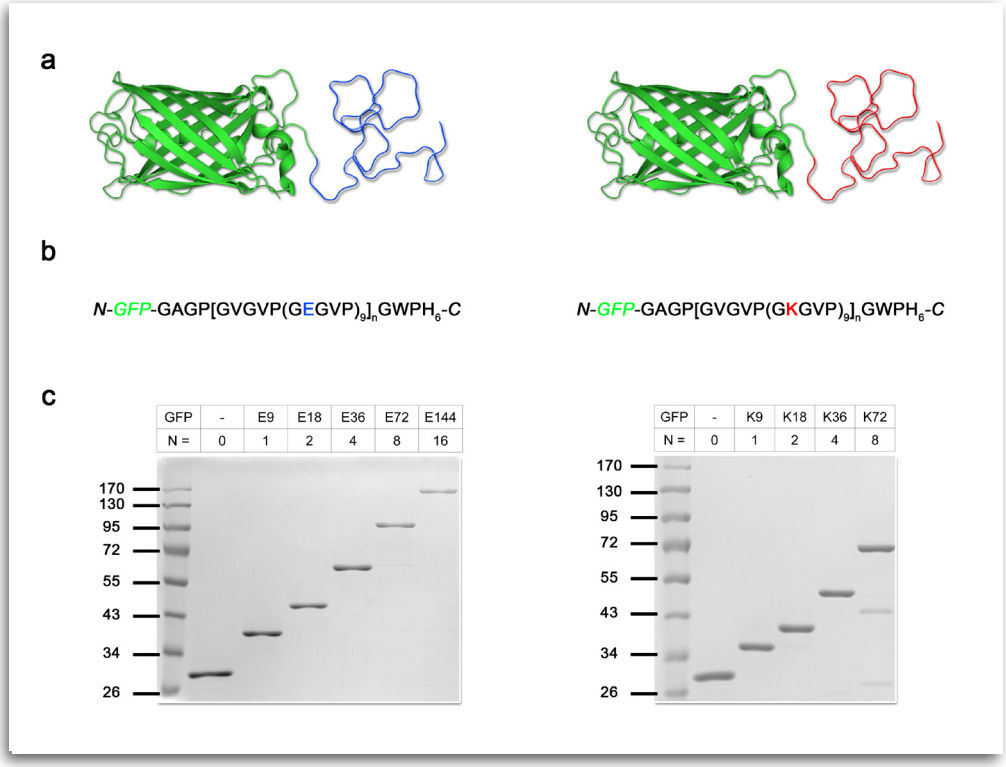

Figure 1. GFP fusion variants of supercharged elastin-like proteins (ELPs). Left: negatively charged ELPs; right: positively charged ELPs. a) Schematic representation of GFP-ELP fusion proteins. GFP (green) shows the characteristic beta-barrel structure, whereas the ELP is presented as an extended coil without exhibiting a defined secondary or tertiary structure. b) Amino acid one letter code of the ELP fusion protein, where n is the number of ELP monomer repeats. The position of GFP close to the N-terminus is indicated in green. c) GFP-ELP fusion proteins separated on a 12% SDS-PAGE gel and stained with Coomassie brilliant blue R250.

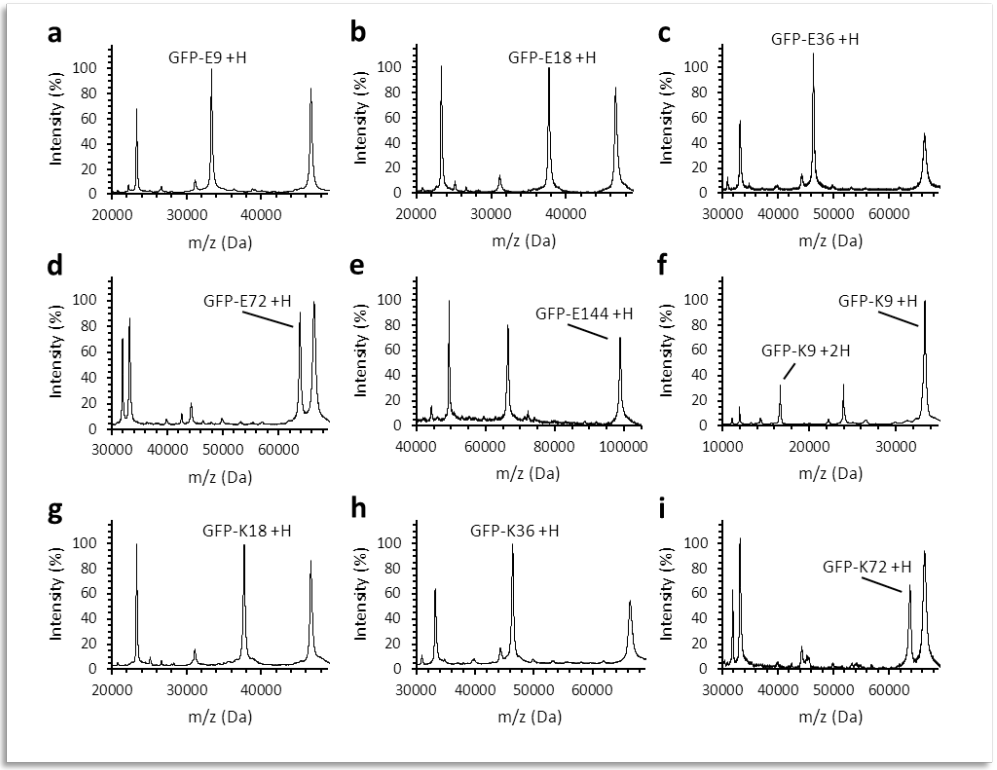

Figure 2. MALDI-TOF mass spectra of supercharged elastin-like proteins fused to GFP. a) GFP-E9; b) GFP-E18; c) GFP-E36; d) GFP-E72; e) GFP-E144; f) GFP-K9; g) GFP-K18; h) GFP-K36; i) GFP-K72. Internal standards are enolase (a, b, g), bovine serum albumin (c-e, h, i) and trypsinogen (f).

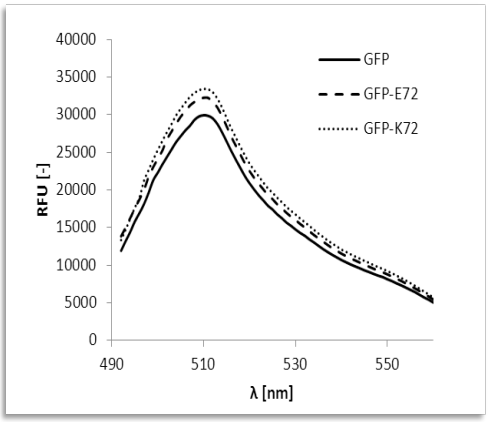

Figure 3. Fluorescence spectra of GFP and GFP-ELP variants GFP-K72 and GFP-E72 upon excitation at 488 nm. Spectra are averages of three measurements.

We have shown that we can supercharge GFP by expression as a fusion protein with charged ELP, following a simple cloning step. We were able to realize GFP-ELP fusion variants carrying up to 144 negative charges and up to 72 positive charges, while preserving the fluorescence of GFP. To our knowledge, these are the highest number of charges realized to date by genetic engineering. The highest net charges achieved by genetic mutation of solvent-exposed amino acids were +48 and -30 charges for a superfolder variant of GFP (stGFP).[15] As folded proteins contain only a limited number of solvent-exposed amino acids, this method is restricted as to the net surface charge values that can be realized. Furthermore, not all surface-exposed amino acids can be mutated without impairing conformational stability and function.[15] Fusing a protein to a charged tag, on the other hand, enables us to fabricate functional proteins with virtually any desired net charge.

CAPSULE PREPARATION AND UPTAKE

A charged tag allows for incorporation of the tagged protein into supramolecular structures that are assembled by means of electrostatic interactions. In this way, such structures can be easily equipped with a desired function (fluorescence in this case) without the need of an extra coupling step. A well-known example for electrostatically assembled structures are polyelectrolyte capsules, which exhibit great potential as carriers for intracellular delivery of biotherapeutics.[29,30] For loading of cargo, either the capsule cavity or the capsule wall can be addressed. While bioactive molecules, like enzymes, antigens and peptides, were mostly loaded into the capsule cavity,[29,31] charged nanoparticles, such as magnetic nanoparticles[32,33], quantum dots[34,35], and noble metal nanoparticles[36,37], were successfully incorporated into the capsule wall. Furthermore, polyelectrolyte capsules containing layers of two enzymes, glucose oxidase and horseradish peroxidase, with high natural net charge (isoelectric points 4.2 and 8.8) were fabricated, and the thus incorporated enzymes showed no loss of activity.[38]

We therefore decided to fabricate hollow polyelectrolyte capsules composed of dextran sulfate (DEXS) and poly(L-arginine) (pARG), with one pARG layer being replaced by GFP-K72. In collaboration with Dr. Loretta L. del Mercato from the University of Salento (Italy) and Prof. Wolfgang Parak from the University of Marburg (Germany), capsules were prepared and characterized as described in chapter 2. In short, ten layers were assembled on a sacrificial $CaCO_3$ core template by the layer-by-layer technique in the following order: $(DEXS/pARG)_3$(DEXS/GFP-K72)(DEXS/pARG). After core removal, the hollow capsules could be visualized by confocal

fluorescence microscopy, proving that fluorescence of GFP was preserved (Figure 4). The capsules had a size between 2.8 and 3.3 µm, comparable to the core template, and retained their spherical shape after core removal, indicating that incorporation of GFP-K72 did not destabilize the capsule wall (Figure 4).

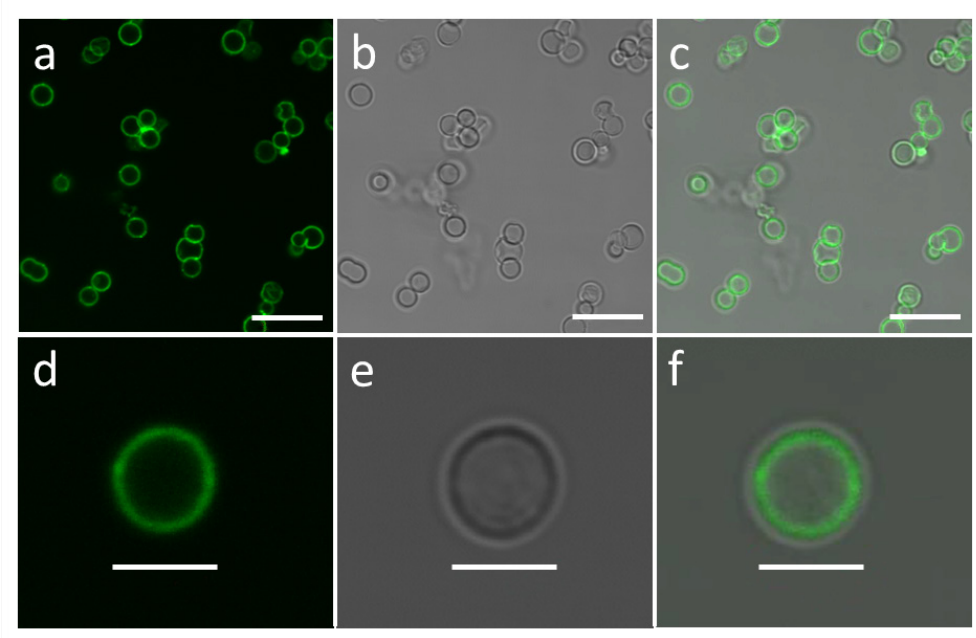

Figure 4. Hollow polyelectrolyte capsules functionalized with GFP-K72. Capsules were prepared from dextran sulfate and poly(L-arginine) with the layer-by-layer technique and are shown after core removal. a) Fluorescence image; b) transmission image; c) overlay; d)-f) magnifications of (a-c). Scale bars: 10 µm (a-c) and 3 µm (d-f).

Next, cellular uptake of the capsules was studied in collaboration with Dr. Pilar Rivera Gil and Prof. Parak from the University of Marburg. Capsules were incubated with MDA-MB-231 P48, a human breast carcinoma cell line, and capsule uptake was followed by confocal fluorescence microscopy, taking advantage of GFP's inherent fluorescence. Directly after addition to the cell culture, capsules aggregated in clusters (Figure 5a). This phenomenon can be explained by the polyionic nature of the capsules, which tend to adsorb proteins present in the cell culture medium, thereby stimulating aggregation of the capsules.[31] After 2 h incubation, capsules were attached to the cell

membrane, probably due to electrostatic interaction between the negatively charged membrane and the positively charged outermost layer of the capsule (Figure 5a). Most capsules were found to colocalize with the cell interior 7 h after addition, and fluorescence started to spread across the cell (Figure 5c). This effect was even more pronounced after 27 h of incubation (Figure 5d). Although the size of the fluorescent spots partly decreased over time, fluorescence still seemed to be restricted to defined areas, even after 27 h, indicating localization in intracellular compartments. This finding is in agreement with previous reports, which stated that micrometer-sized capsules were deformed upon uptake and found in acidic intracellular compartments after internalization.[29,39-43] GFP fluorescence significantly decreased after 31 h of incubation (Figure 5e) and was hardly distinguishable from background fluorescence of untreated cells after 46 h (Figure 5f, untreated cells not shown). Whether the observed decrease in fluorescence is due to dilution or inactivation of GFP in the acidic intracellular compartment, needs to be investigated.

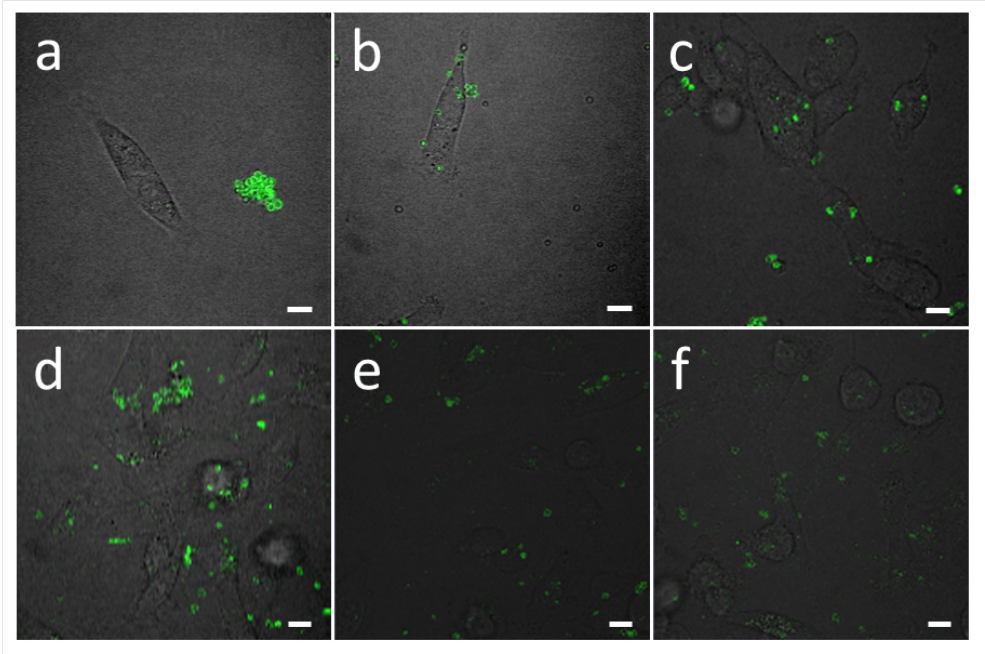

Figure 5. Studying the uptake of capsules by mammalian cells. A culture of human breast carcinoma cells was incubated with GFP-K72-functionalized capsules. Images were obtained a) 0 h; b) 2 h; c) 7 h; d) 27 h; e) 31 h; f) 46 h after addition of capsules to the cell culture. Note that images a) and b) were taken at different settings, resulting in varying fluorescence intensities. Scale bars: 10 µm.

CONCLUSIONS AND OUTLOOK

In this work, we demonstrated that proteins can be supercharged by equipping them with a positively or negatively charged polypeptide tag. Expression as fusion proteins eliminated the need of an extra chemical coupling step for functionalization. We realized GFP-charged tag fusion proteins with up to 144 negative and up to 72 positive charges.

Furthermore, we successfully incorporated the superpositive variant GFP-K72 into the wall of polyelectrolyte multilayer capsules by means of electrostatic interactions, while maintaining the fluorescence of GFP. In initial experiments, uptake of these capsules by mammalian cancer cells was followed by fluorescence microscopy. For capsule preparation, we have chosen GFP with a relatively long positively charged tag. In future experiments it remains to determine the minimum tag length that is needed for stable incorporation of the tagged protein into the capsule wall and whether a cationic or an anionic tag should be preferred. Moreover, the fate of the capsules and the incorporated proteins after uptake need to be investigated in more detail. We are therefore planning to fabricate capsules containing two fluorescent proteins – GFP and mCherry, a red fluorescent protein. As the absorption spectrum of mCherry overlaps with the emission spectrum of GFP, mCherry can serve as an acceptor for the green GFP emission.[44,45] Therefore, fluorescence resonance energy transfer (FRET) will be observed between GFP and mCherry, provided they are in close proximity, as is the case when both proteins are incorporated into the capsule wall. Detection of a FRET signal, i.e. emission of red fluorescence by mCherry upon excitation of GFP, will therefore indicate an intact capsule. Upon disintegration of the capsule, the FRET signal will decrease due to release of the proteins, while their individual fluorescence can still be observed.

Taken together, we have demonstrated that charged tags provide the means to equip polyelectrolye capsules with a functional protein. Furthermore, we believe that this concept can be expanded to the functionalization of surfaces or other electrostatically assembled structures, like polyplexes, for example.[46,47]

EXPERIMENTAL PART

Materials

The pUC19 cloning vector, restriction endonucleases, and GeneJET™ Plasmid Miniprep kit were purchased from Fermentas (St. Leon-Rot, Germany). T4 DNA ligase and antarctic phosphatase were purchased from New England Biolabs (Ipswich,

MA). Digested DNA fragments were purified using QIAquick® spin miniprep kits from QIAGEN, Inc. (Valencia, CA). *E.coli* XL1-Blue competent cells were purchased from Stratagene (Cedar Creek, TX). The pET-25b(+) vector and *E.coli* BLR(DE3) competent cells were purchased from Novagen Inc. (San Diego, CA). Oligonucleotides were ordered from Sigma-Aldrich (St. Louis, MO). Elastin-like polypeptide monomer genes were ordered from Entelechon (Regensburg, Germany). Bacto™ tryptone and BBL™ yeast extract were purchased from Becton, Dickinson and Co. (Sparks, MD). Potassium phosphate monobasic, potassium phosphate dibasic, sodium phosphate monobasic, sodium phosphate dibasic, sodium chloride, glycerol, glycine, acetic acid (glacial, anhydrous), ammonium persulfate and ethylenediaminetetraacetic acid were purchased from Merck KGaA (Darmstadt, Germany). *tris*(hydroxymethyl) amino methane and N,N,N',N'-Tetramethylethylenediamine were purchased from Acros Organics (Geel, Belgium). Methanol was purchased from Lab-Scan (Gliwice, Poland). Acrlyaminde:N,N'-methylene-bis-acrylamide and Tween20 were purchased from Bio-Rad Laboratories (Hercules, CA). Nunc Immobilizer Amino F96 clear plates were purchased from Nunc (Roskilde, Denmark). Antibodies Mouse monoclonal [6AT316] to GFP and Rabbit polyclonal Secondary Antibody to Mouse IgG - H&L (HRP) were purchased from Abcam (Cambridge, United Kingdom). Anti-His antibody was purchased from GE Healthcare (Buckinghamshire, United Kingdom). QuantaBlu™ Fluorogenic Peroxidase Substrate Kit was purchased from Thermo Scientific (Rockford, IL). Sodium dodecyl sulfate was purchased from BDH (Poole, United Kingdom). Carbenicillin, imidazole, Brilliant Blue R250 and bovine serum albumin were purchased from Carl Roth (Karlsruhe, Germany). 3,5 dimethoxy-4-hydroxycinnamic acid and internal standards bovine serum albumin, yeast enolase and trypsinogen for mass spectrometry were purchased from LaserBio Labs (Sophia-Antipolis, France). All chemicals were used as received. Ultrapure water with a resistivity greater than 18.2 MΩ cm was used for all experiments. PGFP was a kind gift from Prof. D. Hilvert, Swiss Federal Institute of Technology, Zurich, Switzerland.

Gene oligomerization

Monomers of the cationic and anionic *ELP* genes (K9 and E9) were ordered from Entelechon and were delivered in the pEN vector. Gene sequences and respective amino acid sequences of monomers are shown in Figure S1. As the recognition sites of the restriction enzymes *Pfl*MI and *Bgl*I had to be preserved, one valine residue per ten pentapeptide repeats was incorporated instead of a lysine or glutamic acid residue. The *ELP* gene was excised from the pEN vector by digestion with *Eco*RI and *Hin*DIII and run on a 1% agarose gel in TAE buffer (per 1L, 108 g Tris base, 57.1 mL glacial acetic acid, 0.05 M EDTA, pH 8.0). The band containing the *ELP* gene was excised

from the gel and purified using a spin column purification kit (QIAGEN). PUC19 was digested with *Eco*RI and *Hin*DIII and was subsequently dephosphorylated. The vector was purified by agarose gel extraction following gel electrophoresis. The linearized pUC vector and the *ELP*-encoding gene were ligated and transformed into XL1-Blue cells. For transformation, 20 µL of chemically competent *E.coli* XL1-Blue cells were combined with 5 µL of the ligation mixture and further treated according to the manufacturer's protocol. Cells were spread on Lysogeni broth (LB) agar plates (for 1 L, 10 g Bacto™ tryptone, 5 g BBL™ yeast extract, 5 g NaCl, 15 g agar) supplemented with 100 µg/mL carbenicillin, and incubated overnight (o/n) at 37ºC. Colonies were picked and grown in 6 mL LB media (for 1 L, 10 g Bacto™ tryptone, 5 g BBL™ yeast extract, 5 g NaCl) supplemented with 100 µg/mL carbenicillin overnight, and plasmids were isolated using the GeneJET Plasmid Miniprep kit. Positive clones were verified by plasmid digestion with *Eco*RI and *Hin*DIII and subsequent gel electrophoresis. The DNA sequence of putative inserts was further verified by DNA sequencing (SequenceXS, Leiden, The Netherlands). Gene oligomerization was performed as described by Chilkoti and co-workers (Figure S2).[48]

Expression vector construction

The expression vector pET 25b(+) was modified by cassette mutagenesis for incorporation of a unique *Sfi*I recognition site as described before.[27,48] The modified pET 25b(+) vector (hence called pET-*Sfi*I from here on) was further digested with *Xba*I and *Nde*I, dephosphorylated and purified using a microcentrifuge spin column kit. The *gfp* gene including the ribosomal binding site was excised from the pGFP vector by digestion with *Xba*I and *Sac*I, and the excised gene (747 bp) was purified by agarose gel extraction following gel electrophoresis. A linker sequence that would connect *gfp* and the *Sfi*I restriction site was constructed in the following way: Oligonucleotides linker_sens (cggtgtagtc ggtttagttc ccagaggaag tca) and linker_ antisens (tatgacttcc tctgggaact aaaccgacta caccgagct), both 5'-phosphorylated, were mixed in equimolar ratios, incubated at 90°C for 1 h and then cooled down stepwise to 20°C for annealing (1°C per 3 min). The resulting linker contained overhangs corresponding to a *Sac*I and an *Nde*I restriction site, respectively. pET-*Sfi*I, the insert containing *gfp* and the linker were ligated, yielding pET-*gfp*-*Sfi*I. For insertion of *ELP* genes, pET-*gfp*-*Sfi*I was digested with *Sfi*I, dephosphorylated and purified using a microcentrifuge spin column kit. The respective *ELP* gene was excised from the pUC19 vector by digestion with *Pfl*MI and *Bgl*I, and the excised gene was purified by agarose gel extraction following gel electrophoresis. The linearized vector and the insert containing the *ELP* gene were ligated, transformed into XL1-Blue cells, and screened as described above.

Protein expression and purification

E.coli BLR (DE3) cells (Novagen) were transformed with the pET-*Sfi*I expression vectors containing the respective *ELP* genes. For protein production, Terrific Broth medium (for 1 L, 12 g tryptone and 24 g yeast extract) enriched with phosphate buffer (for 1 L, 2.31 g potassium phosphate monobasic and 12.54 g potassium phosphate dibasic) and glycerol (4 mL per 1 L TB) and supplemented with 100 µg/mL ampicillin, was inoculated with an overnight starter culture to an initial optical density at 600 nm (OD_{600}) of 0.1 and incubated at 37°C with orbital agitation at 250 rpm until OD_{600} reached 0.7. Protein production was induced by a temperature shift to 30°C. Cultures were then continued for additional 16 h post-induction. Cells were subsequently harvested by centrifugation (7,000 x *g*, 20 min, 4ºC), resuspended in lysis buffer (50 mM sodium phosphate buffer, pH 8.0, 300 mM NaCl, 20 mM imidazole for E variants or 10 mM TrisHCl buffer, pH 8.0, 300 mM NaCl, 20 mM imidazole for K variants) to an OD_{600} of 100 and disrupted with a constant cell disrupter (Constant Systems Ltd., Northands, UK). Cell debris was removed by centrifugation (40,000 x *g*, 90 min, 4ºC). Proteins were purified from the supernatant under native conditions by Ni-sepharose chromatography (GE Healthcare). Product-containing fractions were pooled and dialyzed against Ultrapure water (>18 MΩ). K variants were further purified by affinity chormatography using a Heparin HP column (GE Healthcare), and E variants by anion exchange chromatography using a Q HP column (GE Healthcare). Protein-containing fractions were dialyzed extensively against ultrapure water (>18 MΩ). Purified proteins were frozen in liquid nitrogen, lyophilized and stored at -20ºC until further use.

Protein characterization

The concentrations of the purified ELPs were determined by measuring absorbance at 280 nm using a spectrophotometer (SpectraMax M2, Molecular Devices, Sunnyvale, CA). Protein purity was determined by sodium dodecyl sulfate polyacrylamide gel electrophoresis (SDS-PAGE) on a 12% polyacrylamide gel according to Laemmli[49] and subsequent copper (II) chloride staining as reported by Lee and coworkers.[50] Afterwards, gels were stained with coomassie staining solution (40% methanol, 10% glacial acetic acid, 1 g/L Brilliant Blue R250). Photographs of the gels before and after coomassie staining were taken with a LAS-3000 Image Reader (Fuji Photo Film (Europe) GmbH, Dusseldorf, Germany).

Mass spectrometric analysis was performed using a 4800 MALDI-TOF/TOF Analyzer (Applied Biosystems, Foster City, CA, USA) in the linear positive mode. The protein samples were mixed 1:1 v/v with a recrystallized a-cyano-4-hydroxycinnamic acid matrix (10 mg/mL in 50% ACN and 0.1% TFA, LaserBio Labs). Mass spectra were analyzed and calibrated internally with the Data Explorer software, version 4.9

(Applied Biosystems, Foster City, CA, USA). Trypsinogen (MW = 23,980), enolase (MW = 46,672) and bovine serum albumin (MW = 66,431) were used as calibration standards.

Fluorescence spectra of GFP, GFP-K72 and GFP-E72 were recorded on a fluorimeter (SpectraMax M2, Molecular Devices, Sunnyvale, CA). GFP concentration in phosphate buffer solution (PBS) was determined by measuring absorbance at 488 nm. Volumes were adjusted with PBS until absorbance at 488 nm was between 0.82 and 0.85. Samples were diluted ten times in PBS for fluorescence measurements. Fluorescence spectra were recorded upon excitation at 488 nm. Measurements were carried out in triplicates and average fluorescence values were corrected for differences in absorbance according to

$RFU_{corr} = RFU_{meas} \cdot 0.84 / abs488$,

with RFU_{corr} being the corrected relative fluorescence unit (RFU), RFU_{meas} the measured RFU, and abs488 the measured absorbance at 488 nm of the ten times concentrated solution.

SUPPLEMENTARY DATA

a) ELP monomer lysine (K9)

*Eco*RI *Pfl*MI

A ATT CAT ATG GGC CAC GGC GTG GGT GTT CCG GGC AAA GGT GTT CCG GGT AAA GGT GTG CCG

G V G V P G K G V P G K G V P

GGC AAA GGT GTT CCT GGT AAA GGT GTG CCG GGT AAA GGT GTG CCG GGT AAA GGT GTA CCA

G K G V P G K G V P G K G V P G K G V P

*Bgl*I *Hind*III

GGT AAA GGT GTT CCG GGT AAA GGC GTT CCG GTT AAA GGT GTG CCG GGC GGG CTG GAA TA

G K G V P G K G V P G K G V P

b) ELP monomer glutamic acid (E9)

*Eco*RI *Pfl*MI

A ATT CAT ATG GGC CAC GGC GTG GGT GTT CCG GGC GAA GGT GTT CCG GGT GAA GGT GTG CCG

G V G V P G E G V P G E G V P

GGC GAA GGT GTT CCT GGT GAA GGT GTG CCG GGT GAA GGT GTG CCG GGT GAA GGT GTA CCA

G E G V P G E G V P G E G V P G E G V P

*Bgl*I *Hind*III

GGT GAA GGT GTT CCG GGT GAA GGC GTT CCG GTT GAA GGT GTG CCG GGC GGG CTG GAA TA

G E G V P G E G V P G E G V P

Figure S1. Genes and corresponding polypeptide sequences of **(a)** ELP K9 (monomer lysine) and **(b)** ELP E9 (monomer glutamic acid). Recognition sites for the restriction enzymes *Eco*RI, *Pfl*MI, *Bgl*I, and *Hind*III are underlined.

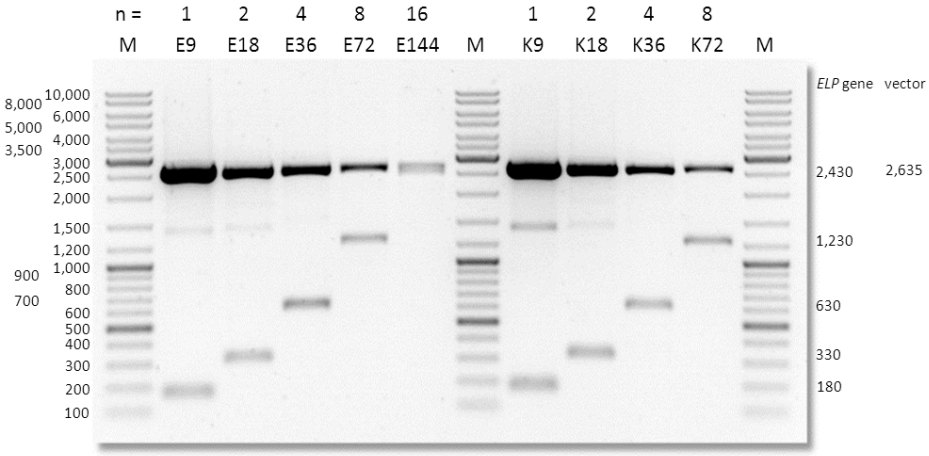

Figure S2. Gel electrophoresis of *ELP* genes. PUC vectors containing the *ELP* genes were digested with *Eco*RI and *Hin*DIII and separated on a 1% agarose gel. DNA bands were visualized by ethidium bromide staining. Digestion produced a vector fragment of 2,635 bp and an *ELP* gene fragment (size in bp is depicted on the right). n = number of monomers with 10 pentapeptide repeats per monomer; E = negatively charged; K = positively charged; 9-144: amount of charges in respective elastin-like polypeptide; M: size standard.

a

AGTTGTCCCAATTCTTGTTGAATTAGATGGTGATGTTAATGGTCACAAATTTTCTGTCAGTGGAGAGGGTGA
AGGTGATGCAACATACGGAAAACTTACCCTTAAATTTATTTGCACTACTGGAAAACTACCTGTTCCATGGCC
AACACTTGTCACTACTTTAACTTATGGTGTTCAATGCTTTTCCCGTTATCCGGATCATATGAAACGTCATGAC
TTTTTCAAGAGTGCCATGCCCGAAGGTTATGTACAGGAACGCACTATATCTTTCAAAGATGACGGTAACTAC
AAGACGCGTGCTGAAGTCAAGTTTGAAGGTGATACCCTTGTTAATCGTATCGAGTTAAAAGGTATTGATTTT
AAAGAAGATGGAAACATTCTCGGACACAAACTCGAGTACAACTATAACTCACACAATGTATACATCACGGC
AGACAAACAAAAGAATGGAATCAAGGCTAACTTCAAAATTCGCCACAACATTGAAGATGGATCCGTTCAAC
TAGCAGACCATTATCAACAAAATACTCCAATTGGCGATGGCCCTGTCCTTTTACCAGACAACCATTACCTGT
CGACACAATCTGCCCTTTCGAAAGATCCCAACGAAAAGCGTGACCACATGGTCCTTCTTGAGTTTGTAACTG
CTGCTGGTATTACACATGGCATGGATGAGCTCTACAAA

b

M A S K G E E L F T G V V P I L V E L D G D V N G H K F S V S G E G E G D A T Y
G K L T L K F I C T T G K L P V P W P T L V T T L T Y G V Q C F S R Y P D H M K R
H D F F K S A M P E G Y V Q E R T I S F K D D G N Y K T R A E V K F E G D T L V
N R I E L K G I D F K E D G N I L G H K L E Y N Y N S H N V Y I T A D K Q K N G I
K A N F K I R H N I E D G S V Q L A D H Y Q Q N T P I G D G P V L L P D N H Y L
S T Q S A L S K D P N E K R D H M V L L E F V T A A G I T H G M D E L Y K

Figure S3. Nucleotide sequence (a) and amino acid one letter code (b) of the green fluorescent protein variant used in this study.

Table S1. Mass determination of GFP-ELP variants

construct	M calc* [Da]	M ms#[Da]
GFP-E9	33,425.3	33,372 +/- 50
GFP-E18	37,790.0	37,725 +/- 50
GFP-E36	46,519.4	46,402 +/- 50
GFP-E72	63,978.2	63,893 +/- 50
GFP-E144	98,895.8	98,874 +/- 50
GFP-K9	33,416.8	33,381 +/- 50
GFP-K18	37,904.2	37,722 +/- 50
GFP-K36	46,485.5	46,377 +/- 50
GFP-K72	63,910.4	63,768 +/- 50

* average molecular weight calculated with ProtParam tool

molecular weight determined by MALDI-TOF mass spectrometry

REFERENCES

[1] A. D. Gounaris, G. E. Perlmann, *J.Biol.Chem.* **1967***, 242*, 2739-&.

[2] D. G. Hoare, D. E. Koshland, *J.Biol.Chem.* **1967***, 242*, 2447-&.

[3] B. F. Shaw, D. T. Moustakas, J. P. Whitelegge, K. F. Faull, *Advances in Protein Chemistry and Structural Biology, Vol 79.* **2010***, 79*, 127-164.

[4] D. B. Thompson, J. J. Cronican, D. R. and Liu, *Methods in Enzymology.* **2012***, 503*, 293-319.

[5] B. F. Shaw, G. F. Schneider, B. Bilgicer, G. K. Kaufman, J. M. Neveu, W. S. Lane, J. P. Whitelegge, G. M. Whitesides, *Protein Sci.* **2008***, 17*, 1446-1455.

[6] H. A. Kosters, K. Broersen, J. de Groot, J. W. F. A. Simons, P. Wierenga, H. H. J. de Jongh, *Biotechnol. Bioeng.* **2003***, 84*, 61-70.

[7] I. Gitlin, K. L. Gudiksen, G. M. Whitesides, *ChemBioChem.* **2006***, 7*, 1241-1250.

[8] R. K. Jain, A. D. Hamilton, *Angewandte Chemie-International Edition.* **2002***, 41*, 641-+.

[9] K. R. Smith, R. T. Borchardt, *Pharm.Res.* **1989***, 6*, 466-473.

[10] D. Fischer, T. Bieber, S. Brusselbach, H. Elsasser, T. Kissel, *Int.J.Pharm.* **2001***, 225*, 97-111.

[11] K. Eisele, R. A. Gropeanu, C. M. Zehendner, A. Rouhanipour, A. Ramanathan, G. Mihov, K. Koynov, C. R. W. Kuhlmann, S. G. Vasudevan, H. J. Luhmann, T. Weil, *Biomaterials.* **2010***, 31*, 8789-8801.

[12] S. Ritz, K. Eisele, J. Dorn, Shaohua Ding, D. Vollmer, S. Puumltz, T. Weil, E. -. Sinner, *Biointerphases Journal.* **2010***, 5*.

[13] J. F. Ng, S. Jaenicke, K. Eisele, J. Dorn, T. Weil, *Biointerphases.* **2010***, 5*, FA41-FA47.

[14] J. F. Ng, T. Weil, S. Jaenicke, *J.Biomed.Mater.Res.Part B.* **2011***, 99B*, 282-290.

[15] M. S. Lawrence, K. J. Phillips, D. R. Liu, *J. Am. Chem. Soc.* **2007***, 129*, 10110-+.

[16] B. R. McNaughton, J. J. Cronican, D. B. Thompson, D. R. Liu, *Proc.Natl.Acad.Sci.U.S.A.* **2009***, 106*, 6111-6116.

[17] J. J. Cronican, D. B. Thompson, K. T. Beier, B. R. McNaughton, C. L. Cepko, D. R. Liu, *Acs Chemical Biology.* **2010***, 5*, 747-752.

[18] A. Karshikoff, R. Ladenstein, *Trends Biochem.Sci.* **2001***, 26*, 550-556.

[19] G. I. Makhatadze, V. V. Loladze, D. N. Ermolenko, X. F. Chen, S. T. Thomas, *J.Mol.Biol.* **2003***, 327*, 1135-1148.

[20] H. N. Ong, B. Arumugam, S. Tayyab, *J.Biochem.* **2009***, 146*, 895-904.

[21] D. L. Nettles, A. Chilkoti, L. A. Setton, *Adv.Drug Deliv.Rev.* **2010***, 62*, 1479-1485.

[22] Z. Megeed, M. Haider, D. Q. Li, B. W. O'Malley, J. Cappello, H. Ghandehari, *J. Control. Release.* **2004***, 94*, 433-445.

[23] R. Dandu, H. Ghandehari, *Prog. Polym. Sci.* **2007***, 32*, 1008-1030.

[24] J. Carlos Rodriguez-Cabello, L. Martin, M. Alonso, F. Javier Arias, A. M. Testera, *Polymer.* **2009***, 50*, 5159-5169.

[25] S. R. MacEwan, A. Chilkoti, *Biopolymers.* **2010***, 94*, 60-77.

[26] G. L. Bidwell III, D. Raucher, *Adv.Drug Deliv.Rev.* **2010***, 62*, 1486-1496.

[27] A. Kolbe, L. L. del Mercato, A. Z. Abbasi, P. Rivera-Gil, S. J. Gorzini, W. H. C. Huibers, B. Poolman, W. J. Parak, A. Herrmann, *Macromol.Rapid Commun.* **2011***, 32*, 186-190.

[28] A. Chilkoti, T. Christensen, J. A. MacKay, *Curr. Opin. Chem. Biol.* **2006***, 10*, 652-657.

[29] S. De Koker, L. J. De Cock, P. Rivera-Gil, W. J. Parak, R. A. Velty, C. Vervaet, J. P. Remon, J. Grooten, B. G. De Geest, *Adv.Drug Deliv.Rev.* **2011***, 63*, 748-761.

[30] M. Dierendonck, S. De Koker, C. Vervaet, J. P. Remon, B. G. De Geest, *Journal of Controlled Release.* **2012***, doi: 10.1016/j.jconrel.2012.03.001*.

[31] P. Rivera Gil, L. L. del Mercato, P. del-Pino, A. Munoz-Javier, W. J. Parak, *Nano Today.* **2008***, 3*, 12-21.

[32] N. Gaponik, I. Radtchenko, G. Sukhorukov, A. Rogach, *Langmuir.* **2004***, 20*, 1449-1452.

[33] S. Mornet, S. Vasseur, F. Grasset, E. Duguet, *J.Mater.Chem.* **2004***, 14*, 2161-2175.

[34] A. Susha, F. Caruso, A. Rogach, G. Sukhorukov, A. Kornowski, H. Mohwald, M. Giersig, A. Eychmuller, H. Weller, *Colloid Surf.A-Physicochem.Eng.Asp.* **2000***, 163*, 39-44.

[35] N. Gaponik, I. Radtchenko, M. Gerstenberger, Y. Fedutik, G. Sukhorukov, A. Rogach, *Nano Lett.* **2003***, 3*, 369-372.

[36] A. Skirtach, C. Dejugnat, D. Braun, A. Susha, A. Rogach, W. Parak, H. Mohwald, G. Sukhorukov, *Nano Lett.* **2005***, 5*, 1371-1377.

[37] A. Angelatos, B. Radt, F. Caruso, *J Phys Chem B.* **2005***, 109*, 3071-3076.

[38] F. Caruso, C. Schuler, *Langmuir.* **2000***, 16*, 9595-9603.

[39] A. Szarpak, D. Cui, F. Dubreuil, B. G. De Geest, L. J. De Cock, C. Picart, R. Auzely-Velty, *Biomacromolecules.* **2010***, 11*, 713-720.

[40] O. Kreft, A. M. Javier, G. B. Sukhorukov, W. J. Parak, *Journal of Materials Chemistry.* **2007***, 17*, 4471-4476.

[41] A. M. Javier, O. Kreft, M. Semmling, S. Kempter, A. G. Skirtach, O. T. Bruns, P. del Pino, M. F. Bedard, J. Raedler, J. Kaes, C. Plank, G. B. Sukhorukov, W. J. Parak, *Adv. Mater.* **2008***, 20*, 4281-4287.

[42] A. Javier, O. Kreft, A. Alberola, C. Kirchner, B. Zebli, A. Susha, E. Horn, S. Kempter, A. Skirtach, A. Rogach, J. Radler, G. Sukhorukov, M. Benoit, W. Parak, *Small.* **2006***, 2*, 394-400.

[43] G. B. Sukhorukov, A. L. Rogach, B. Zebli, T. Liedl, A. G. Skirtach, K. Kohler, A. A. Antipov, N. Gaponik, A. S. Susha, M. Winterhalter, W. J. Parak, *Small.* **2005***, 1*, 194-200.

[44] L. Albertazzi, D. Arosio, L. Marchetti, F. Ricci, F. Beltram, *Photochem.Photobiol.* **2009***, 85*, 287-297.

[45] M. Tramier, M. Zahid, J. Mevel, M. Masse, M. Coppey-Moisan, *Microsc.Res.Tech.* **2006***, 69*, 933-939.

[46] P. Vader, L. J. van der Aa, G. Storm, R. M. Schiffelers, J. F. J. Engbersen, *Curr.Top.Med.Chem.* **2012***, 12*, 108-119.

[47] K. Miyata, N. Nishiyama, K. Kataoka, *Chem.Soc.Rev.* **2012***, 41*, 2562-2574.

[48] D. E. Meyer, A. Chilkoti, *Biomacromolecules.* **2002***, 3*, 357-367.

[49] U. Laemmli, *Nature.* **1970***, 227*, 680-&.

[50] C. Lee, A. Levin, D. Branton, *Anal. Biochem.* **1987***, 166*, 308-312.

Chapter 5

Supercharged Tags for Protein Detection in Nanowire Field-Effect Transistors

Anke Kolbe, Moria Kwiat, Roey Elnathan, Fernando Patolsky, and Andreas Herrmann

Biosensors based on semiconducting nanowire field-effect transistors (NW-FETs) show fast responses with high sensitivity and selectivity and are therefore promising candidates for the detection of disease-related markers. The net charge of the analyte plays a crucial role in detection by these devices, as the electrical response is dependent on changes in the electric field close to the nanowire surface. Understanding the influence of analyte charge on the electric signal will help in improving these biosensors for in-vitro diagnostics. By genetic engineering, the overall charge of a protein can be substantially altered when equipped with a charged protein tag, while leaving the protein itself unchanged. Green fluorescent protein is an excellent model protein, because it exhibits a low net charge at physiological pH and binding to a surface or device can be detected by means of fluorescence. Highly negatively and positively charged variants of elastin-like polypeptide were expressed as fusion proteins with GFP. By changing the length of the supercharged tags, protein markers with varying tag charges (from -144 to +72) can be fabricated. Sensing experiments on nanowire-based devices demonstrate that already short tags with nine positive or negative charges render green fluorescent protein well detectable in NW-FETs.

Detection of disease-related markers has the potential to revolutionize medical diagnostics. These markers are small molecules, peptides, proteins or nucleic acids that are present in body fluids. Early-on stage detection will allow timely treatment, resulting in better prognosis, and has therefore fuelled tremendous efforts in biomedical research to identify disease-related markers. [1-6] To take advantage of these findings for diagnostic purposes, fast and reliable detection schemes are required that can detect marker molecules with high selectivity and sensitivity. Moreover, cancer as well as coronary and chronic inflammatory diseases show complex patterns of different markers in dependence of the course of the disease.[7-12] Therefore, a suitable detection scheme should be able to analyze multiple markers on the same array. Sensors based on semiconducting nanowires (NWs) in field effect transistors (FETs) are promising tools for the sensitive and selective detection of biomarkers like proteins,[13-16] DNA[17-19] and virus particles[20]. Furthermore, their potential for multiplexed detection was demonstrated.[14]

Detection of molecules by NW-FETs is based on the principle that a variation in the electric field or potential close to the NW surface results in a measureable conductivity change.[21] Consequently, the net charge of the analyte has substantial influence on the sensitivity of NW based detection schemes. It is therefore of great interest to study the impact of the analyte charge on the conductivity change. Here, we present a new paradigm for probe design in which proteins with low net charge are genetically engineered to enhance their detectability in NW-FET based devices.

Two main strategies that change the overall charge of a protein were demonstrated in the literature so far. The first strategy relies on chemical posttranslational modification of amino acid residues on the surface of the protein. Lysine residues were chemically modified by acetylation or succinylation, whereas carboxyl groups were methylated. [22,23] Another approach was demonstrated by the group of Liu. Instead of chemical alteration, they employed genetic modification of surface-exposed amino acids to create superpositive and supernegative variants of GFP, streptavidin and glutathione-S-transferase, a process they referred to as "supercharging of proteins".[24] While both methods lead to protein variants with high surface net charge, they might not be suitable to improve detection in biosensors, because binding of the analyte to the sensor is mediated by specific interaction with a capture molecule (e.g. a receptor or antibody in the case of proteins), which strongly relies on conservation of epitopes on the surface of the target. Consequently, exhaustive charge modification of the protein surface will impair recognition by commercially available antibodies. It was therefore our goal to increase the overall charge of a protein by means of a charged tag, leaving the protein itself unchanged. Furthermore, it is advantageous to choose a tag which is not prone to cross-recognition. In this respect, intrinsically disordered polypeptides

are promising candidates, as they lack any secondary or tertiary structure. We have shown earlier that elastin-like polypeptides (ELPs), which are unfolded below their lower critical solution temperature, can be positively or negatively supercharged by introducing a lysine or a glutamic acid residue at the fourth position of the repetitive pentapeptide sequence.[25] Moreover, we demonstrated the supercharging of green fluorescent protein (GFP) by means of fusion with charged variants of ELP (chapter 4 in this thesis). By varying the length of the tag, the overall charge of the protein can be easily tuned. In this work we investigate the influence of the number of charges on the detection of GFP in a silicon NW-FET biosensor.

RESULTS AND DISCUSSION

As mentioned before, the charge of the analyte is a key factor for detection in sensors based on NW-FETs. In the case of sensing of DNA hybridization, the high overall net charge of DNA is taken advantage of, as DNA carries a negatively charged phosphate group at every nucleotide.[19] In contrast, the net charge of proteins varies substantially between different proteins, rendering their detection in NW-FET-based sensors a more demanding task. Moreover, about 84 % of all polypeptides contained in the Protein Data Bank (PDB) carry a net charge that ranges between – 10 and +10, i.e. they are only moderately charged at physiological conditions.[24] As NW-FET sensors are based on detection of changes in the electrical field close to the NW surface, this might result in low sensitivity of these devices for many protein analytes. We therefore decided to study the influence of the net charge of GFP on its detectability in these devices. GFP was chosen as model analyte, because binding to its specific antibody can be easily verified by fluorescence microscopy upon excitation with a standard laser at 488 nm. Furthermore, GFP is only slightly negatively charged at a pH close to 7 (isoelectric point of 6.8, as calculated with the software SwissProtParam) and therefore serves as a good example for proteins with a low overall charge. By genetic engineering, GFP was fused to positively and negatively charged ELP tags of various lengths. GFP-ELP fusion proteins were successfully produced in and purified from *E.coli* cells, as described in chapter 4.

Next, the performance of the charge-tagged GFP variants in sensing experiments was evaluated using a silicon-nanowire field-effect transistor setup in collaboration with Moria Kwiat, Roey Elnathan and Prof. Fernando Patolsky from Tel-Aviv University. The basic nanowire sensor chip contains close to 200 devices that can be addressed individually for simultaneous detection. The electrical contacts were formed by photolithography and metal deposition steps following deposition of the

nanowires on the sensor surface. After their fabrication, the transistors were converted into sensors for the detection of GFP and its charge-tagged variants by modification of the nanowire surface with a monoclonal antibody directed against GFP. Firstly, chemical modification of the naturally formed oxide coating was carried out to allow coupling of the antibody. In a second step, the antibody was covalently linked to the sensor surface, and non-reacted sites were blocked with ethanolamine to avoid unspecific binding of analyte molecules. Subsequently, specific binding of GFP to the immobilized antibody was studied by fluorescence microscopy. As can be seen in Figure 1a, GFP absorbed strongly to the surface that was functionalized with anti-GFP antibody. Incubation of the non-functionalized surface with GFP resulted in only marginal absorption of the protein, indicating that indeed attachment of GFP to the surface is mediated by specific binding to the antibody (Figure 1b). Rinsing of the antibody-functionalized surface after GFP incubation removed loosely-bound protein, resulting in a fluorescence decrease. However, a substantial amount of GFP was retained on the surface, confirming specific binding (Figure 1c and d).

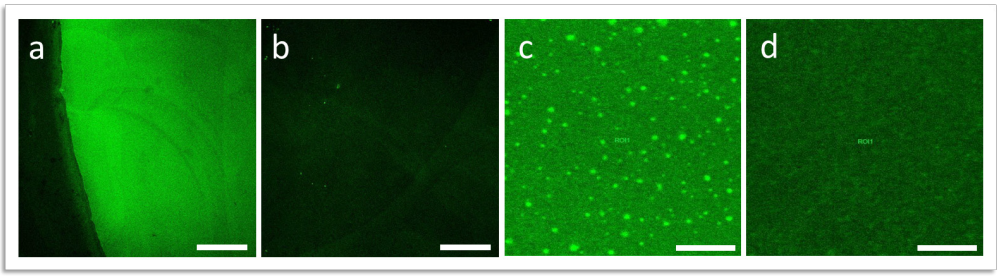

Figure 1. Specific binding of GFP to antibody-functionalized sensor surface. Surfaces were (a) functionalized with monoclonal antibody against GFP or (b) non-functionalized. (c) Higher magnification of the surface shown in (a); (d) surface as in (c), after rinsing with sensing buffer. Scale bars: 50 µm (a and b) and 5 µm (c and d).

After antibody functionalization and confirmation of specific GFP binding, electrical transport characteristics of functional devices were determined. In order to minimize device-to-device variation, the electrical responses of the NWs were calibrated.[26] Protein solutions of GFP-K9, -K36, -K72, -E9, -E36, and -E72 were delivered through a microfluidic channel to the devices and the nanowire conductance was recorded. For clarity, GFP-K36 refers to GFP fused to a tag carrying 36 positive charges, whereas GFP-E36 refers to GFP fused to a tag carrying 36 negative charges. A schematic representation of an antibody-functionalized device is depicted in Figure 2.

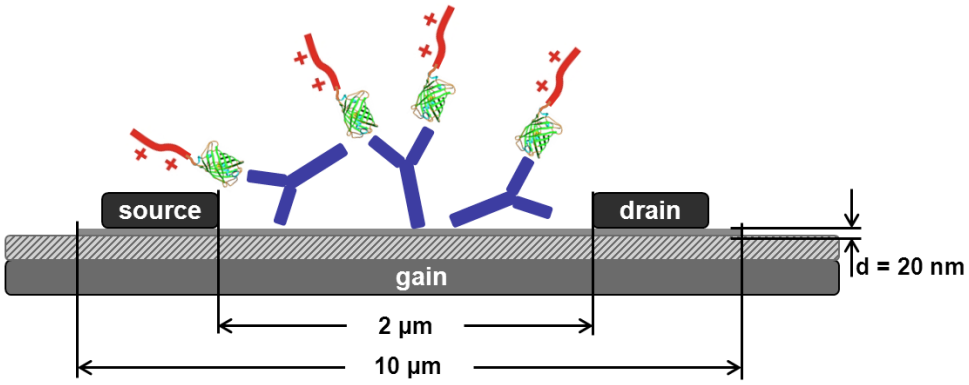

Figure 2. Schematic of a silicon-nanowire FET device functionalized with antibody receptors against GFP (blue). A GFP variant equipped with a charged tag will bind specifically to the receptor and produce a conductance change in the nanowire. Objects are not drawn to scale.

The response of the nanowire devices clearly differed depending on the net charge of the delivered protein. Whereas binding of positively charged GFP-ELPs resulted in reduced conductance of the nanowire, conductance was increased upon binding of negatively charged variants (Figure 3). These findings are in agreement with the expectations, as p-type (boron doped) silicon nanowires were used for nanodevice fabrication. It is well known that binding of negatively charged molecules increases conductance in p-type nanowires, analogously to applying a negative gate voltage.[14] Consequently, binding of positively charged molecules will decrease the conductance, analogously to applying a positive gate voltage. It is noteworthy that these trends were observed for all functional devices in two independent experiments. GFP alone did not induce any measureable change in conductance, as expected from its low net charge close to neutral pH. However, fusion of GFP to an ELP carrying nine positive or negative charges was sufficient to elicit a measureable conductance change. Increasing the number of positive charges on the ELP tag to 36 or 72 resulted in an increased average response. The highest response was observed for GFP-K36, whereas the response to GFP-E36 did not substantially differ from the response to GFP-E9 (Figure 3a). It has to be noted, however, that GFP-K36 and GFP-E36 were not tested in the first experiment. Furthermore, delivery of GFP-E18 did not elicit any response in experiment 1, but induced a decrease in conductance in experiment 2, whereas GFP-K18 was not detectable in experiment 2 (data nor shown). Upon delivery of GFP-ELP variants with 72 and 144 negative charges to the devices in

the first experiment, at a concentration of 100 nM, no change in conductance was observed (data not shown).

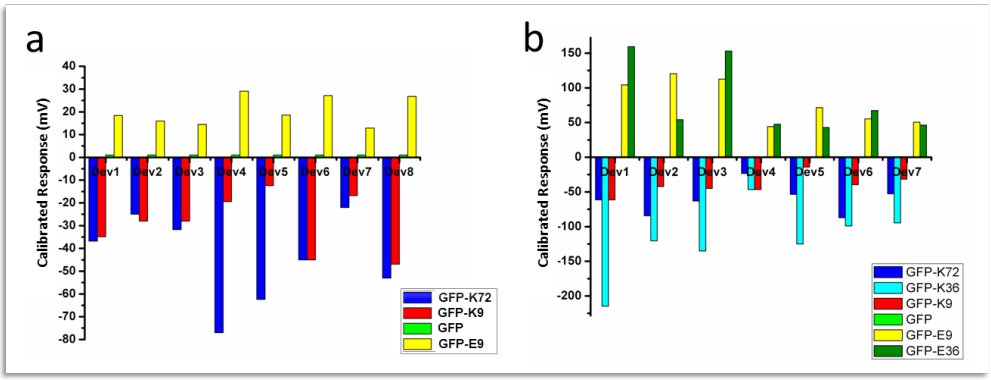

Figure 3. Sensing of GFP-ELP variants on NW-FET sensor chips. Graphs show the calibrated responses of several devices after delivery of the proteins through a fluid-delivery system. Results are from two independent experiments. (a) chip 1, analyte concentration: 100 nM; and (b) chip 2, analyte concentration: 20 nM.

A key factor for real-time sensors is their ability to respond and be regenerated quickly after operation. Representative time-dependent data for an GFP-ELP variant carrying nine positive charges (GFP-K9) show that conductance decreased sharply upon injection of the protein solution and stabilized at a lower value a few minutes after injection (Figure 4a). Upon subsequent washing with pure sensing buffer, the device responded rapidly within 5 min after buffer exchange, and conductance returned to baseline, indicating detachment of the protein from the antibody upon dilution. Contrarily, GFP injection did not change the conductance of the devices (Figure 4b).

To rule out non-specific binding effects due to electrostatic interaction, sensing was performed with the ELP variants K72 and E72, carrying 72 positive and negative charges, respectively. Neither variant elicited a response (Figure 4c and d). These results clearly showed the selectivity of the system, as the response of the devices is strictly dependent upon binding of GFP to the immobilized antibody.

The results raise the question why GFP with the longest negatively charged ELP tag (GFP-E72) did not elicit any response. To check whether binding of GFP to the antibody might be impaired for this variant, we conducted an enzyme-linked immunosorbent assay (ELISA). In brief, GFP and all GFP fusion variants that were tested in the sensing experiments were covalently coupled via the N-terminal amino

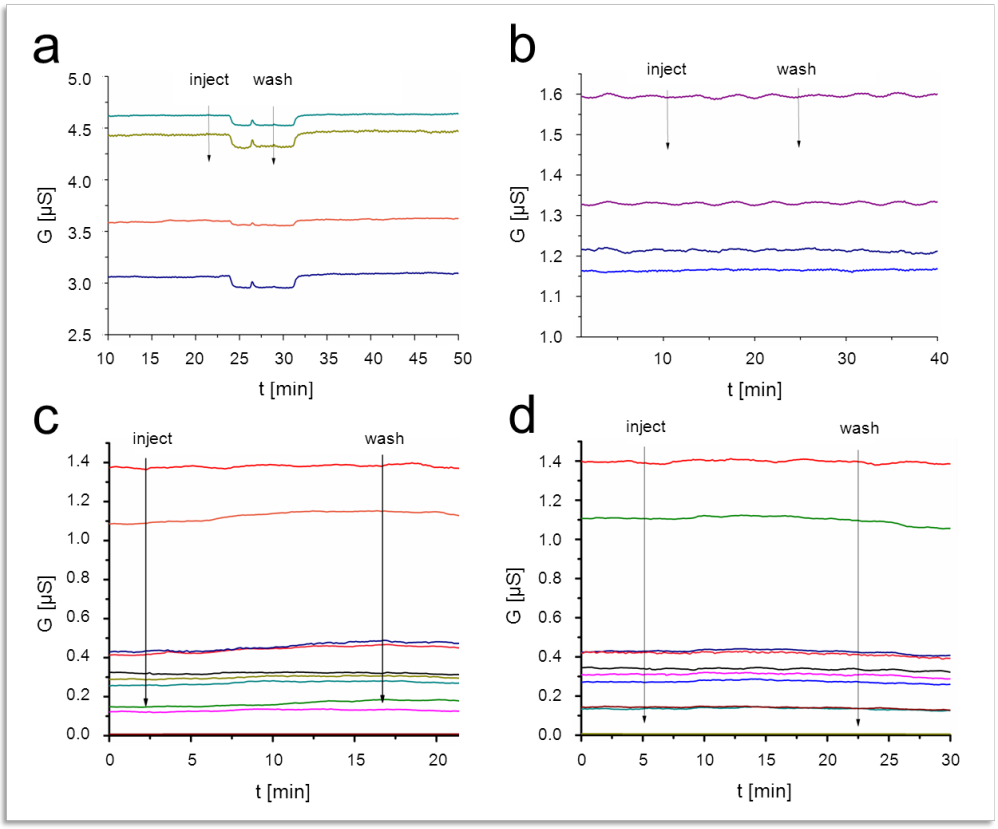

Figure 4. Sensing experiment – real time curves depicting the responses of individual devices to (a) 100 nM GFP-K9; (b) 100 nM GFP; (c) 20 nM K72; (d) 20 nM E72. GFP, K72, and E72 represent negative controls. (a-b) experiment 1; (c-d) experiment 2.

group to amino-reactive groups on the plate surface. The reaction took place in a buffer of pH 7 to favor reaction of the N-terminal amine group over reaction of the lysine ε-amine groups. As lysine ε-amine groups are more prevalent in the positively charged variants, a higher pH might lead to differences in coupling efficiency. The plate was incubated with the mouse monoclonal antibody against GFP, which was used in the sensing experiments. Binding of the anti-GFP antibody was detected by an enzyme-linked secondary antibody, which catalyzed the reaction of a non-fluorescent substrate to a fluorescent product. Fluorescence intensity in GFP-E9 functionalized wells was similar to the signal for wells with GFP absorbed. Intensity decreased with increasing length of the negatively charged tag (Figure 5a).

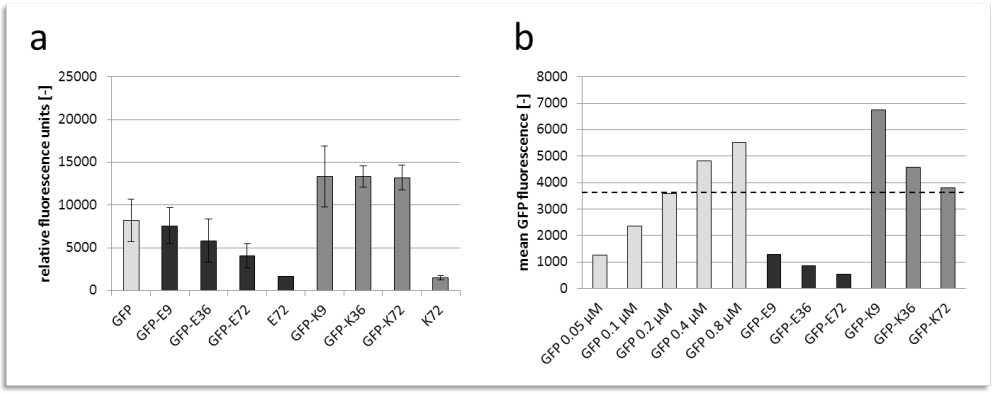

Figure 5. Relative binding affinities of anti-GFP antibody to GFP-ELP variants. (a) ELISA with primary antibody against GFP and enzyme-linked secondary antibody for detection via formation of a fluorescent product. GFP-ELP concentration was 0.2 µM for all variants during incubation on the plate. Relative fluorescence values are averages of two experiments with each experiment performed in hexaplicate. (b) Mean fluorescence of GFP-ELP variants absorbed to ELISA plate, determined by fluorescence microscopy and background-subtracted. Fluorescence micrographs were taken after incubation with the protein solution and washing. Dashed line: mean fluorescence of GFP, after incubation of 0.2 µM GFP solution. Protein concentration was 0.2 µM during incubation on the plate, if not otherwise stated.

Intensity for all positively charged GFP-ELP variants was substantially higher than for GFP. It can be ruled out that these differences result from unspecific electrostatic interactions between the antibody and the positively charged tag, as for the negative control K72 only a weak signal was detected, comparable to E72. It was therefore necessary to assess whether these differences can be assigned to different binding affinities of the antibody depending on the variant, or whether the variants only had different reactivities with the plate surface during immobilization. Fluorescence microscopy was used to estimate the amounts of protein adsorbed to the plate, taking advantage of the inherent fluorescence of GFP. Despite the fact that the same concentration was used for all GFP variants during incubation, the mean fluorescence was strongly reduced for negatively charged variants and strongly increased for the shorter positively charged variants (Figure 5b). These findings indicate that adsorption is highly dependent on the charge nature and the amount of charges on the ELP tag. We therefore conclude that the performed ELISA test is not suitable to answer the question why GFP-E72 did not elicit any response in the sensing experiments.

A sandwich ELISA was tried and proved to be unsuitable as well. In this second ELISA setup the anti-GFP antibody was coupled to the plate, and binding of GFP was assessed by detection with a second antibody directed against the C-terminal His tag. This assay resembled more closely the situation in the sensing device, where the antibody was immobilized on the plate and GFP was delivered in the mobile phase. However, the background signal was found to be in the range of the signal, due to unspecific absorption of GFP to the plate (data not shown).

CONCLUSIONS AND OUTLOOK

In this work, we successfully demonstrated that proteins targets equipped with a supercharged ELP tag are suitable for detection in SiNW-FETs, while the pristine protein does not elicit any signal at all. Already a moderate change in net charge due to fusion with a short charged ELP tag greatly enhances the detectability of a protein target in a nanowire field-effect transistor setup. Initial experiments with ELP tags carrying different numbers of charges indicate that longer tags induce a larger change in nanowire conductivity. However, a very high number of charges can suppress the signal, as was seen for the longest negatively charged tags E72 and E144. Further experiments are needed to determine the optimal length of supercharged tags in SiNW-FET devices. A detailed statement about the optimum length to elicit maximum response cannot be given at this point. Furthermore, it remains to clarify the mechanisms by which the charged ELP tag influences the device response. We tried to elucidate whether the ELP tag interferes with the binding of the GFP-fusion protein by the antibody, and, if yes, whether this interference is dependent on the length of the tag. However, all ELISA setups that were employed proved to be unsuitable to answer this question. Instead, this question might be addressed by confocal fluorescence imaging. As shown in this work, binding of GFP by the antibody immobilized on the sensor surface can be directly visualized. Binding affinities of the antibody to the different GFP-ELP variants need to be quantified by determining fluorescence intensity on the modified sensor surface after incubation with the fusion proteins.

Taken together, further experiments are needed to determine the optimum tag length and charge and to elucidate the mechanisms by which the ELP tag influences GFP detection by the device. Nevertheless, the results presented here are very promising and provide a successful proof-of-concept of the application of supercharged fusion proteins in NW-FET devices.

EXPERIMENTAL PART

Materials

All chemicals were used as purchased without any further purification. Fabrication and characterization of the analyte proteins was described in chapter 4. Mouse monoclonal [6AT316] antibody to GFP and rabbit anti-Mouse IgG H&L (HRP) secondary antibody were purchased from Abcam (Cambridge, UK). Phosphate buffer solution (PBS) tablets were obtained from Sigma-Aldrich (Steinheim, Germany). Tween20 was purchased from Bio-Rad Laboratories (Hercules, CA). Bovine serum albumin was obtained from Carl Roth GmbH (Karlsruhe, Germany). Solvents were purchased from Biolab Ltd., Israel. Silicon wafers with 600 nm thermal oxide, SSP prime grade, were obtained from Silicon Quest International. Glutaraldehyde, sodium cyanoborohydride and ethanolamine were purchased from Sigma-Aldrich (Israel). All other chemicals were purchased from KGaA (Darmstadt, Germany). Water with a resistivity > 18 MΩ was used for all experiments.

SiNW synthesis, device fabrication, and surface functionalization

Si-NW synthesis and device array fabrication

Silicon nanowires were synthesized by chemical vapor deposition as described previously.[27] Briefly, 20-nm-diameter gold nanoparticles served as catalyst sites for the growth of SiNWs on Si (100) growth substrates, covered with poly-lysine to promote adhesion of the gold nanoparticles to the substrate. For growth of p-doped SiNWs, the Si wafer was placed in a horizontal tube furnace, with silane (SiH_4) and diborane (B_2H_6) as reactants in a ratio of 1:4000 in the gas phase. SiNW FET devices and the polydimethylsiloxane (PDMS) fluid delivery system were fabricated as described previously.[19] In short, source and drain electrodes were deposited on the Si-NWs using a multilayer photoresist structure. After exposure and development of the electrode pattern, the contacts were metallized by e-beam and thermal evaporation of Ti/Pd/Ti (5/60/8) nm. Contacts were passivated with an insulating layer (100 nm) of Si_3N_4 deposited by plasma-enhanced chemical vapor deposition. The fluid delivery system was fabricated from flexible PDMS elastomer, using a master-SU8 template. PDMS was mixed 10:1 with base as a curing agent, cured overnight at 60 °C and cut into rectangular pieces of 10 x 10 x 5 cm. The PDMS channel was clamped to the wafer in respect to the NW-devices.

Surface Functionalization with anti-GFP antibody

Prior to chemical modification, the sensor device was cleaned by oxygen plasma treatment for effective chemical modification of the hydroxyl-terminated surface.

Substrates were then modified with 1% (v/v) 3-aminopropyltriethoxysilane (APTES) in ethanol/H_2O (95%/5%) for 1 h at room temperature, followed by a thorough rinse with isopropyl alcohol and baking on a hot plate at 115 °C for 3 hr. In order to provide aldehyde terminal groups, the APTES-modified surface was modified with glutaraldehyde by immersing the sensor chip in phosphate buffer solution (PBS) containing 2.5% glutaraldehyde with 4mM sodium cyanoborohydride ($NaBH_3CN$) at pH 8 for 2 h, followed by a through wash with water and isopropyl alcohol. A solution of monoclonal anti-GFP antibody (100 μg/ml (in 10 mM phosphate buffer, pH 8.4, containing 4 mM $NaBH_3CN$ was delivered into the PDMS channel for 4 h at a flow rate of 4 μl/min at room temperature, followed by a washing step with 10 mM phosphate buffer, pH 8.4. Unreacted terminal aldehyde groups were passivated by flushing the PDMS chamber for 1-2 h with 100 mM ethanolamine in 10 mM phosphate buffer, pH 8.4, containing 4 mM $NaBH_3CN$, followed by washing with 10 mM phosphate buffer, pH 8.4.

Analyte Binding Control with Confocal Fluorescence Imaging

A rectangular piece of cured PDMS with 2 to 3 mm holes was sealed to a Si/SiO_2 wafer functionalized with anti-GFP antibody as described above. A wafer that was not functionalized with the antibody served as a control. GFP at a concentration of 100 μg/ml in sensing buffer (PBS, 1:1000 in MilliQ) was added to the holes and incubated for 2 h. The GFP solution was removed and the chip was rinsed with sensing buffer for 1 min. Fluorescence micrographs of the surfaces were taken before and after rinsing of the wafers. Micrographs were recorded on a Leica SP5 confocal microscope equipped with an X63 1.4 NA Plan-Apo oil immersion objective. Images were acquired upon excitation at 488 nm and by recording emission between 500 and 550 nm using LASAF software.

Analyte Preparation, Sensing and Electrical Characterization

Protein sample preparation

Lyophilized proteins were dissolved in 50 mM NaCl solution to a concentration of 1 mg/mL, frozen in liquid nitrogen in aliquots and stored at -18 °C until further use. For sensing experiments, an aliquot (2×10^{-12} mol) was thawed on ice, filled up to 100 μL with sensing buffer to reach a final concentration of 200 nM, and dialyzed against sensing buffer overnight. The sample was then diluted with sensing buffer to the desired protein concentration (200 pM to 200 nM).

Sensing experiments were performed as described previously.[19] Briefly, the conductance of the Si-NW FET was measured by application of an AC bias (70 kHz, 100 mV) by means of a lock-in amplifier (Stanford Research System model SR830

DSP). The drain current was amplified with a variable-gain amplifier (model 99539 Amplifier System) and filtered by the lock-in amplifier with a time-constant setting of 300 ms. Data were recorded using a multichannel I/O adaptor panel (BNC-2090, National Instrument). Prior to real time electrical detection, the sensor chip was washed with sensing buffer. Protein analytes were delivered to the SiNW FET sensor chip by the microfluidic system using a syringe pump (Solomite Mitos Syringe Pump XS) at a flow rate of 5 µL/min, and conductance of the SiNW devices was monitored over time. All studies were carried out at room temperature. In order to decrease device-to-device variation, the device responses were calibrated by dividing the absolute response, i.e. the absolute change in current ΔI, by the NW gate dependence (dI_{ds}/dV_g) for each device.[26]

Enzyme-linked immunosorbent assay (ELISA)

Freeze-dried proteins were dissolved in coupling buffer (0.1 M sodium phosphate buffer, pH 7.0). Insoluble protein was removed by centrifugation (16,000 x g, 5 min, 6 °C), and protein concentration in the supernatant was determined by measuring absorbance at 280 nm. Protein solutions were diluted in coupling buffer to a concentration of 0.2 µM. 100 µl of protein solution was added to each well of a Nunc Immobilizer Amino F96 black plate. During all incubation steps the plate was wrapped in cling film to prevent evaporation of liquid. For coupling, the plate was incubated at 7°C o/n. After incubation, the liquid was removed. To block unreacted sites on the plate, 300 µl of blocking buffer (2% bovine serum albumin in 0.1 M sodium phosphate buffer, pH 8.0) were added to each well. The plate was incubated for 2 h at 7°C. Each well was washed 4 times with sensing buffer. Mouse monoclonal [6AT316] immunoglobulin G (IgG) antibody to GFP was diluted 1:1,000 in sensing buffer. 100 µl of antibody solution was added to each well and incubated for 30 min at room temperature (RT) whilst shaking at 800 rpm. Antibody solution was removed and wells were washed once with 300 µl sensing buffer and 5 times with 300 µl wash buffer (0.1 % bovine serum albumin and 0.1 % Tween20 in PBS) per well. HRP conjugated rabbit polyclonal antibody to mouse IgG was diluted 1:1,000 in wash buffer. 100 µl were added to each well and incubated for 30 min at RT whilst shaking at 800 rpm. All wells were washed 5 times with wash buffer and once with sensing buffer. Antibody detection was performed with the QuantaBlu detection kit according to the manufacturer's protocol. 100 µl of the freshly mixed substrate/peroxide solution was added to each well. Fluorescence at 420 nm after excitation at 325 nm was measured on a SpectraMax M2 (Molecular Devices, Sunnyvale, CA) for 4 h in intervals of 2 min.

Fluorescence microscopy of ELISA plates

Concentrated protein solutions were prepared as described for ELISA. A dilution series (0.05 to 0.8 µM) of GFP in coupling buffer was prepared. GFP-ELP variants were diluted in coupling buffer to a concentration of 0.2 µM. 100 µl of protein solution were added to each well of a Nunc Immobilizer Amino F96 clear plate. During all incubation steps the plate was wrapped in cling film to prevent evaporation of liquid. For coupling, the plate was incubated at 7°C o/n. After incubation, the liquid was removed. To block unreacted sites on the plate, 300 µl of blocking buffer (2% bovine serum albumin (BSA) in 0.1 M Na-P, pH 8.0) were added to each well. The plate was incubated for 2 h at 7°C. Blocking solution was exchanged for 300 µl of PBS per well.

Fluorescence images were recorded in epifluorescence mode using an EM-CCD camera (ImagEM / Hamamatsu, Japan) connected to an inverted microscope (IX71 / Olympus, Germany). GFP was excited with a continuous-wave solid-state laser at 488 nm, which was coupled into the microscope and focused onto the sample via an air objective (LUCPlanFLN 40x/0.6 / Olympus, Germany). The power at the focal point amounted to 570 µW. The emitted fluorescence was collected and separated from the excitation wavelength using a single-band dichroic filter (T495LP, Chroma, VT, USA) and a bandpass filter (HQ550/100m, Chroma, VT, USA). During each measurement, a sequence of 1000 frames was recorded with an exposure time of 100 ms. These images were averaged afterwards and then evaluated. Since the images just showed a slight uniform gradient in fluorescence due to the beam-profile (but no additional structures) the same inset in all averaged images was analyzed statistically.

REFERENCES

[1] T. H. S. Dent, *Atherosclerosis.* **2010***, 213*, 352-362.

[2] L. Hermus, J. D. Lefrandt, R. A. Tio, J. Breek, C. J. Zeebregts, *Atherosclerosis.* **2010***, 213*, 21-29.

[3] H. F. Escobar-Morreale, M. Luque-Ramirez, F. Gonzalez, *Fertil.Steril.* **2011***, 95*, 1048-U249.

[4] M. Kowalewska, R. Nowak, M. Chechlinska, *Biochimica Et Biophysica Acta-Reviews on Cancer.* **2010***, 1806*, 163-171.

[5] M. Zaninotto, M. M. Mion, E. Novello, S. Altinier, M. Plebani, *Clinica Chimica Acta.* **2007***, 381*, 14-20.

[6] P. Mullenix, C. Andersen, B. Starnes, *Ann.Vasc.Surg.* **2005***, 19*, 130-138.

[7] J. A. P. Bons, M. P. van Dieijen-Visser, W. K. W. H. Wodzig, *Proteomics Clinical Applications.* **2007***, 1*, 1123-1133.

[8] S. I. Mohammed, M. Rahman, *Proteomics Clinical Applications.* **2008***, 2*, 1194-1207.

[9] M. Pardo, R. A. Dwek, N. Zitzmann, *Expert Review of Proteomics.* **2007***, 4*, 273-286.

[10] L. D. Ralton, G. I. Murray, *Current Proteomics.* **2010***, 7*, 212-221.

[11] E. D. Avgerinos, N. P. E. Kadoglou, K. G. Moulakakis, T. G. Giannakopoulos, C. D. Liapis, *International Journal of Stroke.* **2011***, 6*, 337-345.

[12] E. P. Rhee, R. E. Gerszten, *Clin.Chem.* **2012***, 58*, 139-147.

[13] E. Stern, J. F. Klemic, D. A. Routenberg, P. N. Wyrembak, D. B. Turner-Evans, A. D. Hamilton, D. A. LaVan, T. M. Fahmy, M. A. Reed, *Nature.* **2007***, 445*, 519-522.

[14] G. Zheng, F. Patolsky, C. Lieber, *Abstr.Pap.Am.Chem.Soc.* **2005***, 229*, U782-U782.

[15] G. Zheng, X. P. A. Gao, C. M. Lieber, *Nano Lett.* **2010***, 10*, 3179-3183.

[16] Y. Cui, Q. Wei, H. Park, C. Lieber, *Science.* **2001***, 293*, 1289-1292.

[17] J. Hahm, C. Lieber, *Nano Lett.* **2004***, 4*, 51-54.

[18] L. Soleymani, Z. Fang, E. H. Sargent, S. O. Kelley, *Nat.Nanotechnol.* **2009***, 4*, 844-848.

[19] M. Kwiat, R. Elnathan, M. Kwak, J. W. de Vries, A. Pevzner, Y. Engel, L. Burstein, A. Khatchtourints, A. Lichtenstein, E. Flaxer, A. Herrmann, F. Patolsky, *J.Am.Chem.Soc.* **2012***, 134*, 280-292.

[20] F. Patolsky, G. Zheng, O. Hayden, M. Lakadamyali, X. Zhuang, C. Lieber, *Proc.Natl.Acad. Sci.U.S.A.* **2004***, 101*, 14017-14022.

[21] F. Patolsky, G. Zheng, C. Lieber, *Anal.Chem.* **2006***, 78*, 4260-4269.

[22] B. F. Shaw, G. F. Schneider, B. Bilgicer, G. K. Kaufman, J. M. Neveu, W. S. Lane, J. P. Whitelegge, G. M. Whitesides, *Protein Sci.* **2008***, 17*, 1446-1455.

[23] K. Broersen, M. Weijers, J. de Groot, R. J. Hamer, H. H. J. de Jongh, *Biomacromolecules.* **2007***, 8*, 1648-1656.

[24] M. S. Lawrence, K. J. Phillips, D. R. Liu, *J. Am. Chem. Soc.* **2007***, 129*, 10110-+.

[25] A. Kolbe, L. L. del Mercato, A. Z. Abbasi, P. Rivera-Gil, S. J. Gorzini, W. H. C. Huibers, B. Poolman, W. J. Parak, A. Herrmann, *Macromol.Rapid Commun.* **2011***, 32*, 186-190.

[26] F. N. Ishikawa, M. Curreli, H. Chang, P. Chen, R. Zhang, R. J. Cote, M. E. Thompson, C. Zhou, *Acs Nano.* **2009***, 3*, 3969-3976.

[27] F. Patolsky, G. Zheng, C. M. Lieber, *Nature Protocols.* **2006***, 1*, 1711-1724.

Chapter 6

Summary

Electrostatic interactions rely on the effect that positive and negative charges attract each other, whereas two positive or two negative charges repel each other. Electrostatic effects play an important role in many processes that take place in living organisms, and many structures and molecules inside the cell bear charges. The carrier of genetic information, deoxyribonucleic acid (DNA) is negatively charged. Proteins, on the other hand, can be positively or negatively charged. As they carry out many functions in living organisms, a great variety of different proteins is needed. This variety is attained by the fact that the 20 natural amino acids (i.e. the building blocks of proteins) can be used in virtually any combination. Among the natural amino acids two positively and two negatively charged ones occur under physiological conditions. Structure and function of a protein are defined by the amino acid sequence, which is encoded in the genetic information. Changing the genetic information - a process called genetic manipulation - therefore actually means to modify the "construction plan" of a protein. The genetic information is delivered into a host organism (a bacterial cell, for example), which then produces the modified protein. In this way, also the charge of a protein can be altered: When negatively charged amino acids are exchanged by positively charged ones, the modified protein is highly positively charged, and *vice versa*. Two such proteins repel each other, but are attracted to everything that is negatively charged. **Chapter 1** describes how such "supercharged" proteins are used for a wide variety of applications in medicine, biological research and material science.

Many proteins form compact, well-defined structures in solution. The proteins described in this thesis, however, exhibit a flexible backbone. They were designed in such a way that they have positive or negative charges at equal distances along the amino acid chain and are able to interact with oppositely charged molecules and objects (**chapter 2**). As they do not fold into three-dimensional structures in solution, they are called supercharged, unfolded proteins (SUPs). We decided to investigate whether positively charged (cationic) SUPs can bind to mucins, highly negatively charged proteins with sugar chains attached along the protein chain (**chapter 3**). Mucins are a component of saliva and are responsible for lubrication in the mouth: They form a viscous film on teeth, tongue and mucosa to reduce friction between sliding surfaces. Saliva needs to be constantly produced, because the salivary conditioning film can be damaged due to mechanical stress (during speaking and chewing) or dilution (during eating and drinking). Patients who suffer from dry-mouth disease do not produce enough saliva and consequently experience pain when they speak or eat. These patients are prescribed special toothpastes or mouth-rinses, but their effect does not last very long, and most patients still complain about a perception of dryness in the mouth after the application. Together with Dr. Prashant Sharma and Deepak

Veeregowda at the University Medical Center Groningen, we investigated whether treatment with cationic SUPs could stabilize salivary conditioning films in these patients. We therefore mimicked the real situation in which a patient would rinse his/her mouth with the protein solution. Salivary conditioning films were created on a plain surface, which were first rinsed with the protein solution and then with saliva. We observed that the films indeed became more resistant to mechanical stress after treatment with a long variant of cationic SUP. Moreover, the lubrication properties of the treated films were considerably improved compared to untreated films. These results raise the hope that treatment with cationic SUPs will increase the comfort of patients with dry-mouth disease in the future.

Next, we examined whether it is possible to build structures from SUPs on the micro-and nanometer scale (i.e. a thousandth to a millionth part of a millimeter in size). Such structures can find applications as carrier systems for drugs and other bioactive compounds that are injected into the blood stream. The use of a carrier system has at least two advantages: Firstly, the active compound is shielded from agents that can inactivate it before it reaches its target. Secondly, the carrier system can be directed to the target site and trigger the uptake of its load by those cells that are to be treated, but not by other cells in the body. In this way, side effects can be substantially reduced. In collaboration with Prof. Parak's group at the University of Marburg, Germany, we fabricated micrometer-sized, hollow capsules from SUPs (**chapter 2**). We built the capsule wall of consecutive layers of anionic and cationic SUPs on a spherical core; thereby the electrostatic attraction between oppositely charged SUPs served as a kind of "glue" between the ten or more layers. After the assembly of the wall, the core was destroyed, and the hollow shell proved to be stable, as it preserved its round shape. It had been shown before that proteins can be loaded into the cavity of electrostatically assembled capsules and that these capsules are taken up by cells in culture (i.e. cells that are grown in a culture medium in the laboratory). We wanted to see whether proteins can also be loaded into the capsule wall (**chapter 4**). To this end a cationic SUP variant was fused to green fluorescent protein (GFP). As GFP is fluorescent, it lights up as green spots under a fluorescence microscope when excited with blue light. This enables us to see where GFP is located in a sample. The SUP served as an electrostatic "anchor" to incorporate GFP into the capsule wall. The capsules were fabricated as described in chapter 2, but this time one layer was composed of the GFP fusion protein. The capsules were indeed taken up by cells in culture, and we were able to follow their fate inside the cells under a fluorescence microscope. These results serve as a proof-of-principle that the shell of multilayer capsules can be functionalized by electrostatic anchoring using a SUP tag fused to a charge neutral or moderately charged protein.

Finally, we investigated how GFP-SUP fusion proteins perform in supersensitive detection (**chapter 5**). Supersensitive detectors are able to sense compounds even at very low concentrations. Therefore they are promising tools for a broad range of applications like the fast diagnosis of heart attacks or dangerous infections and the detection of explosives or pesticides, just to name a few. Together with Prof. Patolski's group at Tel-Aviv University, Israel, we developed a detector for GFP based on a nanowire field-effect transistor (NW-FET). This kind of detector senses changes in the charge distribution around a semiconducting wire. The field is changed when a charged object comes into close proximity with the wire surface. Due to the fact that the wires have a large surface to volume ratio, even small particles (like proteins, for example) cause a measureable field change. We created series of positively and negatively charged GFP-SUP fusion proteins with various lengths of the SUP part and measured the effect of the charged tag on the detectability of GFP. As GFP is only moderately charged, it was not detectable by our system. However, already the smallest tags with nine charges were sufficient to sense binding of GFP to the nanowires. Furthermore, the results indicated that positively charged tags perform slightly better than negatively charged ones. Experiments like these will help to better understand the factors that influence measurements in NW-FETs and to improve the performance of these sensors.

Chapter 7

Samenvatting

Elektrostatische interacties zijn gebaseerd op het effect dat positieve en negatieve ladingen elkaar aantrekken, terwijl twee positieve of twee negatieve ladingen elkaar afstoten. Elektrostatische effecten spelen een belangrijke rol in veel processen die plaatsvinden in levende organismen, en veel onderdelen en moleculen in de cel hebben ladingen. De drager van genetische informatie, desoxyribonucleïnezuur (DNA), is negatief geladen. Eiwitten aan de andere kant kunnen positief of negatief geladen zijn. Omdat ze veel functies in levende organismen vervullen, is een grote variëteit aan verschillende eiwitten nodig. Deze variëteit wordt verkregen door het feit dat de 20 natuurlijke aminozuren (de bouwstenen van eiwitten) gebruikt kunnen worden in vrijwel elke combinatie. Onder de natuurlijke aminozuren komen twee positief en twee negatief geladen voor onder fysiologische condities. De structuur en functie van een eiwit worden bepaald door de aminozuur volgorde, die is vastgelegd in de genetische code. Verandering van de genetische code – een proces genaamd genetische manipulatie – houdt dus eigenlijk een verandering van het "bouwplan" van een eiwit in. De genetische informatie wordt bezorgd in een host organisme (een bacterie bijvoorbeeld), die vervolgens het gemodificeerde eiwit produceert. Via deze weg kan ook de lading van een eiwit worden veranderd: wanneer negatief geladen worden vervangen door positief geladen eiwitten, dan is het gemodificeerde eiwit hoog positief geladen, en *vice versa*. Twee van zulke eiwitten stoten elkaar af, maar worden aangetrokken door alles wat negatief geladen is. **Hoofdstuk 1** beschrijft hoe zulke "supergeladen" eiwitten worden gebruikt in een verscheidenheid aan applicaties in medicijnen, biologisch onderzoek en materiaalwetenschapen.

Veel eiwitten vormen compacte, goed gedefinieerde structuren in oplossingen. Echter, de eiwitten beschreven in dit proefschrift vertonen een flexibele structuur. Ze zijn zo ontworpen dat ze positieve of negatieve ladingen op gelijke afstand hebben over de gehele lengte van aminozuren en hebben interactie met moleculen en objecten van tegengestelde lading (**hoofdstuk 2**). Omdat ze in oplossing niet in een driedimensionale structuur vouwen, worden ze "supercharged, unfolded proteins" (hoogeladen, ongevouwen eiwitten; SUPs) genoemd. We hebben besloten te onderzoeken of positief geladen (kationische) SUPs kunnen binden aan mucines, hoog negatief geladen eiwitten met suiker ketens aan de eiwit keten (**hoofdstuk 3**). Mucines zijn een onderdeel van het speeksel en zijn verantwoordelijk voor de smering van de mond: ze vormen een viskeuze film op de tanden, tong en het slijmvlies om de frictie tussen schuivende oppervlakken te verminderen. Speeksel moet constant geproduceerd worden omdat de film beschadigd kan worden door mechanische stress (tijdens het praten of kauwen) of verdunning (tijdens het eten en drinken). Patiënten die aan de droge mond ziekten lijden produceren niet genoeg speeksel en ervaren pijn tijdens het praten en eten. Deze patiënten krijgen speciale tandpasta of mondwater

voorgeschreven, maar hiervan duurt het effect niet lang en de meeste patiënten klagen nog steeds over droogte in de mond na het nemen hiervan. Samen met Dr. Prashant Sharma en Deepak Veeregowda van het Universitair Medisch Centrum Groningen hebben we onderzocht of behandeling met kationische SUPs de speekselfilm van deze patiënten kan stabiliseren. Daarom hebben we de werkelijke situatie nagebootst waarin een patiënt zijn/haar mond spoelt met de eiwitoplossing. Speekselfilms zijn gemaakt op een recht oppervlak en vervolgens eerst met de eiwit oplossing gewassen en daarna met speeksel. Er is gebleken dat de films inderdaad beter resistent waren tegen mechanische stress na behandeling met de lange variant van kationische SUPs. Bovendien bleek de smering van de behandelde films behoorlijk verbeterd te zijn in vergelijking met onbehandelde films. Deze resultaten bieden de hoop dat behandeling waarbij gebruik wordt gemaakt van kationische SUPs het leven voor patiënten met een droge mond aandoening in de toekomst dragelijker zal maken.

Vervolgens hebben we onderzocht of het mogelijk is om structuren te maken van SUPs op micro- en nanometer schaal (een duizendste en een miljoenste meter omvang). Zulke structuren kunnen gebruikt worden als dragersystemen voor medicijnen en andere bioactieve verbindingen die worden geïnjecteerd in de bloedbaan. Het gebruik van dragersystemen heeft tenminste twee voordelen: Ten eerste is het actieve middel beschermd tegen vernietiging voordat het doel wordt bereikt. Ten tweede kan het systeem gestuurd worden naar de doellocatie en de opname door de beoogde cellen versterken terwijl andere lichaamscellen buiten schot blijven. Hierdoor kunnen bijwerkingen aanzienlijk worden verminderd. In samenwerking met Prof. Parak's groep aan de universiteit van Marburg, Duitsland, hebben we micrometer grote holle capsules gemaakt van SUPs (**hoofdstuk 2**). We hebben de capsule wand gebouwd van opeenvolgende lagen van anionische en kationische SUPs op een ronde kern; waarbij de elektrostatische interactie tussen de tegengesteld geladen SUPs als een soort lijm dient tussen de tien of meer lagen. Na vorming van de wand is de kern verwijderd en bleken de holle capsules hun ronde vorm te behouden. Er is eerder getoond dat eiwitten geladen kunnen worden in de ruimte van elektrostatisch gevormde capsules en dat deze capsules opgenomen worden door cultuur cellen (dit zijn cellen die gegroeid worden in cultuur medium in een laboratorium). Wij hebben onderzocht of dergelijke eiwitten ook in de wand kunnen worden ingebouwd (**hoofdstuk 4**). Zodoende is de kationische SUP variant gefuseerd met het "green fluorescent protein" (GFP). Omdat GFP fluoriserend is, is het zichtbaar als een groene plek onder een fluorescentie microscoop wanneer er belicht wordt met blauw licht. Dit maakt het mogelijk te zien waar de GFP gesitueerd is in het monster. De SUP dient als een elektrostatisch anker om de GFP te incorporeren in de capsule wand. De capsules zijn gemaakt zoals beschreven in hoofdstuk 2, maar deze keer is een laag gemaakt van

het GFP fusie eiwit. Deze capsules worden inderdaad opgenomen door cultuur cellen en we waren in staat om hun bestemming in de cel te volgen met behulp van een fluorescentie microscoop. Deze resultaten dienen als proof-of-concept voor het feit dat een meerderelaags capsule gefunctionaliseerd kan worden door het elektrostatisch verankeren met een SUP gefuseerd met een neutraal of licht geladen eiwit.

Tenslotte hebben we onderzocht hoe GFP-SUP fusie eiwitten presteren in supergevoelige detectie (**hoofdstuk 5**). Supergevoelige detectoren zijn in staat om verbindingen te herkennen op zeer lage concentraties. Daarom zijn ze veelbelovend gereedschap voor een brede range aan toepassingen zoals snelle diagnose van een hartstilstand of gevaarlijke infecties en de opsporing van explosieven en pesticiden. Samen met Prof. Patolski's groep aan de universiteit van Tel-Aviv, Israel, is een detector voor GFP ontwikkeld die gebruik maakt van "nanowire field-effect transistors" (NW-FETs). Dergelijke detectoren zijn gevoelig voor een verandering in de ladingsverdeling rondom een halfgeleidende draad. Het veld wordt veranderd wanneer een geladen object in de nabijheid komt van het oppervlak. Doordat de draden een grote oppervlak-volume ratio hebben kunnen zelfs kleine deeltjes (zoals eiwitten bijvoorbeeld) een meetbare verandering in het veld veroorzaken. Wij hebben een serie van verschillende positief en negatief geladen GFP-SUP fusie eiwitten gemaakt, met verschillende lengtes van het SUP gedeelte, en het effect gemeten van het geladen label aan GFP. Omdat GFP licht geladen is, is het niet detecteerbaar met ons systeem. Echter, het kleinste label met negen ladingen was genoeg om binding van GFP aan de nanometer dikke draad te detecteren. Bovendien laten de resultaten zien dat positief geladen labels iets beter werken dan negatief geladen labels. Dergelijke experimenten helpen een beter inzicht te krijgen in de factoren die een rol spelen in metingen met NW-FETs en om de prestaties van deze sensors te verbeteren.

Chapter 8

Acknowledgements

A chapter of my life is about to be closed – the right moment to look back and to thank all the people who contributed in some form or other to this work.

First of all, I would like to thank my supervisor, Prof. Andreas Herrmann, for the opportunity to become a PhD student in his group and for all his support during my PhD studies. Andreas, your door was always open when I needed advice or some information or just a signature from you. You showed me that you were greatly interested in the progress of my research and at the same time you gave me a lot of freedom. I greatly admire your networking abilities: You often made contact with people who could help me further, initiated several collaborations and made it possible that I could to travel to Tel-Aviv, Stuttgart, Enschede and Fribourg. Thank you so much!

Secondly, I would like to thank the members of the reading committee – Prof. Katja Loos, Prof. Bert Poolman and Prof. Wolfgang Parak - for the evaluation of my thesis and for helpful comments.

Many thanks to all people in the department of Polymer Chemistry and especially to the members of the "Polymer Chemistry and Bioengineering" group! Thank you for all the good moments – for the VvP activities, the talks in the coffee room and the time we spent together during conferences and meetings. I would just like to name a few people in particular: Jan-Willem, Agnieszka, Tobias and Ralph, thank you for hiking trips, dinners, watching football matches and other activities we did together! You were much more than colleagues to me. Manfred, thank you so much for all advice in questions regarding my research and for your encouragement! Diego, thank you for always lending me an ear and for sharing your collection of great music in the lab! Alessio, you were always willing to help, especially with figures for presentations, posters and papers, and you did everything with a smile. Thank you! I really admire your patience and friendliness. Andrew, thank you so much for all the dinners at your place and for the amazing conversations we had! Your wedding in the south of France was a wonderful experience, Andrew and Leila! Deepak, Minseok and Andreas, you were my first colleagues in Groningen. Together we built the lab and tried to find our way at the university and through the Dutch bureaucracy. Minseok, I greatly admire your "kwakabilities" and I will never forget your help, especially in the first months! Deepak, you are a wonderful person! Knowing you makes my life richer. Andreas, thank you for all the great moments at your place and at the university! Salomeh, it was always encouraging talking to you, having you around. Your Swiss-German accent is beautiful! Jan, it was a pity that you left our group after such a short time. Thank you for all your advice and for all you invested into me and into others! Alberto, thank you so much for your friendship and your trust!

What would my PhD studies and this thesis have been without my collaborators? I would like to thank Dr. Loretta del Mercato, Dr. Pilar Rivera Gil and Prof. Wolfgang Parak from the University of Marburg, Germany, for all contributions and for fruitful discussions on the phone and face-to-face here in Groningen. Two chapters of this thesis would not have been written without you. Deepak Veeregowda, Dr. Prashant Sharma, Prof. Henny van der Mei and Prof. Henk Busscher from the University Medical Center Groningen I would like to mention here as well - we started a joint project only in the second-last year of my PhD. Still, we were able to get conclusive results and to write a well-founded paper together, which will hopefully be accepted and published soon. I would like to thank Noam Sidelman and Dr. Shachar Richter, as well as Dr. Moria Kwiat, Dr. Roey Elnathan and Prof. Fernando Patolski from Tel-Aviv University. During my stays at the Nanocenter I got insight into two fields that were mostly new to me. Special thanks to you, Moria, for sending me all the data I needed for the last chapter of my thesis and for answering most patiently all my questions during a time which was a most difficult one for you! Thanks to Melanie Brasch and Prof. Jeroen Cornelissen from Twente University, Dr. Ilja Voets from Technical University Eindhoven, Dr. Stefan Ernst and Prof. Michael Börsch from the University of Stuttgart, Germany, Dr. Jacek Mika and Prof. Bert Poolman from the University of Groningen and all other people I worked with during my PhD studies for everything I could learn from you! Especially I would like to thank the Membrane Enzymology group and the Protein Crystallography group at the University of Groningen: You generously allowed me to use your labs and equipment; moreover, so many people helped me with the machines and gave me valuable advice. Your support, especially in the first year of my PhD when I was the only biologist in the whole Polymer Chemistry department, cannot be valued too high. Furthermore, I would like to thank Maria de Vries, Marius Uebel and Lieke van Gijtenbeek, who worked under my supervision and greatly supported me in my research. It was great pleasure working with you. Last but not least I express my deep gratitude to Dr. Sekineh (Sheyda) Jafari Gorzini from the Max-Planck-Institute in Mainz, Germany – your initial work on the supercharged proteins and the training I got from you laid a good foundation for my research.

Next to direct support at the university, many people indirectly supported me. Very important were the international christian student organization HOST and the International Christian Church in Assen (now Vineyard Groningen). There I met so many wonderful people from all over the world. I don't dare to write some names here – I could easily forget someone and the list would be far too long anyway. So Iet me just tell you all that I am very thankful for having met you. Thank you so much for your friendship, for caring, for providing, for praying! I am blessed to have such

a family. Hester, although you are a member of Vineyard Groningen now, I still want to mention you especially. Door de jaren hebben we elkaar beter leren kennen en hebben we veel samen beleefd. Ik hoop dat we nog vaker samen op vakantie gaan – volgend jaar weer naar Ierland? Ik ben ook heel blij dat je de omslag van dit boekje hebt ontworpen. Hij is geweldig! Ik zeg nog een keer van harte: "Dank je wel!".

Besides work I spent a lot of time "at home", of course, in our cozy, shared flat in the "Grote Lelie" with wonderful and very special housemates. Christina, unser gemeinsames Jahr wird mir immer in Erinnerung bleiben. Hab vielen, vielen Dank für all die schönen Stunden und für deine Unterstützung in schwierigen Zeiten! Judith en Lasse – jullie waren geweldige huisgenoten! Ook dankzij jullie heb ik mijn Nederlands kunnen verbeteren. Rebecka, fast drei Jahre lang haben wir Freud und Leid geteilt, haben so viel zusammen erlebt. Es hat mir so gut getan, dass ich nicht nur mit dir reden, sondern auch mit dir beten konnte, und ich kann nur staunen über Gottes Führung. Jan, es ist eine wunderbare Sache, dass ich dich durch Rebecka kennen lernen durfte – unseren sporadischen vierten Mitbewohner und Partner in vielen Gesprächen über einfach alles. Bald bildet ihr beiden hoffentlich eine WG fürs Leben und ich wünsche euch von ganzem Herzen Gottes Segen dazu. Eliyahu, you were an amazing neighbor and are a wonderful friend. Thank you with all my heart for your friendship, your generosity and your valuable advice in many things! And thank you so much for all your help with preparing this thesis! Thinking of you, I also remember my friends in Israel – Noam, Amir, Yaron and Maia: You received me with open arms and hearts. Thank you for having given me such an amazing time during my stays in Tel-Aviv!

For my family I am deeply grateful, especially for my nearest relatives – for my parents and my grandmother, for my brother Bernd with his wife Jasmin and his daughters Hannah and Elinor, for my sister Christine and her boyfriend Matthias. Liebe Mama, lieber Papa, ich danke euch aus tiefstem Herzen für eure Liebe, Geduld, Erziehung und Unterstützung in jeder Hinsicht, am meisten aber für eure treuen Gebete und dass ihr mir den Glauben vorgelebt habt! Liebe Großmama, auch du bist für mich einer der wichtigsten Menschen in meinem Leben. Ich danke dir von ganzem Herzen für alles, was du für mich getan hast und dass du mir immer wieder gezeigt und gesagt hast, wie lieb und wertvoll ich dir bin. Lieber Bernd, liebe Christine, ich bin so froh, dass ich euch habe und dass wir als Geschwister zusammen aufwachsen durften. Habt Dank für all die besonderen Stunden mit euch bis jetzt! Ich habe euch alle sehr, sehr lieb!

Now I have thanked so many people, who have been part of my life during the last five years or even before, and there are still many more. However, there is one who deserves my thanks most of all: my Lord and Savior, Jesus Christ. You created me;

You provide for all my needs and You have given me the capability to do this PhD. Therefore You are the one who deserves all praise.

I trust in your unfailing love;
my heart rejoices in your salvation.
I will sing the Lord's praise,
for he has been good to me.
Psalm 13: 5-6 (NIV)

Anke Kollee